ANALYSIS OF CRACKS IN THREE-DIMENSIONAL LINEAR ELASTIC MEDIA WITH CONSIDERATION OF SURFACE STRESS EFFECTS

Mr. Binh Thai Nguyen

A Dissertation Submitted in Partial Fulfillment of the Requirements
for the Degree of Doctor of Philosophy Program in Civil Engineering
Department of Civil Engineering
Faculty of Engineering
Chulalongkorn University
Academic Year 2013

การวิเคราะห์รอยร้าวในตัวกลางยืดหยุ่นเชิงเส้นสามมิติโดยพิจารณาหน่วยแรงที่ผิว

นายบิน ไทย เหงียน

วิทยานิพนธ์นี้เป็นส่วนหนึ่งของการศึกษาตามหลักสูตรปริญญาวิศวกรรมศาสตรดุษฎีบัณฑิต
สาขาวิชาวิศวกรรมโยธา ภาควิชาวิศวกรรมโยธา
คณะวิศวกรรมศาสตร์ จุฬาลงกรณ์มหาวิทยาลัย
ปีการศึกษา 2556

Thesis Title	ANALYSIS OF CRACKS IN THREE-DIMENSIONAL LINEAR ELASTIC MEDIA WITH CONSIDERATION OF SURFACE STRESS EFFECTS
By	Mr. Binh Thai Nguyen
Field of Study	Civil Engineering
Thesis Advisor	Associate Professor Jaroon Rungamornrat, Ph.D.
Thesis Co-Advisor	Professor Teerapong Senjuntichai, Ph.D.
	Associate Professor Anil C. Wijeyewickrema, Ph.D.

Accepted by the Faculty of Engineering, Chulalongkorn University in Partial Fulfillment of the Requirements for the Doctoral Degree

.....Dean of the Faculty of Engineering

(Professor Bundhit Eua-arporn, Ph.D.)

THESIS COMMITTEE

.....Chairman

(Professor Thaksin Thepchatri, Ph.D.)

.....Thesis Advisor

(Associate Professor Jaroon Rungamornrat, Ph.D.)

.....Thesis Co-Advisor

(Professor Teerapong Senjuntichai, Ph.D.)

.....Thesis Co-Advisor

(Associate Professor Anil C. Wijeyewickrema, Ph.D.)

.....Examiner

(Associate Professor Akhrawat Lenwari, Ph.D.)

.....Examiner

(Assistant Professor Watanachai Smittakorn, Ph.D.)

.....External Examiner

(Assistant Professor Arnon Wongkaew, Ph.D.)

บิน ไทย เหงียน : การวิเคราะห์รอยร้าวในตัวกลางยืดหยุ่นเชิงเส้นสามมิติโดยพิจารณาหน่วยแรงที่ผิว. (ANALYSIS OF CRACKS IN THREE-DIMENSIONAL LINEAR ELASTIC MEDIA WITH CONSIDERATION OF SURFACE STRESS EFFECTS) อ.ที่ปรึกษาวิทยานิพนธ์หลัก: รศ.ดร. จรูญ รุ่งอมรรัตน์, อ.ที่ปรึกษาวิทยานิพนธ์ร่วม: ศ.ดร. ธีรพงศ์ เสนจันทร์ฒิไชย, Assoc. Prof. Anil C. Wijeyewickrema Ph.D., 89 หน้า.

ดุษฎีนิพนธ์นี้นำเสนอระเบียบวิธีเชิงตัวเลขที่มีประสิทธิภาพสำหรับจำลองรอยแตกร้าวในระนาบ ในตัวกลางยืดหยุ่นเชิงเส้นสามมิติซึ่งพิจารณาอิทธิพลของหน่วยแรงที่ผิวด้วย หลักการของหน่วยแรงที่ผิวซึ่งนิยมใช้แพร่หลายในการศึกษาปัญหาในระดับนาโนถูกนำมาใช้ในการพัฒนาแบบจำลองเชิงคณิตศาสตร์ซึ่งสามารถจำลองรอยแตกร้าวขนาดนาโนได้ แผ่นผิวบางของวัสดุบนผิวรอยแตกร้าวจำลองเป็นพื้นผิวที่มีความหนาเป็นศูนย์ ซึ่งยึดแน่นกับวัสดุบัลก์โดยพฤติกรรมถูกกำกับโดยความสัมพันธ์เชิงวัสดุของเกอร์ตินและเมอร์ดอค ในการสร้างปัญหาค่าขอบเขต ทฤษฎีความยืดหยุ่นเชิงเส้นพื้นฐานถูกนำมาใช้ในการสร้างสมการกำกับของวัสดุบัลก์ในรูปแบบของสมการเชิงปริพันธ์พื้นผิวที่ลดดีกรีความเป็นเอกฐานสำหรับการขจัดและแรงพื้นผิวบนผิวรอยแตกร้าว ส่วนสมการกำกับของพื้นผิวที่มีความหนาเป็นศูนย์ซึ่งรวมผลของหน่วยแรงที่ผิวถูกพัฒนาในรูปแบบอ่อนโดยอาศัยระเบียบวิธีน้ำหนักคงค้าง ผลเฉลยของระบบสมการผสมที่พัฒนาขึ้นหาได้จากกระบวนการเชิงตัวเลขร่วมระหว่างระเบียบวิธีไฟไนต์เอลิเมนต์และระเบียบวิธีบาวดารีเอลิเมนต์แบบสมมาตร เนื่องจากสมการกำกับเชิงปริพันธ์เป็นแบบเอกฐานต่ำ ทำให้สามารถใช้ฟังก์ชันต่อเนื่องมาตรฐานในการประมาณปริมาณไม่ทราบค่าบนผิวของรอยแตกร้าวได้ และจำเป็นต้องใช้เทคนิคเชิงตัวเลขพิเศษเฉพาะในการหาค่าปริพันธ์เชิงเอกฐานและใกล้เคียงเอกฐานเท่านั้น หลังจากสอบเทียบกับผลเฉลยอ้างอิงแล้ว ระเบียบวิธีเชิงตัวเลขที่พัฒนาขึ้นถูกนำมาใช้ในการศึกษาอิทธิพลในระดับนาโนที่มีต่อรอยแตกร้าวขนาดนาโน ตัวอย่างที่นำเสนอแสดงให้เห็นถึงความสามารถและประสิทธิภาพเชิงคำนวณของระเบียบวิธีที่พัฒนาขึ้น นอกจากนี้ผลที่ได้จากการศึกษาอิทธิพลของตัวแปรต่างๆที่เกี่ยวข้องชี้ให้เห็นว่า หน่วยแรงที่ผิวบนผิวรอยแตกร้าวไม่เพียงแต่เพิ่มความแข็งแกร่งของวัสดุที่บริเวณใกล้ผิว แต่ยังส่งผลให้ผลเฉลยของปัญหาขึ้นอยู่กับขนาดของรอยแตกร้าวและหน่วยแรงที่บริเวณใกล้กับขอบของรอยแตกร้าวมีค่าลดลงอีกด้วย

ภาควิชา วิศวกรรมโยธา
สาขาวิชา วิศวกรรมโยธา
ปีการศึกษา 2556

ลายมือชื่อนิสิต .....
ลายมือชื่อ อ.ที่ปรึกษาวิทยานิพนธ์หลัก .....
ลายมือชื่อ อ.ที่ปรึกษาวิทยานิพนธ์ร่วม .....
ลายมือชื่อ อ.ที่ปรึกษาวิทยานิพนธ์ร่วม .....

5371844721 : MAJOR CIVIL ENGINEERING
KEYWORDS: FEM-SGBEM COUPLING / GURTIN-MURDOCH MODEL / NANO-CRACKS / SIZE DEPENDENCY / SURFACE STRESSES

BINH THAI NGUYEN: ANALYSIS OF CRACKS IN THREE-DIMENSIONAL LINEAR ELASTIC MEDIA WITH CONSIDERATION OF SURFACE STRESS EFFECTS. ADVISOR: ASSOC. PROF. JAROON RUNGAMORNRAT, Ph.D., CO-ADVISOR: PROF. TEERAPONG SENJUNTICHAI, Ph.D., ASSOC. PROF. ANIL C. WIJEYEWICKREMA, Ph.D., 89 pp.

An efficient numerical procedure for modeling planar cracks in three dimensional, linear elastic, infinite medium which accounts for the influence of surface stresses is presented in this dissertation. The concept of surface stresses, which has been widely employed in the investigation of nano-scale problems, is adopted to derive a suitable mathematical model capable of simulating nano-sized cracks. An infinitesimally thin layer of material on the crack surface is modeled by a zero-thickness surface perfectly bonded to the bulk material, with its behavior governed by the Gurtin-Murdoch constitutive relation. In the formulation, the classical theory of isotropic linear elasticity is utilized to establish the governing equation of the bulk material in terms of singularity-reduced boundary integral equations for the displacement and traction on the crack surface. For the zero-thickness surface, the final governing equation incorporating the surface stress effect is obtained in a weak form following the standard weighted residual technique. The fully coupled system of equations is then solved by the FEM-SGBEM coupling numerical procedure. Due to the weakly singular nature of all involved boundary integral equations, standard continuous interpolation functions can be employed everywhere in the approximation of crack-face data and only special quadrature for evaluating nearly and weakly singular integrals is required. Once the implemented numerical scheme is validated with available benchmark solutions, it is applied to investigate the nano-scale influence on nano-sized cracks. Several examples are presented to demonstrate the capability and robustness of the method. Results from an extensive parametric study reveal that, the presence of surface stresses not only increases the near-surface material stiffness but also introduces size dependent behavior of solutions and the reduction of stresses in the region ahead of the crack front.

Department:	Civil Engineering	Student's Signature	.....
Field of Study:	Civil Engineering	Advisor's Signature	.....
Academic Year:	2013	Co-Advisor's Signature	.....
		Co-Advisor's Signature	.....

ACKNOWLEDGEMENTS

First and foremost I offer my sincerest gratitude to my advisor, Associate Professor Dr. Jaroon Rungamornrat and co-advisor, Professor Dr. Teerapong Senjuntichai, whose encouragement, guidance and support from the initial to the final level enabled me to develop an understanding of the subject, continuous and unconditional guidance and support at each step of the study. I also wish to express my appreciation and gratitude to my co-advisor, Associate Professor Dr. Anil C. Wijeyewickrema at Tokyo Institute of Technology (TIT), Japan, for his kindness and invaluable advice on the research work and very warm welcome during the visits at TIT from October 2012 to May 2013. This dissertation would not have been a real fulfillment without the backing and cooperation of these people who have supported me throughout my thesis with their patience and knowledge.

I would like to express my sincere gratitude to ASEAN University Network – Southeast Asia Engineering Education Development Network Project (AUN/SEED-Net) for giving me the opportunity to pursue a Doctoral's Degree in Civil Engineering in the field of Structure Engineering. I also thank the International School of Engineering (ISE) at Chulalongkorn University for their supporting programs. I express my gratitude to Chulalongkorn University for providing a wonderful educational environment for studying.

My sincere thanks to all committee members, namely, Professor Dr. Thaksin Thepchatri, Associate Professor Dr. Akhrawat Lenwari, Assistant Professor Dr. Watanachai Smittakorn and Assistant Professor Dr. Arnon Wongkaew for their helpful suggestions and comments.

I would like to extend my thanks to all my colleagues and friend who has helped directly and indirectly in the preparation of this thesis. Finally, I would like to thank my parents and my sisters, for their endless love and efforts that encouraged me to realize my goals.

CONTENTS

Page

Page

LIST OF ABBREVIATIONS

a	crack radius, the semi-major axis;
b	the semi-minor axis;
$D_t(\cdot)$	surface operator;
$i,\ j$	Latin subscripts denote field quantities associated with the bulk take the values 1, 2, 3;
$n_i^+,\ n_i^-$	unit normal vector in the *i*-direction of upper and lower crack surface, respectively;
N	number of nodal points;
r	radial coordinate;
S_c^+	upper crack surface;
S_c^-	lower crack surface;
$S_c \equiv S_c^+$	considered crack surface;
$\mathbf{t}^{0+},\ \mathbf{t}^{0-}$	applied traction on upper and lower crack surface, respectively;
$\mathbf{t}^{+b},\ \mathbf{t}^{-b}$	unknown traction apply on the bulk exerted directly by the layers S_c^+ and S_c^-, respectively;
$\mathbf{t}^{+s},\ \mathbf{t}^{-s}$	unknown traction on the layers S_c^+ and S_c^-, respectively, obtained from applied traction with consideration surface stress effects;
$T^{\Sigma}_{3(q-1)+i}$	nodal degrees of freedom associated with the sum of the traction across the crack surfaces;
$\mathbf{T}^{\Sigma}$	vector of nodal quantities of the sum of the traction;
u_i	displacement components;
u_α^s	displacement components within the surface;
$U^{\Sigma}_{3(q-1)+i}$	nodal degrees of freedom associated with the sum of the displacement across the crack surfaces;
$U^{\Delta}_{3(q-1)+i}$	nodal degrees of freedom associated with the jump of the displacement across the crack surfaces;
$\mathbf{U}^{\Sigma}$	vector of nodal quantities of the sum of the displacement;

$\mathbf{U}^{\Delta}$	vector of nodal quantities of the jump of the displacement;
x_i	coordinate in the *i*-direction;
α, β	Greek subscripts denote field quantities associated with the surface take the values 1 and 2;
δ_{ij}	Kronecker delta;
ε_{irt}	standard alternating symbol;
ε_{ij}	Strain components;
$\varepsilon^{s}_{\alpha\beta}$	strain components within the surface;
θ	angular coordinate measured from the major-axis;
κ^{s}	surface material constant;
λ, μ	Lamé constants of the bulk material;
λ^{s}, μ^{s}	Lamé constants of the surface material;
ν	Poisson's ratio of the bulk material;
σ_0	applied normal traction;
σ_{ij}	stress components;
$\sigma^{s}_{\alpha\beta}$	stress components within the surface;
τ^{s}	residual surface stress under unstrained condition;
τ_0	applied tangential traction;
Λ	material characteristic length;
" Σ "	indicate the sum of quantities across the crack surface;
" Δ "	indicate the jump of quantities across the crack surface;
Φ_q	nodal basis functions at node *q*

LIST OF FIGURES

CHAPTER 1
INTRODUCTION

Nowadays, Nanotechnology has become one of the most interesting research area in various fields such as biology, chemistry, physics, medicine and engineering. Although nanotechnology deals only with extremely tiny objects with their length scale of few nanometers (where one nanometer is approximately about 50,000 times smaller than the average of a human hair), its applications tend to be substantial. For instance, nano-crystals are examples of a new invention at a nano-scale level. Metal nano-crystals can be incorporated into car bumpers, making the parts stronger, or into aluminum, making it more durable. Other applications of the metal nano-crystals can be found in the production of bearings, new types of sensors and components for computers and electronic hardware. The nano-crystals of various metals have been shown to be 100 percent, 200 percent and even as much as 300 percent harder than the same materials in the bulk form. Since the wear resistance is often dictated by the hardness of a metal, parts made from the nano-crystals might last significantly longer than conventional parts. In a field of medicine and healthcare, ones apply the nanotechnology to produce a nano-particulate-based synthetic bone. It is well known that the human bone is made of a calcium and phosphate composite called hydroxyapatite. By manipulating the calcium and phosphate at a molecular level, ones can create a patented material that is identical in structure and composition to the natural bone. This novel synthetic bone can be used in areas where the natural bone is damaged or removed, such as in the treatment of fractures and soft tissue injuries. For public utilities, nano-filters are capable of filtering the smallest particles of impurities. Such performance results directly from the nano-sized alumina fiber attracting and retaining sub-micron and nano-sized particles. This disposable filter retains 99.9999 percentages of viruses at water flow rates several hundred times greater than virus-rated ultra-porous membranes. This product can be exploited to sterilize drinking water, allowing inhabitants in third-world countries to access the clean water. In a field of materials, advanced researches of nano-science and nanotechnology such as nano-tubes, nano-wires, nano-composites and nano-films have grown rapidly and continuously. For examples, the carbon nano-tube which was discovered by Iijima in 1991 (Iijima 1991, Iijima and Ichihashi 1993) has been known as an ideal material that possesses excellent mechanical properties. For instance, Young's modulus, tensile strengths and failure strains of a defect-free single-walled carbon

nano-tube are up to 1 TPa, greater than 100 GPa and about 15-30%, respectively (Peng *et al.* 2008). All above excellent products come from advanced researches conducted at the nano-scale level. What we have seen is just the beginning of a revolution, caused by the ability to work on the same scale as nature. The nanotechnology is going to affect every aspect of our life. It will become the next industrial revolution (Ratner and Ratner 2003). The nanotechnology can be compared to a dawn of the digital revolution that totally changes the face of technology and human life. Unlike the internet, the nanotechnology can equally be applied to old things and processes. It is about creating entirely new materials, products, and systems as well as making existing products faster, stronger and better.

1.1 Statement of Research Problem

Due to enormous benefits that nanotechnology has brought out for the human, applications of nano-sized devices and nano-structured materials rapidly grow in various field. The physical modeling and corresponding comprehensive analysis to gain an insight into the complex behavior of nano-sized devices and nano-structured materials become crucial aspects in the optimal design of nano-scale products. Failure/damage analysis and assessment is one of the essential steps that must be properly considered to ensure their safety and integrity in the design procedure. In recent years, there are many researches conducted to investigate the nano-sized crack problems by the various methods. Some researchers attempted to use the experimental methods to deal with the nano-sized crack problems (Karimi *et al.* 2002, Sumomogi *et al.* 2002, Sundararajan and Bhushan 2002, Chen *et al.* 2008, Peng *et al.* 2008, Zhao and Xing 2008, Qin *et al.* 2009, Zhao and Xing 2010, Yan *et al.* 2011). While experimental approaches yield results reflecting the real responses or behaviors, they are highly dependent on experimental settings and, generally, expensive due to requiring high precision testing devices and procedures. Other researchers used the mathematical modeling and simulations based on the discrete atomic-scale model to handle the nano-sized crack problems (Buehler *et al.* 2003, Zhang *et al.* 2005, Buehler and Gao 2006, Rafii-Tabar *et al.* 2006, Pugno *et al.* 2008, Huang *et al.* 2009, Masuda-Jindo *et al.* 2009, Phan and Tippur 2009, Adnan and Sun 2010). Those proposed models have been verified to yield accurate prediction of responses of interest due to their effectiveness in detailing of bonds or atoms; however, such simulations require enormous computational effort and resources to treat billions of atoms at a Nano scale. This therefore renders the discrete atomic-scale models impractical in various

applications. Hence, a classical approach based on the stress analysis of a body containing pre-existing defects or cracks becomes an attractive alternative due to their advantages of saving computational resources. Unlike macro-structures, in the case of nano-sized objects (e.g., thin films, quantum dots, nano-wires, nano-tubes and nano-composites), the surface to volume ratio is much higher and, as a direct consequence, the surface free energy often plays a crucial role in the mechanical behavior (Yakobson 2003). Therefore, the classical theory of continuum-based mechanics commonly used in the modeling of macroscopic bodies cannot be directly applied to accurately treat the problem of nano-sized cracks. While conventional linear elastic fracture mechanics has been well established and employed in the modeling of cracks in linear elastic media, an enhancement of the classical model to incorporate the nano-scale influence is essentially required. On the basis of an extensive literature survey, work towards using continuum-based theories to model defects/fractures at the nano-scale level has been very limited. Most of them are restricted to situations where cracks can be treated either within the context of two-dimensional boundary value problems (Fu *et al.* 2008, Wang *et al.* 2008, Fang *et al.* 2009, Fu *et al.* 2010, Kim *et al.* 2010, Kim *et al.* 2011, Kim *et al.* 2011, Nan and Wang 2012, Kim *et al.* 2013, Nan and Wang 2013) or within the context of relatively simple three-dimensional problems (Intarit *et al.* 2012, Intarit 2013). It is remarked, however, that bodies or components involved in the real practices are, in general, relatively complex in terms of geometries, loading conditions, and influences to be treated (e.g., surface free energy). Existing simplified mathematical models are therefore of limited capabilities and insufficient to be used in the prediction of responses of those practical cases. This, as a result, necessitates the development of a fully three-dimensional models supplemented by efficient and powerful numerical procedures.

1.2 Research Objectives

The primary objectives of the present research is to:

(i) develop a physically suitable mathematical model based on the continuum theory capable of modeling nano-sized cracks,

(ii) develop an efficient and accurate numerical procedure to determine mechanical field quantities and essential fracture information such as crack-opening displacements and stress in the vicinity of the crack front of nano-sized cracks and

(iii) investigate the size-dependent behavior of nano-sized cracks.

1.3 Research Scope

This research is conducted within the following context: (i) the body containing cracks is a three-dimensional, homogeneous, isotropic elastic infinite medium; (ii) the medium is free of the body force and remote loadings; (iii) crack surfaces are planar and are subjected to general surface tractions; and (iv) only Gurtin-Murdoch surface elasticity model is utilized to treat the surface stress effects.

1.4 Research Methodology

This dissertation concerns the development of a computationally efficient numerical technique capable of modeling planar cracks embedded in three-dimensional isotropic, linear elastic media including the influence of surface stresses. To be capable of capturing the surface free energy effect, a model that properly takes into account the surface free energy is utilized. The most widely used continuum-based model which incorporates the surface free energy effects is that using Gurtin-Murdoch surface elasticity theory. Gurtin and Murdoch (1975, 1978), and Gurtin *et al.* (1998) proposed a mathematical framework to study the mechanical behavior of material surfaces through a continuum-based model which includes surface stresses. This well recognized model is chosen in the present investigation to explore the nano-scale influence. A numerical procedure based primarily on the coupling of a standard finite element method (FEM) and a weakly singular, symmetric Galerkin boundary element method (SGBEM) is employed. The former technique is utilized to efficiently handle the governing equations of the surface whereas the latter is employed to discretize the governing equations of the bulk material. Extensive numerical simulations are conducted and the results are compared with available benchmark solutions to verify both the formulation and numerical implementations.

Above methodology can further be summarized in details as follows:

(i) A cracked body is first decomposed into two parts: a bulk and a surface with zero thickness perfectly bonded to the crack surface of the bulk.

(ii) The behavior of the bulk is modeled by a classical theory of linear elasticity. The governing equations are established in terms of weakly

singular boundary integral equations following the work of Rungamornrat and Mear (2008a).

(iii) The behavior of the surface is modeled by a full version of Gurtin-Murdoch surface elasticity model. A weak-form statement is established using standard weight residual approach.

(iv) The weak-form equation of the surface part is discretized into a set of linear algebraic equations using standard finite element procedure.

(v) A set of weakly singular integral equations are discretized into a set of linear algebraic equations using weakly singular SGBEM similar to that employed by Rungamornrat and Mear (2008b).

(vi) Continuity conditions between the surface part and the bulk material are utilized to obtain a fully coupled system of linear algebraic equations.

(vii) A final system of linear equations is solved by a selected linear solver.

(viii) All field quantities within the bulk material can be obtained from a set of boundary integral relations appearing in the work of Rungamornrat and Mear (2008a).

(ix) Extensive numerical experiments are conducted and results are compared with available Benchmark solutions to validate the proposed numerical technique.

(x) Extensive parametric study is performed to explore the nano-scale influence on responses of cracked media.

1.5 Research Significance

Expected outcomes from the proposed research should enhance or strengthen the capability in the modeling of nano-sized crack problems using an alternative, computationally cheap continuum-based model along with the proper treatment of surface stress effects via Gurtin-Murdoch surface elasticity model. The developed mathematical model and the implemented numerical procedure allow more practical planar nano-sized fracture problems to be investigated, e.g. cracks of arbitrary shapes under general loading conditions. Availability of a computational tool of such high capability should be very significant in the parametric study to investigate and gain an insight into various crucial responses of interest in the nano-scale level such as the size-dependent behavior of an elastic field and all other related quantities.

1.6 Outline of Dissertation

This dissertation is a reflection of the entire research process and findings, which is divided into the following chapters:

Chapter 1 introduces the applications and the benefits of nano technology that has brought to humans nowadays, states research problem, research objective, research scopes, research methodology, and research significance.

Chapter 2 presents an extensive literature review on the surface elasticity theory, the nano-sized crack problem and the Boundary Element Method and Coupling Finite Element Method and Boundary Element Method in solving the boundary value problem.

Chapter 3 clearly states the description of the boundary value problem considered in this study and briefly summarizes the formulation of the key governing equations for both the bulk material and the zero-thickness layer on the crack surface. The fully coupled system of governing equations resulting from the enforcement of interfacial conditions is also presented at the end of the chapter.

Chapter 4 briefly discusses all numerical treatments including the discretization, element shape functions utilized in the approximation of primary unknowns and numerical integration. In general, standard procedures for the weakly singular SGBEM and those for the standard finite element method to form the discretized system of linear algebraic equations are summarized.

In chapter 5, numerical results for a penny-shaped crack embedded in an unbounded domain under mode-I loading conditions and with consideration of the surface stress effects are reported and compared with existing benchmark solution to verify the formulation and numerical implementation of the proposed technique. Then, various examples of crack problems such as a penny-shaped crack under mixed-mode loading, an elliptical crack under mode-I and mixed-mode loading conditions, and multiple cracks embedded in an unbounded domain are considered to demonstrate the capability and robustness of the proposed FEM-SGBEM numerical technique. The influence of surface stresses on the elastic field and the size-dependent behavior of nano-sized cracks are also reported and discussed.

Chapter 6 briefly summarizes research findings, conclusion and remarks, and possible extensions of this research.

CHAPTER 2
LITERATURE REVIEW

This chapter provides a summary of background and recent advances in the area relevant to the present study. It begins with the review of the surface elasticity theory and the Gurtin-Murdoch surface elasticity model. Then, previous studies concerning the investigations of nano-sized crack problems by various approaches such as experimental methods, discrete atomic-scale models and approaches based on the continuum-based theories are summarized. Review of computational techniques relevant to the current work such as the boundary element method and the coupling of standard finite element techniques and boundary element methods is presented in the last section of this chapter.

2.1 Background and Review of Surface Elasticity Model

In general, to investigate the nano-scale problems, either experimental methods (by using a scanning force microscope (SFM), a scanning laser microscope (SLM), an atomic force microscopy, electron microscopy, etc.) or mathematical modeling and simulations by using quantum mechanics can be employed. However, both methods costly or computationally expensive due to the requirement of high precision testing devices and procedures in the experiments and enormous computational effort and resources to deal with billions of atoms at a nano scale in the modeling. Therefore, an alternative computationally cheap continuum-based model has become an attractive choice to treat nano-scale problems. To be agreed with results obtained from both experiments and atomistic calculations, influences appearing or dominating in the nano-scale level must be suitably incorporated in the classical continuum-based model. Atomistic simulations pointed out that atoms near the free surface of solids behave differently from their bulk. In this sense, the whole body is not completely homogeneous, but when its size is comparable to the scale of micrometers or larger, a surface free energy effect can be neglected due to its insignificant influence on overall properties. Unlike macro-structures, in the case of nano-sized objects (e.g., thin films, quantum dots, nano-wires, nano-tubes and nano-composites) their surface-to-volume-ratio is much higher and, as a direct consequence, the influence of the surface free energy often becomes prominent.

The concepts of surface free energy effect and surface stresses were first formulated by Gibbs (1906). Gibbs (1906) first introduced the concept of surface phenomena and a quantity γ that represents the excess free energy per unit area owing to the existence of such free surface. He was the first person who demonstrated that for solid-solid interfaces, there is a fundamental parameter called a surface stress, which critically affects the behavior of surfaces. It means that to deform such a solid, excessive work is needed to stretch the surface in addition to straining the bulk. Extensive historical review on the surface free energy effect and the Gibbsian formulation of the thermodynamics of surfaces can be found in various researches on surface and interface stresses (e.g., Shuttleworth 1950, Cammarata 1994, Cammarata 1997, Fischer *et al.* 2008). In particular, Cammarata (1994) gave an excellent explanation of the concept of the surface stress and showed that the difference between the surface stresses and the surface free energy γ is equal to the change in the surface free energy per unit change in the elastic strain of the surface. It should be noted that γ is simply a scalar quantity whereas the surface stresses are a second order tensor in the tangent plane of the surface with the strain normal to the surface being excluded. Besides, Nix and Gao (1998) used a microscopic model to show that an interface stress gives a work effect associated with the elastic straining of the interface and this quantity causes the bending of a substrate. The surface energy γ has usually been accepted as an excess energy term since a surface can be interpreted as a layer to which certain energy is attached (Fischer *et al.* 2008). The reduced coordination of atoms in a surface layer versus atoms within the bulk induces a corresponding redistribution of electronic charge, and the altered binding situation in the surface is the modified layer spacing (interlayer separation), which deviates from the bulk value (Sander 2003). As a result, in general, the energy at a free surface is different from that of the atoms in the bulk (Dingreville *et al.* 2005). The ratio of surface free energy γ (J/m^2) and Young's modulus E(J/m^3), γ /E, is an inevitable parameter of materials (Yakobson 2003). For conventional metallic materials, the ratio is normally less than one Angstrom. For some soft solids, such as polymer gels and biological materials, however, the surface energy (or surface stress) is a little less than that of a metal, but the elastic modulus can be nearly 7-8 orders smaller than that of conventional solids. Therefore, the corresponding intrinsic length scale of soft solids is much larger, implying that the surface energy can play an important role on the properties of the materials, thus their properties become size-dependent (He and Lim 2006). In past decades, several researchers have attempted to incorporate the effects of surface stresses into a classical continuum-based model to be capable of predicting

the behavior of soft materials or to obtain correct responses for nano-scale bodies. Within the context of nano-sized crack problems, Gao and Ji (2003) investigated fractures in nano-materials by using a virtual-internal-bond (VIB) method. Hasheminejad *et al.* (2011) studied the flexural vibrations of cracked micro- and nano-beams with consideration of surface effects by using the cracked-beam model, which is set up by dividing a classical cracked beam element into two segments connected by a rotational spring located at the cracked section.

Nevertheless, the most popular continuum-based models with consideration of surface energy effects are those using Gurtin-Murdoch surface elasticity theory. Gurtin and Murdoch (1975), Gurtin and Murdoch (1978) and Gurtin *et al.* (1998) proposed a mathematical framework to study the mechanical behavior of material surfaces through the continuum-based model with the surface stresses. An elastic surface is assumed to be very thin and modeled as a mathematical layer of zero thickness perfectly bonded to the bulk without slipping. In addition, such idealized surface has different elastic moduli from those of the bulk. During the last ten years, Gurtin-Murdoch model has been widely used to investigate various size-dependent, nano-scale problems. For instance, Cammarata (1994), He *et al.* (2004), Dingreville *et al.* (2005), Huang (2008), Wang *et al.* (2008), Song *et al.* (2011) employed Gurtin-Murdoch model to clearly elucidate the size-dependent elastic properties of nano-structured elements such as beams, plates, wires, and films. Results of Dingreville *et al.* (2005) and Wang *et al.* (2008) calculated from Gurtin-Murdoch model agree reasonably well with direct atomistic simulations of Miller and Shenoy (2000) and Shenoy (2002). Furthermore, Cammarata (1997), Sharma *et al.* (2003), Sharma and Ganti (2004), Duan *et al.* (2005), Wang and Wang (2006), Tian and Rajapakse (2006), (2007), Ou *et al.* (2008), Zhao and Rajapakse (2009) applied the Gurtin-Murdoch surface elasticity model to point out the significance of the surface effects and conduct analytical solutions for nano-inhomogeneities problems. Fang and Liu (2006), Liu and Fang (2007), Mogilevskaya *et al.* (2008), Jammes *et al.* (2009), (Fang *et al.* 2009) also investigated interactions of multiple inhomogeneities problems at nano-scale by using Gurtin-Murdoch surface elasticity model.

2.2 Review of Nano-Sized Crack Problems

Research focusing on the investigation of nano-sized defects and fractures has become of central interest in the past two decades. Basic approaches proposed in those investigations can be categorized into two groups, namely experimental

methods and theoretical simulations. Some of previous studies in the first group can be briefly summarized as follows. Sumomogi *et al.* (2002) investigated both subsurface and surface cracks of single-crystal silicon by using a scanning force microscope (SFM) and a scanning laser microscope (SLM). Sundararajan and Bhushan (2002) evaluated the elastic modulus and bending strength and estimated the fracture toughness of nanometer-scale fixed-end beam specimens made of single-crystal silicon and SiO_2 by using a quasi-static bending test technique that was developed by using an atomic force microscope. Karimi *et al.* (2002) combined a depth sensing nano-indentation and a nano-scratch testing along with the atomic force microscopy and electron microscopy observations to study mechanical properties and fracture behavior of a number of TiAlN(Si, C) hard thin films. Chen *et al.* (2008) carried out an experiment of the composite to examine the local mechanical and fracture behavior of an EPON 862 based-epoxy with 12 nm (primary) and 100 nm (secondary) fumed silica particles by using the atomic force microscopy/digital image correlation (AFM/DIC) method. Peng *et al.* (2008) conducted an experiment by using an in-situ transmission electron microscopy (TEM) method. They employed a MEMS material testing system that allows accurate measurement of both load and displacement along with the TEM imaging to measure a single shell failure for multiwalled carbon nano-tubes that display the fracture strengths of about 100 GPa and also showed that fracture strains are very close to theoretical predictions. Zhao and Xing (2008), (2010) experimentally investigated a micro-crack in silicon by using high-resolution transmission electron microscopy (HRTEM) and a combination of geometric phase analysis (GPA), the numerical moiré method (NM) and the transmission electron microscopy (TEM). Qin *et al.* (2009) quantitatively investigated the effect of the density of nano-scale twin bundles on the tensile strength and fracture toughness. In their study, the fracture surface characteristics were elucidated by using scanning electron microscopy (SEM) and focused ion beam (FIB) microscopy analysis. The fracture toughness was measured by a conventional three-point bending test based on ASTM-E399. Most recently, Yan *et al.* (2011) experimentally investigated crack initiation and propagation along the Cu/Si interface in multilayered films (Si/Cu/SiN) with different thicknesses of the Cu layer (20 and 200 nm) by using a nano-cantilever and millimeter-sized four-point bending specimens. Those experiments demonstrated that the elastic modulus, bending strength, and fracture toughness were size-dependent at the nano-scale. Values of mechanical properties had a tendency higher compared with those obtained from experiments of macro-scale structures. The experimental approaches offer results reflecting the real responses or behaviors, they are, however, highly dependent on

experimental settings and, generally, expensive due to the requirement of high precision testing devices and procedures.

Another alternative is based on the mathematical modeling and simulations. In this group, a set of governing physics and assumptions is chosen to construct a set of mathematical equations governing representative quantities of interest and a solution methodology is developed to obtain such representative solutions for describing the real behavior. The discrepancy between the real responses and the representative solutions depends primarily on the choice of governing physics and assumptions and the accuracy of the solution strategy. Based on a careful literature review, most of existing studies employed two different types of mathematical models, one employing discrete-based models and the other utilizing modified continuum-based models.

Within the context of modeling nano-sized cracks, several studies based on the discrete atomic-scale model have been recognized. For instance, Buehler *et al.* (2003), Zhang *et al.* (2005), Buehler and Gao (2006), Rafii-Tabar *et al.* (2006), Huang *et al.* (2009), Masuda-Jindo *et al.* (2009), Adnan and Sun (2010) and Sakib and Adnan (2012) investigated the crack by using molecular dynamics (MD) atomistic simulations. Phan and Tippur (2009) presented a numerical method to evaluate the quantized fracture mechanics (QFM) stress intensity factors (SIFs). Pugno *et al.* (2008) combined quantized fracture mechanics and molecular dynamics atomistic simulations to study atomistic fractures. While those proposed models have been verified to yield accurate prediction of responses of interest due to their effectiveness in detailing of bonds or atoms, such simulations require enormous computational effort and resources to treat billions of atoms at a nano-scale. This therefore renders the discrete atomic-scale models impractical in various applications.

Consequently, a group of approaches based upon continuum-based theories is considered attractive since it can substantially reduce both the computational cost and complexity of the governing physics. Work towards applying the surface elasticity model to simulate the nano-scale influence of nano-sized fracture problems has become one of an interesting research area. Based upon the investigation of an elliptical void, Wu (1999) argued that presence of the surface stresses can effectively reduce an applied stress-intensity factor to a lower effective stress-intensity factor. Wu and Wang (2000), (2001) proposed the method using a pair of point forces, one at each crack tip, a uniformly distributed compressive load on the convex side of the crack, and a uniformly distributed tensile load on the concave side to study the influence of

surface stress on two-dimensional crack problems and pointed out that the singularity of the crack-tip stress fields becomes $1/r$ instead of being $1/\sqrt{r}$. Wang *et al.* (2007) explored the dependent relationship of crack-tip stresses on surface elastic parameters for both mode-I (opening mode) and mode-III (tearing mode) cracks based on the Gurtin Murdoch surface elasticity theory along with a local asymptotic approach. They found in their study, that the stress intensities in the vicinity of the crack tip are significantly affected by the surface energy when the curvature radius of a blunt crack front decreases to nanometers. Fu *et al.* (2008), (2010) incorporated the effect of surface elasticity into the finite element analysis (via ANSYS® and ABAQUS®) to study the influence of surface stresses on the mode-I (opening mode) and mode-II (sliding mode) crack tip fields. They found that when the curvature radius of the crack root decreases to micro-/nano-meters, the surface elasticity exhibits significant influence on stresses near the crack tip. Fang *et al.* (2009) investigated the influence of surface stresses on the dislocation emission from an elliptically blunt crack under mode-I and mode-II loading conditions and reported that the impact of the surface stresses on the critical stress intensity factors for dislocation emission becomes remarkable when the size of the blunted crack is very small, typically of a nanometer scale. However, their results for stresses are valid only in the vicinity ahead the crack-tip of the blunt crack.

Use of a sharp crack-tip model has also been commonly employed in the modeling of nano-sized cracks. The fundamental problem of mode-I crack was elaborated by Oh *et al.* (2005) based upon an extension of continuum mechanics by incorporating effects of the nano-scale through the long-range intermolecular force obtained from atomistic simulations. They concluded that the fracture tip should be sharp rather than blunt and, unlike the classical case, there is no stress singularity at the fracture tip when considered at a nano-scale level. It is also important to remark that the surface energy is generally nonzero and a function of position on the fracture surface. Sendova and Walton (2010) examined mode-I crack in an infinite elastic medium using various models of surface energy effects (e.g., a model of constant surface tension and a model of curvature dependent surface tension). In their study, they proposed that the stress singularity at the crack tip was reduced to the logarithmic singularity in the case of the constant surface tension, whereas the finite stress at the crack tip was observed for the case of the curvature dependent surface tension. Kim *et al.* (2010) first examined a mode-III crack problem (i.e., anti-plane shear deformations of a linearly elastic solid) subjected to non-uniform surface tractions. Later, Kim *et al.* (2011) studied the plane deformations of a linearly elastic solid containing a crack under either mode-I or mode-II loading conditions. Kim *et al.* (2011) considered the

contribution of the surface elasticity to the anti-plane deformations of a linearly elastic bi-material containing mode-III interface crack. For above three studies, the continuum-based surface/interface model of Gurtin and Murdoch was employed in the formulation of the boundary value problem and complex variable techniques were applied in the solution procedure. They pointed out that the surface stresses result in elastic responses and corresponding stress fields being size-dependent and also argued that, in contrast to classical results from linear elastic fracture mechanics, their model yielded the finite stresses at the sharp crack-tips. Recently, Kim *et al.* (2013) examined the role of surface stresses on the singularity behavior of near-tip stress field. They showed that the necessary and sufficient conditions for bounded stresses at the crack tip cannot be satisfied with the first-order (curvature-independent) theory of surface effects, which leads, at most, to the reduction of the classical strong square-root singularity to the weaker logarithmic singularity. This finding agrees with the previous study of Sendova and Walton (2010) in the case of the constant surface tension. Nan and Wang (2012) considered the effect of the residual surface stress on the crack surface and obtained solutions of the crack opening displacement (COD) and the mode-I stress intensity factor (K_I). Their obtained results demonstrated that the influence of the surface stresses on the crack deformation and crack-tip field is prominent at the nano-scale. Moreover, the COD and K_I are influenced by the residual surface stress not only on the surface near the crack-tip region but also on the entire crack-face. Most recently, Nan and Wang (2013) investigated a problem of a nano-scale crack in piezoelectric nano-materials by considering the effect of the residual surface stress on the crack surface. They pointed out that the electromechanical coupling fracture behavior of the piezoelectric materials is influenced by the residual surface stress on the entire crack surface.

On the basis of an extensive literature survey, it can be said that work related to the modeling of defects/cracks at nano-scale level has been very limited. Most of existing studies regarding to the analysis of nano-sized fractures, the corresponding boundary value problems were formulated within the context of two-dimensional settings and most of them were solved by using analytical techniques such as complex variable techniques, complex potential method and Chebyshev polynomials technique. Due to limitations of both inherent simplified assumptions and solution techniques, complex but more practical loading conditions and fracture geometries cannot readily be treated in those existing works. Recently, Intarit *et al.* (2012) and Intarit (2013) analytically investigated a nano-sized crack in a three-dimensional elastic media under a mode-I loading conditions. Although a complete Gurtin-Murdoch

surface elasticity model was employed to model the effect of surface stresses, it was still limited to a crack of circular shape and axisymmetric loading conditions. However, bodies or components containing existing defects/flaws involved in practical applications are, in general, relatively complex in terms of geometries, loading conditions, and influences to be treated (e.g., surface free energy). The existing mathematical models are therefore of limited scope and insufficient for the prediction of responses in practical cases. This, as a result, necessitates the development of fully three-dimensional models, supplemented by efficient and powerful numerical procedures. This current gap of knowledge is to be fully investigated in the present study.

2.3 Review of BEM and FEM-BEM Coupling for Crack Problems

Numerical techniques based on boundary integral equations have been well-established and proven powerful for both two-dimensional and three-dimensional fracture analysis (e.g., Blandford *et al.* 1981, Cruse 1988, Gray *et al.* 1990, Sáez *et al.* 1997, Pan and Yuan 2000, Sutradhar and Paulino 2004). The techniques possess attractive characteristics, such as governing equations with spatially reduced dimensions and simplicity of treating remote boundaries and infinite bodies, rendering them computationally efficient and convenient for modeling crack problems. The weakly singular, symmetric Galerkin boundary element method (SGBEM), which is a principal numerical technique proposed to model the cracks in the present study, is a particular boundary integral equation method that has been continuously developed and widely adopted by various investigators in the past four decades. This special numerical technique has been widely and successfully employed to solve both linear elasticity and linear elastic fracture problems (Gu and Yew 1988, Xu and Ortiz 1993, Bonnet 1995, Li and Mear 1998, Li *et al.* 1998, Xu 1999, Frangi *et al.* 2002, Rungamornrat 2006, Rungamornrat and Mear 2008, Rungamornrat and Mear 2008, Rungamornrat and Senjuntichai 2009), since it possesses several important and desirable features. For instance, the governing integral equations contain only weakly singular kernels of $\mathcal{O}(1/r)$; the technique is applicable for modeling cracks with arbitrary configurations and under general loading conditions and for treating an infinite body efficiently; and the formulation is established in a symmetric weak-form such that it gives rise to a system of linear equations with a symmetric coefficient matrix. The first feature renders that all involved integrals exist in an ordinary sense and their validity requires only the continuity of the boundary data; i.e., in the numerical implementation, it is possible to

employ standard C^0 elements in the approximation of the primary unknowns and to apply existing quadrature schemes to numerically evaluate all involved integrals (e.g., Li and Mear 1998, Li *et al.* 1998, Rungamornrat and Mear 2008, Rungamornrat and Senjuntichai 2009). In addition, the last feature also allows the SGBEM to be conveniently coupled with the standard finite element procedure to enhance its computational efficiency and capability (e.g., Frangi and Novati 2003, Rungamornrat and Mear 2011). Extensive review of the weakly singular SGBEM can be found in Bonnet *et al.* (1998), in Rungamornrat and Mear (2008) and Rungamornrat and Senjuntichai (2009) for its application to three-dimensional fracture analysis, and in Rungamornrat and Mear (2011) for its coupling with the standard FEM.

While the SGBEM and FEM-SGBEM coupling have been well-established and extensively employed in the modeling of classical crack problems, their applications to performing stress analysis of defects/flaws at the nano-scale level has not been well-recognized in the literature. This motivates the present investigation with the primary objective to fill the existing gap of knowledge. The potential advantages of using the FEM-SGBEM coupling in the analysis of nano-cracks are as follows: the SGBEM can be used to efficiently treat an infinite bulk material containing cracks whereas the standard FEM is suitable for modeling the nano-scale influence on the crack surface. The positive features of both techniques should not only enhance both the accuracy and computational efficiency of the proposed technique but also allow fracture problems to be solved within the general context.

CHAPTER 3
GOVERNING EQUATIONS

This chapter begins with the clear problem description and assumptions essential for the formulation of the boundary value problem that is the main focus of the present study. All basic field equations and the development of governing equations for both the bulk material and the crack surface are then presented. Finally, the fully coupled system of weak-form equations governing the primary unknowns on the crack surface is derived.

3.1 Problem Description

Consider a three-dimensional, linearly elastic, infinite medium Ω containing an isolated, planar crack of arbitrary shape with a selected reference Cartesian coordinate system $\{O;\ x_1;\ x_2;\ x_3\}$, as shown schematically in Figure 3.1(a).

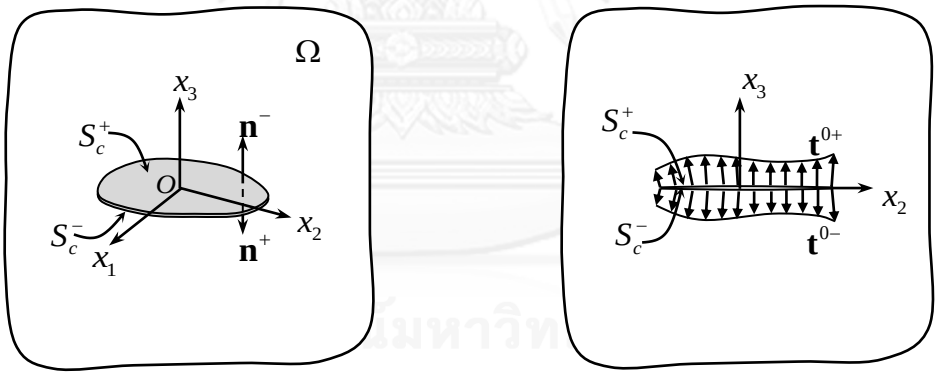

Figure 3.1: (a) Schematic of three-dimensional infinite elastic medium containing an isolated crack and (b) prescribed traction on crack surfaces.

The crack is represented by two geometrically identical surfaces, denoted by S_c^+ and S_c^- with the corresponding outward unit normal vectors $\mathbf{n}^+$ and $\mathbf{n}^-$, for convenience in further development, are oriented perpendicular to the x_3-axis. In the present study, the medium is assumed free of body forces and remote loading, but subjected to prescribed, self-equilibrated, normal tractions $\mathbf{t}^{0+}$ and $\mathbf{t}^{0-}$ on the crack surfaces S_c^+ and S_c^-, respectively (see Figure 3.1(b)). An infinitesimally thin layer on

each crack surface possesses a constant residual surface tension τ^s (under unstrained conditions) and the surface Lamé constants λ^s and μ^s, whereas the rest of the medium, termed the "*bulk material*", is made of a homogeneous, isotropic, linearly elastic material with shear modulus μ and Poisson's ratio ν.

A clear problem statement of the present study is to determine the complete elastic field including the displacements and stresses within the bulk material by taking the influence of surface stresses into account. Fracture-related information such as the relative crack-face displacement and the local stress field in the vicinity of the crack front is also of primary interest.

3.2 Domain Decomposition

In the formulation of the boundary value problem, the medium is decomposed into three parts: the bulk material, the zero-thickness layer S_c^+ and the zero-thickness layer S_c^- as shown in Figure 3.2. The bulk material is simply the whole medium without the two infinitesimally thin layers on the crack surfaces. Since both layers have zero thickness, the geometry of the bulk material is therefore identical to that of the whole medium (i.e., it can also be completely described by the region Ω and the two crack surfaces S_c^+ and S_c^-).

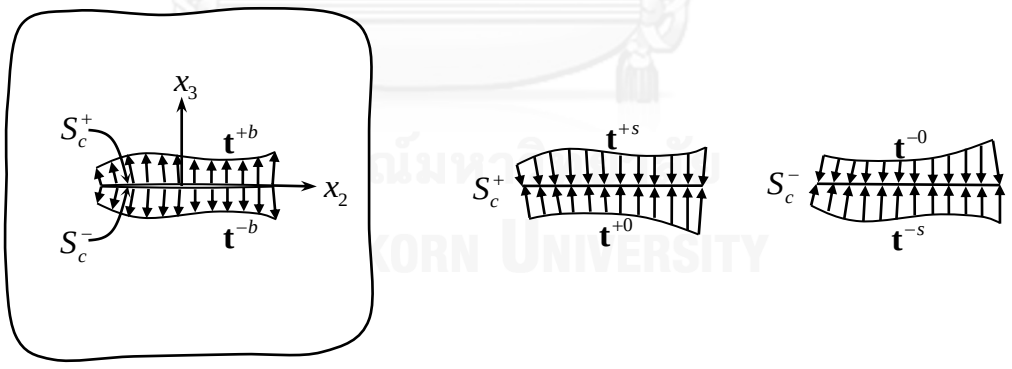

(a) (b) (c)

Figure 3.2: Schematics of (a) the bulk material, (b) the zero-thickness layer S_c^+ and (c) the zero-thickness layer S_c^-.

The key difference between the bulk material and the original medium is that the bulk material is homogeneous and the crack surfaces S_c^+ and S_c^- in the bulk material part are subjected to unknown tractions (exerted directly by the two layers)

$\mathbf{t}^{+b}$ and $\mathbf{t}^{-b}$, respectively. The layer S_c^+ is treated as a two-sided surface with one side subjected to the prescribed traction $\mathbf{t}^{+0}$ and the other side subjected to the traction $\mathbf{t}^{+s}$ exerted by the bulk material (Figure 3.2(b)). Similarly, the layer S_c^- is treated as a two-sided surface with one side subjected to the prescribed traction $\mathbf{t}^{-0}$ and the other side subjected to the traction $\mathbf{t}^{-s}$ exerted by the bulk material (Figure 3.2(c)). In what follows, Greek subscripts denote field quantities associated with the surface and take the values 1, 2 while the Latin subscripts take the values 1, 2, 3. It is remarked that, in the development to follow, it will suffice to make reference to the single crack surface $S_c \equiv S_c^+$.

3.3 Governing Equations of Bulk Material

Since the bulk material is made of homogeneous, isotropic, linear elastic material, its behavior is governed by the classical theory of linear elasticity. From results developed in the work of Rungamornrat and Mear (2008a) and Rungamornrat and Senjuntichai (2009), the displacement and stress components at any interior point $\mathbf{x}$, denoted respectively by $u_p(\mathbf{x})$ and $\sigma_{ij}(\mathbf{x})$, can be expressed in terms of the traction data $\mathbf{t}^{+b}$ and $\mathbf{t}^{-b}$ and the displacement data $\mathbf{u}^{+b}$ and $\mathbf{u}^{-b}$ on the crack surfaces S_c^+ and S_c^- as

$$\begin{aligned} u_p(\mathbf{x}) &= \int_{S_c} U_j^p(\boldsymbol{\xi}-\mathbf{x}) t_j^{b\Sigma}(\boldsymbol{\xi}) dS(\boldsymbol{\xi}) \\ &\quad + \int_{S_c} G_{mj}^p(\boldsymbol{\xi}-\mathbf{x}) D_m u_j^{b\Delta}(\boldsymbol{\xi}) dS(\boldsymbol{\xi}) - \int_{S_c} H_{ij}^p(\boldsymbol{\xi}-\mathbf{x}) n_i(\boldsymbol{\xi}) u_j^{b\Delta}(\boldsymbol{\xi}) dS(\boldsymbol{\xi}) \end{aligned} \tag{3.1}$$

$$\begin{aligned} \sigma_{ij}(\mathbf{x}) &= \int_{S_c} \varepsilon_{irt} C_{lk,r}^{tj}(\boldsymbol{\xi}-\mathbf{x}) D_l u_k^{b\Delta}(\boldsymbol{\xi}) dS(\boldsymbol{\xi}) \\ &\quad + \int_{S_c} \varepsilon_{irt} G_{tj,r}^p(\boldsymbol{\xi}-\mathbf{x}) t_p^{b\Sigma}(\boldsymbol{\xi}) dS(\boldsymbol{\xi}) - \int_{S_c} H_{ij}^p(\boldsymbol{\xi}-\mathbf{x}) t_p^{b\Sigma}(\boldsymbol{\xi}) dS(\boldsymbol{\xi}) \end{aligned} \tag{3.2}$$

where $D_t(\cdot) = \varepsilon_{tmj} n_m \partial(\cdot)/\partial \xi_j$ is a surface differential operator, $t_j^{b\Sigma} = t_j^{+b} + t_j^{-b}$, $u_j^{b\Delta} = u_j^{+b} - u_j^{-b}$, ε_{irt} is the standard alternating symbol, the kernels $\{U_j^p, G_{mj}^p, C_{mj}^{tk}, H_{ij}^p\}$ for isotropic elastic materials are given explicitly by

$$U_j^p(\boldsymbol{\xi}-\mathbf{x}) = \frac{1}{16\pi(1-\nu)\mu r}\left[(3-4\nu)\delta_{pj} + \frac{(\xi_p - x_p)(\xi_j - x_j)}{r^2}\right] \tag{3.3}$$

$$G_{mj}^p(\boldsymbol{\xi}-\mathbf{x}) = \frac{1}{8\pi(1-\nu)r}\left[(1-2\nu)\varepsilon_{mpj} + \frac{(\xi_p - x_p)(\xi_a - x_a)}{r^2}\varepsilon_{ajm}\right] \tag{3.4}$$

$$C_{mj}^{tk}(\boldsymbol{\xi}-\mathbf{x})=\frac{\mu}{4\pi(1-\nu)r}\left[(1-\nu)\delta_{tk}\delta_{mj}+2\nu\delta_{km}\delta_{tj}-\delta_{kj}\delta_{tm}-\frac{(\xi_k-x_k)(\xi_j-x_j)}{r^2}\delta_{tm}\right] \tag{3.5}$$

$$H_{ij}^{p}(\boldsymbol{\xi}-\mathbf{x})=-\frac{(\xi_i-x_i)\delta_{jp}}{4\pi r^3} \tag{3.6}$$

with $r=\|\boldsymbol{\xi}-\mathbf{x}\|$ and ν,μ are Poisson's ratio and the shear modulus, respectively. The boundary integral relations (3.1) and (3.2) allow the displacement and stress at any interior point to be determined once the data $\mathbf{t}^{+b}$, $\mathbf{t}^{-b}$, $\mathbf{u}^{+b}$ and $\mathbf{u}^{-b}$ are known. To establish the boundary integral equations governing the unknown data $\mathbf{t}^{+b}$, $\mathbf{t}^{-b}$, $\mathbf{u}^{+b}$ and $\mathbf{u}^{-b}$, the integral relations (3.1) and (3.2) are utilized along with the limiting process to any point on the crack surface and the standard integration by parts procedure using Stokes' theorem to obtain the weak-form equations. The final weak-form, boundary integral equations are given by (see details of the development in Rungamornrat and Mear (2008a) and Rungamornrat and Senjuntichai (2009))

$$\begin{aligned}\frac{1}{2}\int_{S_c}\tilde{t}_p^{\Sigma}(\mathbf{y})u_p^{b\Sigma}(\mathbf{y})dS(\mathbf{y})=&\int_{S_c}\tilde{t}_p^{\Sigma}(\mathbf{y})\int_{S_c}U_j^{p}(\boldsymbol{\xi}-\mathbf{y})t_j^{b\Sigma}(\boldsymbol{\xi})dS(\boldsymbol{\xi})dS(\mathbf{y})\\&+\int_{S_c}\tilde{t}_p^{\Sigma}(\mathbf{y})\int_{S_c}G_{mj}^{p}(\boldsymbol{\xi}-\mathbf{y})D_m u_j^{b\Delta}(\boldsymbol{\xi})dS(\boldsymbol{\xi})dS(\mathbf{y})\\&-\int_{S_c}\tilde{t}_p^{\Sigma}(\mathbf{y})\int_{S_c}H_{ij}^{p}(\boldsymbol{\xi}-\mathbf{y})n_i(\boldsymbol{\xi})u_j^{b\Delta}(\boldsymbol{\xi})dS(\boldsymbol{\xi})dS(\mathbf{y})\end{aligned} \tag{3.7}$$

$$\begin{aligned}-\frac{1}{2}\int_{S_c}\tilde{u}_k^{\Delta}(\mathbf{y})t_k^{b\Delta}(\mathbf{y})dS(\mathbf{y})=&\int_{S_c}D_t\tilde{u}_k^{\Delta}(\mathbf{y})\int_{S_c}C_{mj}^{tk}(\boldsymbol{\xi}-\mathbf{y})D_m u_j^{b\Delta}(\boldsymbol{\xi})dS(\boldsymbol{\xi})dS(\mathbf{y})\\&+\int_{S_c}D_t\tilde{u}_k^{\Delta}(\mathbf{y})\int_{S_c}G_{tk}^{j}(\boldsymbol{\xi}-\mathbf{y})t_j^{b\Sigma}(\boldsymbol{\xi})dS(\boldsymbol{\xi})dS(\mathbf{y})\\&+\int_{S_c}\tilde{u}_k^{\Delta}(\mathbf{y})\int_{S_c}H_{lk}^{j}(\boldsymbol{\xi}-\mathbf{y})n_l(\mathbf{y})t_j^{b\Sigma}(\boldsymbol{\xi})dS(\boldsymbol{\xi})dS(\mathbf{y})\end{aligned} \tag{3.8}$$

where $u_j^{b\Sigma}=u_j^{+b}+u_j^{-b}$, $t_j^{b\Delta}=t_j^{+b}-t_j^{-b}$, and $\{\tilde{t}_p^{\Sigma},\ \tilde{u}_k^{\Delta}\}$ are sufficiently smooth test functions. The pair of equations (3.7) and (3.8) has been well recognized as the weak-form boundary integral equations for the sum of the displacement $u_j^{b\Sigma}$ and the jump of the traction $t_j^{b\Delta}$ across the crack surface, respectively. It is worth noting that both integral equations contain only weakly singular kernels $\{U_j^{p},G_{mj}^{p},C_{mj}^{tk},H_{ij}^{p}n_j\}$ of $\mathcal{O}(1/r)$. This positive feature renders all involved double surface integrals to exist in an ordinary sense and their validity requires only C^0- boundary data.

3.4 Governing Equations of Two Layers

The two layers S_c^+ and S_c^- shown in Figures 3.2(b) and 3.2(c) are considered as infinitesimally thin membranes adhered perfectly to the bulk material. The behavior of these two layers is modeled by the full version of Gurtin-Murdoch surface elasticity theory. The equilibrium equations, the surface constitutive relations and the strain-displacement relationship of the layers S_c^+ and S_c^- are therefore given by (Gurtin and Murdoch, 1975; Gurtin and Murdoch, 1978; Gurtin *et al.*, 1998)

$$\sigma^s_{i\beta,\beta} + t^s_i + t^o_i = 0 \tag{3.9}$$

$$\sigma^s_{\alpha\beta} = \tau^s\delta_{\alpha\beta} + \left(\lambda^s + \tau^s\right)\varepsilon^s_{\gamma\gamma}\delta_{\alpha\beta} + 2\left(\mu^s - \tau^s\right)\varepsilon^s_{\alpha\beta} + \tau^s u^s_{\alpha,\beta} \quad , \quad \sigma^s_{3\beta} = \tau^s u^s_{3,\beta} \tag{3.10}$$

$$\varepsilon^s_{\alpha\beta} = \tfrac{1}{2}\left(u^s_{\alpha,\beta} + u^s_{\beta,\alpha}\right) \tag{3.11}$$

where $\sigma^s_{i\beta}$, $\varepsilon^s_{\alpha\beta}$, u^s_i represent stress, strain and displacement components within the layer. It is important to remark that, in this case, the full version of Gurtin-Murdoch surface elasticity theory including both the surface Lamé constants (or in-plane elastic constants) and the residual surface tension is considered. This model should suit the treatment of general loading conditions when both the normal and tangential tractions can be applied simultaneously on the crack surfaces.

To construct the weak-form equation, the equilibrium equation (3.9) is multiplied by a sufficiently smooth test function $\tilde{u}^s_i$ and the result is integrated over the entire crack surface to obtain

$$\int_{S_c} \tilde{u}^s_\alpha \sigma^s_{\alpha\beta,\beta} dS + \int_{S_c} \tilde{u}^s_3 \sigma^s_{3\beta,\beta} dS + \int_{S_c} \tilde{u}^s_i t^s_i dS + \int_{S_c} \tilde{u}^s_i t^0_i dS = 0 \tag{3.12}$$

By performing the integration by parts of the first term using the Gauss-divergence theorem, it leads to

$$\int_{S_c} \tilde{u}^s_{\alpha,\beta} \sigma^s_{\alpha\beta} dS + \int_{S_c} \tilde{u}^s_{3,\beta} \sigma^s_{3\beta} dS - \int_{S_c} \tilde{u}^s_i t^s_i dS = \int_{\partial S_c} \tilde{u}^s_\alpha \sigma^s_{\alpha\beta} n_\beta dS + \int_{\partial S_c} \tilde{u}^s_3 \sigma^s_{3\beta} n_\beta dS + \int_{S_c} \tilde{u}^s_i t^0_i dS \tag{3.13}$$

Substituting (3.10) into (3.13) finally yields

$$\lambda^s \int_{S_c} \tilde{u}^s_{\alpha,\alpha} u^s_{\gamma,\gamma} dS + \frac{\mu^s}{2} \int_{S_c} \left(\tilde{u}^s_{\alpha,\beta} + \tilde{u}^s_{\beta,\alpha}\right)\left(u^s_{\alpha,\beta} + u^s_{\beta,\alpha}\right) dS + \tau^s \int_{S_c} \tilde{u}^s_{3,\beta} u^s_{3,\beta} dS - \int_{S_c} \tilde{u}^s_i t^s_i dS =$$
$$\lambda^s \int_{\partial S_c} \tilde{u}^s_\alpha n_\alpha u^s_{\gamma,\gamma} d\Gamma + \frac{\mu^s}{2} \int_{\partial S_c} \left(\tilde{u}^s_\alpha n_\beta + \tilde{u}^s_\beta n_\alpha\right)\left(u^s_{\alpha,\beta} + u^s_{\beta,\alpha}\right) d\Gamma + \tau^s \int_{\partial S_c} \tilde{u}^s_3 u^s_{3,\beta} n_\beta d\Gamma + \int_{S_c} \tilde{u}^s_i t^0_i dS \tag{3.14}$$

Note that the weak-form equation (3.14) applies to both crack surfaces. In particular, the weak-form equations for the surface S_c^+ and surface S_c^- can be obtained explicitly by

$$\lambda^s \int_{S_c} \tilde{u}^{s+}_{\alpha,\alpha} u^{s+}_{\gamma,\gamma} dS + \frac{\mu^s}{2} \int_{S_c} \left(\tilde{u}^{s+}_{\alpha,\beta} + \tilde{u}^{s+}_{\beta,\alpha}\right)\left(u^{s+}_{\alpha,\beta} + u^{s+}_{\beta,\alpha}\right) dS + \tau^s \int_{S_c} \tilde{u}^{s+}_{3,\beta} u^{s+}_{3,\beta} dS - \int_{S_c} \tilde{u}^{s+}_i t^{s+}_i dS =$$
$$\lambda^s \int_{\partial S_c} \tilde{u}^{s+}_\alpha n_\alpha u^{s+}_{\gamma,\gamma} d\Gamma + \frac{\mu^s}{2} \int_{\partial S_c} \left(\tilde{u}^{s+}_\alpha n_\beta + \tilde{u}^{s+}_\beta n_\alpha\right)\left(u^{s+}_{\alpha,\beta} + u^{s+}_{\beta,\alpha}\right) d\Gamma + \tau^s \int_{\partial S_c} \tilde{u}^{s+}_3 u^{s+}_{3,\beta} n_\beta d\Gamma + \int_{S_c} \tilde{u}^{s+}_i t^{0+}_i dS \tag{3.15}$$

$$\lambda^s \int_{S_c} \tilde{u}^{s-}_{\alpha,\alpha} u^{s-}_{\gamma,\gamma} dS + \frac{\mu^s}{2} \int_{S_c} \left(\tilde{u}^{s-}_{\alpha,\beta} + \tilde{u}^{s-}_{\beta,\alpha}\right)\left(u^{s-}_{\alpha,\beta} + u^{s-}_{\beta,\alpha}\right) dS + \tau^s \int_{S_c} \tilde{u}^{s-}_{3,\beta} u^{s-}_{3,\beta} dS - \int_{S_c} \tilde{u}^{s-}_i t^{s-}_i dS =$$
$$\lambda^s \int_{\partial S_c} \tilde{u}^{s-}_\alpha n_\alpha u^{s-}_{\gamma,\gamma} d\Gamma + \frac{\mu^s}{2} \int_{\partial S_c} \left(\tilde{u}^{s-}_\alpha n_\beta + \tilde{u}^{s-}_\beta n_\alpha\right)\left(u^{s-}_{\alpha,\beta} + u^{s-}_{\beta,\alpha}\right) d\Gamma + \tau^s \int_{\partial S_c} \tilde{u}^{s-}_3 u^{s-}_{3,\beta} n_\beta d\Gamma + \int_{S_c} \tilde{u}^{s-}_i t^{0-}_i dS \tag{3.16}$$

where superscripts "+" and "−" are added to differentiate quantities defined on each crack surface. Since the boundary integral equations governing the bulk material are derived in terms of the unknown sum and jump of quantities across the crack surface, it is natural to establish the weak-form equations governing the surface in terms of the same type of unknowns. This can be readily accomplished by forming two linear combinations of (3.15) and (3.16) as follows: (i) choosing $\tilde{u}_i^{s+} = \tilde{u}_i^{s-} \equiv \tilde{u}_i^{s\Sigma}$ and then adding (3.15) to (3.16) and (ii) choosing $\tilde{u}_i^{s+} = \tilde{u}_i^{s-} \equiv \tilde{u}_i^{s\Delta}$ and then subtracting (3.15) from (3.16). Such pair of equivalent weak-form equations is given by

$$\lambda^s \int_{S_c} \tilde{u}^{s\Sigma}_{\alpha,\alpha} u^{s\Sigma}_{\gamma,\gamma} dS + \frac{\mu^s}{2} \int_{S_c} \left(\tilde{u}^{s\Sigma}_{\alpha,\beta} + \tilde{u}^{s\Sigma}_{\beta,\alpha}\right)\left(u^{s\Sigma}_{\alpha,\beta} + u^{s\Sigma}_{\beta,\alpha}\right) dS + \tau^s \int_{S_c} \tilde{u}^{s\Sigma}_{3,\beta} u^{s\Sigma}_{3,\beta} dS - \int_{S_c} \tilde{u}^{s\Sigma}_i t^{s\Sigma}_i dS =$$
$$\lambda^s \int_{\partial S_c} \tilde{u}^{s\Sigma}_\alpha n_\alpha u^{s\Sigma}_{\gamma,\gamma} d\Gamma + \frac{\mu^s}{2} \int_{\partial S_c} \left(\tilde{u}^{s\Sigma}_\alpha n_\beta + \tilde{u}^{s\Sigma}_\beta n_\alpha\right)\left(u^{s\Sigma}_{\alpha,\beta} + u^{s\Sigma}_{\beta,\alpha}\right) d\Gamma + \tau^s \int_{\partial S_c} \tilde{u}^{s\Sigma}_3 u^{s\Sigma}_{3,\beta} n_\beta d\Gamma + \int_{S_c} \tilde{u}^{s\Sigma}_i t^{0\Sigma}_i dS \tag{3.17}$$

$$\lambda^s \int_{S_c} \tilde{u}^{s\Delta}_{\alpha,\alpha} u^{s\Delta}_{\gamma,\gamma} dS + \frac{\mu^s}{2} \int_{S_c} \left(\tilde{u}^{s\Delta}_{\alpha,\beta} + \tilde{u}^{s\Delta}_{\beta,\alpha}\right)\left(u^{s\Delta}_{\alpha,\beta} + u^{s\Delta}_{\beta,\alpha}\right) dS + \tau^s \int_{S_c} \tilde{u}^{s\Delta}_{3,\beta} u^{s\Delta}_{3,\beta} dS - \int_{S_c} \tilde{u}^{s\Delta}_i t^{s\Delta}_i dS =$$

$$\lambda^s \int_{\partial S_c} \tilde{u}^{s\Delta}_\alpha n_\alpha u^{s\Delta}_{\gamma,\gamma} d\Gamma + \frac{\mu^s}{2} \int_{\partial S_c} \left(\tilde{u}^{s\Delta}_\alpha n_\beta + \tilde{u}^{s\Delta}_\beta n_\alpha\right)\left(u^{s\Delta}_{\alpha,\beta} + u^{s\Delta}_{\beta,\alpha}\right) d\Gamma + \tau^s \int_{\partial S_c} \tilde{u}^{s\Delta}_3 u^{s\Delta}_{3,\beta} n_\beta d\Gamma + \int_{S_c} \tilde{u}^{s\Delta}_i t^{0\Delta}_i dS \tag{3.18}$$

where superscripts " Σ " and " Δ " indicate the sum and jump of quantities across the crack surface. It should be remarked further that since the jump of the displacement along the crack-front vanishes identically, the test function $\tilde{u}^{s\Delta}_i$ is chosen to satisfy the homogeneous condition $\tilde{u}^{s\Delta}_i = 0$ on ∂S_c. The weak-form equations (3.17) and (3.18) now take the form

$$\lambda^s \int_{S_c} \tilde{u}^{s\Sigma}_{\alpha,\alpha} u^{s\Sigma}_{\gamma,\gamma} dS + \frac{\mu^s}{2} \int_{S_c} \left(\tilde{u}^{s\Sigma}_{\alpha,\beta} + \tilde{u}^{s\Sigma}_{\beta,\alpha}\right)\left(u^{s\Sigma}_{\alpha,\beta} + u^{s\Sigma}_{\beta,\alpha}\right) dS + \tau^s \int_{S_c} \tilde{u}^{s\Sigma}_{3,\beta} u^{s\Sigma}_{3,\beta} dS - \int_{S_c} \tilde{u}^{s\Sigma}_i t^{s\Sigma}_i dS =$$

$$\lambda^s \int_{\partial S_c} \tilde{u}^{s\Sigma}_\alpha n_\alpha u^{s\Sigma}_{\gamma,\gamma} d\Gamma + \frac{\mu^s}{2} \int_{\partial S_c} \left(\tilde{u}^{s\Sigma}_\alpha n_\beta + \tilde{u}^{s\Sigma}_\beta n_\alpha\right)\left(u^{s\Sigma}_{\alpha,\beta} + u^{s\Sigma}_{\beta,\alpha}\right) d\Gamma + \tau^s \int_{\partial S_c} \tilde{u}^{s\Sigma}_3 u^{s\Sigma}_{3,\beta} n_\beta d\Gamma + \int_{S_c} \tilde{u}^{s\Sigma}_i t^{0\Sigma}_i dS \tag{3.19}$$

$$\lambda^s \int_{S_c} \tilde{u}^{s\Delta}_{\alpha,\alpha} u^{s\Delta}_{\gamma,\gamma} dS + \frac{\mu^s}{2} \int_{S_c} \left(\tilde{u}^{s\Delta}_{\alpha,\beta} + \tilde{u}^{s\Delta}_{\beta,\alpha}\right)\left(u^{s\Delta}_{\alpha,\beta} + u^{s\Delta}_{\beta,\alpha}\right) dS + \tau^s \int_{S_c} \tilde{u}^{s\Delta}_{3,\beta} u^{s\Delta}_{3,\beta} dS - \int_{S_c} \tilde{u}^{s\Delta}_i t^{s\Delta}_i dS = \int_{S_c} \tilde{u}^{s\Delta}_i t^{0\Delta}_i dS \tag{3.20}$$

Equations (3.19) and (3.20) constitute a set of weak-form equations governing the unknown quantities $\{ u^{s\Sigma}_i, t^{s\Sigma}_i, u^{s\Delta}_i, t^{s\Delta}_i \}$.

3.4.1 Special case with Only Residual Surface Tension

It has been pointed out by various investigators that the influence of the surface Lamé constants on the out-of-plane responses in the local region very near the surface is negligibly weak (Intarit *et al.* 2012, Nan and Wang 2012, Intarit 2013, Pinyochotiwong *et al.* 2013). The simplified version of the Gurtin-Murdoch model without the in-plane surface elasticity is therefore considered suitable for modeling planar cracks subjected to pure mode-I loading conditions. By simply setting the

surface Lamé constants λ^s and μ^s to zero in the constitutive relation for the surface (3.10), it leads to

$$\sigma^s_{\alpha\beta} = \tau^s\delta_{\alpha\beta} + \tau^s\varepsilon^s_{\gamma\gamma}\delta_{\alpha\beta} - 2\tau^s\varepsilon^s_{\alpha\beta} + \tau^s u^s_{\alpha,\beta} \quad , \quad \sigma^s_{3\beta} = \tau^s u^s_{3,\beta} \tag{3.21}$$

Since the same equilibrium equation and strain-displacement relation as those employed in the general case (i.e., equations (3.9) and (3.11)) are also considered, the model is not restricted mathematically to applied tractions normal to the crack surface although it is physically suitable for treating pure mode-I loading conditions. Due to the vanishing of the term $\sigma^s_{\alpha\beta,\beta}$, which can readily be verified by the relation (3.21), the equilibrium equation (3.9) then implies that the applied shear traction is transmitted directly to the crack surface of the bulk medium. To construct the weak-form statement for this particular case, the procedure similar to that employed in the previous section is adopted. The final weak-form equations of the two layers take the following form:

$$\tau^s \int_{S_c} \tilde{u}^{s\Sigma}_{3,\beta} u^{s\Sigma}_{3,\beta} dS - \int_{S_c} \tilde{u}^{s\Sigma}_i t^{s\Sigma}_i dS = \int_{\partial S_c} \tilde{u}^{s\Sigma}_3 \sigma^{s\Sigma}_{3\beta} n_\beta dS + \int_{S_c} \tilde{u}^{s\Sigma}_i t^{0\Sigma}_i dS \tag{3.22}$$

$$\tau^s \int_{S_c} \tilde{u}^{s\Delta}_{3,\beta} u^{s\Delta}_{3,\beta} dS - \int_{S_c} \tilde{u}^{s\Delta}_i t^{s\Delta}_i dS = \int_{S_c} \tilde{u}^{s\Delta}_i t^{0\Delta}_i dS \tag{3.23}$$

3.4.2 Special case with Only In-plane Surface Elasticity

Another simplified version of the Gurtin-Murdoch model considered in the present study is the one with only the effect of the in-plane surface elasticity being treated. The simplified constitutive relation of the layers S_c^+ and S_c^- is obtained by substituting the residual surface tension τ^s to zero in (3.10) and this results in

$$\sigma^s_{\alpha\beta} = \lambda^s\varepsilon^s_{\gamma\gamma}\delta_{\alpha\beta} + 2\mu^s\varepsilon^s_{\alpha\beta} \quad , \quad \sigma^s_{3\beta} = 0 \tag{3.24}$$

It is evident from (3.24) that this simplified model always predicts zero out-of-plane shear stresses and this result, when combined with the equilibrium equation (3.9), dictates that the applied normal traction is transmitted directly to the crack surface of the bulk material. Similar to the previous special case, this simplified model is still applicable to general loading conditions on the crack surface. To obtain the weak-form statement for this particular case, the procedure similar to that employed in the general case is utilized and the resulting weak-form equations are given by

$$\lambda^s \int_{S_c} \tilde{u}^{s\Sigma}_{\alpha,\alpha} u^{s\Sigma}_{\gamma,\gamma} dS + \frac{\mu^s}{2} \int_{S_c} \left(\tilde{u}^{s\Sigma}_{\alpha,\beta} + \tilde{u}^{s\Sigma}_{\beta,\alpha}\right)\left(u^{s\Sigma}_{\alpha,\beta} + u^{s\Sigma}_{\beta,\alpha}\right) dS - \int_{S_c} \tilde{u}^{s\Sigma}_i t^{s\Sigma}_i dS =$$
$$\lambda^s \int_{\partial S_c} \tilde{u}^{s\Sigma}_\alpha n_\alpha u^{s\Sigma}_{\gamma,\gamma} d\Gamma + \frac{\mu^s}{2} \int_{\partial S_c} \left(\tilde{u}^{s\Sigma}_\alpha n_\beta + \tilde{u}^{s\Sigma}_\beta n_\alpha\right)\left(u^{s\Sigma}_{\alpha,\beta} + u^{s\Sigma}_{\beta,\alpha}\right) d\Gamma + \int_{S_c} \tilde{u}^{s\Sigma}_i t^{0\Sigma}_i dS \tag{3.25}$$

$$\lambda^s \int_{S_c} \tilde{u}^{s\Delta}_{\alpha,\alpha} u^{s\Delta}_{\gamma,\gamma} dS + \frac{\mu^s}{2} \int_{S_c} \left(\tilde{u}^{s\Delta}_{\alpha,\beta} + \tilde{u}^{s\Delta}_{\beta,\alpha}\right)\left(u^{s\Delta}_{\alpha,\beta} + u^{s\Delta}_{\beta,\alpha}\right) dS - \int_{S_c} \tilde{u}^{s\Delta}_i t^{s\Delta}_i dS = \int_{S_c} \tilde{u}^{s\Delta}_i t^{0\Delta}_i dS \tag{3.26}$$

3.5 Governing Equations of Whole Medium

Since the two layers S_c^+ and S_c^- are adhered perfectly to the bulk material, the displacements and tractions along the interface of the two layers and the bulk material must be continuous. This yields the following continuity conditions:

$$u_i^{s\Delta} = u_i^{b\Delta} \equiv u_i^{\Delta} \tag{3.27}$$

$$u_i^{s\Sigma} = u_i^{b\Sigma} \equiv u_i^{\Sigma} \tag{3.28}$$

$$t_i^{s\Delta} = -t_i^{b\Delta} \equiv -t_i^{\Delta} \tag{3.29}$$

$$t_i^{s\Sigma} = -t_i^{b\Sigma} \equiv -t_i^{\Sigma} \tag{3.30}$$

Substituting (3.27) - (3.30) into (3.7), (3.8), (3.19) and (3.20), leads to a system of four equations involving four unknown functions $\{u_i^{\Sigma}, t_i^{\Sigma}, u_i^{\Delta}, t_i^{\Delta}\}$ as follows

$$\begin{aligned}\frac{1}{2}\int_{S_c} \tilde{t}_p^{\Sigma}(\mathbf{y}) u_p^{\Sigma}(\mathbf{y}) dS(\mathbf{y}) = &\int_{S_c} \tilde{t}_p^{\Sigma}(\mathbf{y}) \int_{S_c} U_j^p(\boldsymbol{\xi}-\mathbf{y}) t_j^{\Sigma}(\boldsymbol{\xi}) dS(\boldsymbol{\xi}) dS(\mathbf{y}) \\ &+ \int_{S_c} \tilde{t}_p^{\Sigma}(\mathbf{y}) \int_{S_c} G_{mj}^p(\boldsymbol{\xi}-\mathbf{y}) D_m u_j^{\Delta}(\boldsymbol{\xi}) dS(\boldsymbol{\xi}) dS(\mathbf{y}) \\ &- \int_{S_c} \tilde{t}_p^{\Sigma}(\mathbf{y}) \int_{S_c} H_{ij}^p(\boldsymbol{\xi}-\mathbf{y}) n_i(\boldsymbol{\xi}) u_j^{\Delta}(\boldsymbol{\xi}) dS(\boldsymbol{\xi}) dS(\mathbf{y})\end{aligned} \tag{3.31}$$

$$\begin{aligned}-\frac{1}{2}\int_{S_c} \tilde{u}_k^{\Delta}(\mathbf{y}) t_k^{\Delta}(\mathbf{y}) dS(\mathbf{y}) = &\int_{S_c} D_t \tilde{u}_k^{\Delta}(\mathbf{y}) \int_{S_c} C_{mj}^{tk}(\boldsymbol{\xi}-\mathbf{y}) D_m u_j^{\Delta}(\boldsymbol{\xi}) dS(\boldsymbol{\xi}) dS(\mathbf{y}) \\ &+ \int_{S_c} D_t \tilde{u}_k^{\Delta}(\mathbf{y}) \int_{S_c} G_{tk}^j(\boldsymbol{\xi}-\mathbf{y}) t_j^{\Sigma}(\boldsymbol{\xi}) dS(\boldsymbol{\xi}) dS(\mathbf{y}) \\ &+ \int_{S_c} \tilde{u}_k^{\Delta}(\mathbf{y}) \int_{S_c} H_{lk}^j(\boldsymbol{\xi}-\mathbf{y}) n_l(\mathbf{y}) t_j^{\Sigma}(\boldsymbol{\xi}) dS(\boldsymbol{\xi}) dS(\mathbf{y})\end{aligned} \tag{3.32}$$

$$\lambda^s \int_{S_c} \tilde{u}^{s\Sigma}_{\alpha,\alpha} u^{\Sigma}_{\gamma,\gamma} dS + \frac{\mu^s}{2} \int_{S_c} \left(\tilde{u}^{s\Sigma}_{\alpha,\beta} + \tilde{u}^{s\Sigma}_{\beta,\alpha} \right) \left(u^{\Sigma}_{\alpha,\beta} + u^{\Sigma}_{\beta,\alpha} \right) dS + \tau^s \int_{S_c} \tilde{u}^{s\Sigma}_{3,\beta} u^{\Sigma}_{3,\beta} dS + \int_{S_c} \tilde{u}^{s\Sigma}_i t^{\Sigma}_i dS =$$

$$\lambda^s \int_{\partial S_c} \tilde{u}^{s\Sigma}_{\alpha} n_\alpha u^{\Sigma}_{\gamma,\gamma} d\Gamma + \frac{\mu^s}{2} \int_{\partial S_c} \left(\tilde{u}^{s\Sigma}_{\alpha} n_\beta + \tilde{u}^{s\Sigma}_{\beta} n_\alpha \right) \left(u^{\Sigma}_{\alpha,\beta} + u^{\Sigma}_{\beta,\alpha} \right) d\Gamma + \tau^s \int_{\partial S_c} \tilde{u}^{s\Sigma}_{3} u^{\Sigma}_{3,\beta} n_\beta d\Gamma + \int_{S_c} \tilde{u}^{s\Sigma}_i t^{0\Sigma}_i dS \tag{3.33}$$

$$\lambda^s \int_{S_c} \tilde{u}^{s\Delta}_{\alpha,\alpha} u^{\Delta}_{\gamma,\gamma} dS + \frac{\mu^s}{2} \int_{S_c} \left(\tilde{u}^{s\Delta}_{\alpha,\beta} + \tilde{u}^{s\Delta}_{\beta,\alpha} \right) \left(u^{\Delta}_{\alpha,\beta} + u^{\Delta}_{\beta,\alpha} \right) dS + \tau^s \int_{S_c} \tilde{u}^{s\Delta}_{3,\beta} u^{\Delta}_{3,\beta} dS + \int_{S_c} \tilde{u}^{s\Delta}_i t^{\Delta}_i dS = \int_{S_c} \tilde{u}^{s\Delta}_i t^{0\Delta}_i dS \tag{3.34}$$

It is obvious from (3.32) and (3.34) that terms involving the unknown jump of the traction t_i^{Δ} are similar and, by choosing $\tilde{u}_i^{s\Delta} = \tilde{u}_i^{\Delta}$, the two equations can be combined and those terms containing t_i^{Δ} can be eliminated. The above system (3.31)-(3.34) now becomes a system of three equations involving three unknown functions $\{u_i^{\Sigma}, t_i^{\Sigma}, u_i^{\Delta}\}$ given by

$$\begin{aligned} \mathcal{A}(\tilde{\mathbf{u}}^{s\Sigma}, \mathbf{u}^{\Sigma}) \; &+ \mathcal{B}(\tilde{\mathbf{u}}^{s\Sigma}, \mathbf{t}^{\Sigma}) \qquad\qquad &= \mathcal{R}_1(\tilde{\mathbf{u}}^{s\Sigma}) \\ \mathcal{B}(\tilde{\mathbf{t}}^{\Sigma}, \mathbf{u}^{\Sigma}) \; &+ \mathcal{C}(\tilde{\mathbf{t}}^{\Sigma}, \mathbf{t}^{\Sigma}) \; + \mathcal{D}(\tilde{\mathbf{t}}^{\Sigma}, \mathbf{u}^{\Delta}) \; &= 0 \\ \mathcal{D}(\mathbf{t}^{\Sigma}, \tilde{\mathbf{u}}^{\Delta}) \; &+ \mathcal{E}(\tilde{\mathbf{u}}^{\Delta}, \mathbf{u}^{\Delta}) \; &= \mathcal{R}_2(\tilde{\mathbf{u}}^{\Delta}) \end{aligned} \tag{3.35}$$

where the bilinear integral operators $\mathcal{A}, \mathcal{B}, \mathcal{C}, \mathcal{D}, \mathcal{E}$ are defined by

$$\mathcal{A}(\mathbf{X}, \mathbf{Y}) = \frac{\lambda^s}{2} \int_{S_c} X_{\alpha,\alpha} Y_{\gamma,\gamma} dS + \frac{\mu^s}{4} \int_{S_c} \left(X_{\alpha,\beta} + X_{\beta,\alpha} \right) \left(Y_{\alpha,\beta} + Y_{\beta,\alpha} \right) dS + \frac{\tau^s}{2} \int_{S_c} X_{3,\beta} Y_{3,\beta} dS$$

$$- \left[\frac{\lambda^s}{2} \int_{\partial S_c} X_\alpha n_\alpha Y_{\gamma,\gamma} d\Gamma + \frac{\mu^s}{4} \int_{\partial S_c} \left(X_\alpha n_\beta + X_\beta n_\alpha \right) \left(Y_{\alpha,\beta} + Y_{\beta,\alpha} \right) d\Gamma + \frac{\tau^s}{2} \int_{\partial S_c} X_3 Y_{3,\beta} n_\beta d\Gamma \right] \tag{3.36}$$

$$\mathcal{B}(\mathbf{X}, \mathbf{Y}) = \frac{1}{2} \int_{S_c} X_p(\mathbf{y}) Y_p(\mathbf{y}) dS(\mathbf{y}) \tag{3.37}$$

$$\mathcal{C}(\mathbf{X}, \mathbf{Y}) = -\int_{S_c} X_p(\mathbf{y}) \int_{S_c} U^p_j(\xi - \mathbf{y}) Y_j(\xi) dS(\xi) dS(\mathbf{y}) \tag{3.38}$$

$$\begin{aligned} \mathcal{D}(\mathbf{X}, \mathbf{Y}) = &-\int_{S_c} X_p(\mathbf{y}) \int_{S_c} G^p_{mj}(\xi - \mathbf{y}) D_m Y_j(\xi) dS(\xi) dS(\mathbf{y}) \\ &+ \int_{S_c} X_p(\mathbf{y}) \int_{S_c} H^p_{ij}(\xi - \mathbf{y}) n_i(\xi) Y_j(\xi) dS(\xi) dS(\mathbf{y}) \end{aligned} \tag{3.39}$$

$$\mathcal{E}(\mathbf{X},\mathbf{Y}) = -\int_{S_c} D_t X_k(\mathbf{y}) \int_{S_c} C_{mj}^{tk}(\boldsymbol{\xi}-\mathbf{y}) D_m Y_j(\boldsymbol{\xi}) dS(\boldsymbol{\xi}) dS(\mathbf{y}) + \mathcal{F}(\mathbf{X},\mathbf{Y}) \tag{3.40}$$

$$\mathcal{F}(\mathbf{X},\mathbf{Y}) = \frac{\lambda^s}{2}\int_{S_c} X_{\alpha,\alpha} Y_{\beta,\beta} dS + \frac{\mu^s}{4}\int_{S_c} \left(X_{\alpha,\beta} + X_{\beta,\alpha}\right)\left(Y_{\alpha,\beta} + Y_{\beta,\alpha}\right) dS + \frac{\tau^s}{2}\int_{S_c} X_{3,\beta} Y_{3,\beta} dS \tag{3.41}$$

and the linear integral operators $\{\mathcal{R}_1, \mathcal{R}_2\}$ are defined, in terms of prescribed data $\mathbf{t}^{0\Sigma}$ and $\mathbf{t}^{0\Delta}$, by

$$\mathcal{R}_1(\mathbf{X}) = \frac{1}{2}\int_{S_c} X_l(\mathbf{y}) t_l^{0\Sigma}(\mathbf{y}) dS(\mathbf{y}) \tag{3.42}$$

$$\mathcal{R}_2(\mathbf{X}) = \frac{1}{2}\int_{S_c} X_l(\mathbf{y}) t_l^{0\Delta}(\mathbf{y}) dS(\mathbf{y}) \tag{3.43}$$

3.5.1 Special case with Only Residual Surface Tension

For the special case when only the residual surface tension is considered, the fully coupled system of governing equations (3.35) can readily be simplified by ignoring the surface elastic constants to

$$\begin{aligned} \bar{\mathcal{A}}(\tilde{\mathbf{u}}^{s\Sigma}, \mathbf{u}^{\Sigma}) &+ \mathcal{B}(\tilde{\mathbf{u}}^{s\Sigma}, \mathbf{t}^{\Sigma}) && = \mathcal{R}_1(\tilde{\mathbf{u}}^{s\Sigma}) \\ \mathcal{B}(\tilde{\mathbf{t}}^{\Sigma}, \mathbf{u}^{\Sigma}) &+ \mathcal{C}(\tilde{\mathbf{t}}^{\Sigma}, \mathbf{t}^{\Sigma}) + \mathcal{D}(\tilde{\mathbf{t}}^{\Sigma}, \mathbf{u}^{\Delta}) && = 0 \\ \mathcal{D}(\mathbf{t}^{\Sigma}, \tilde{\mathbf{u}}^{\Delta}) &+ \bar{\mathcal{E}}(\tilde{\mathbf{u}}^{\Delta}, \mathbf{u}^{\Delta}) && = \mathcal{R}_2(\tilde{\mathbf{u}}^{\Delta}) \end{aligned} \tag{3.44}$$

where the additional bilinear integral operators $\bar{\mathcal{A}}$ and $\bar{\mathcal{E}}$ are defined by

$$\bar{\mathcal{A}}(\mathbf{X},\mathbf{Y}) = \frac{\tau^s}{2}\int_{S_c} X_{3,\beta} Y_{3,\beta} dS - \frac{\tau^s}{2}\int_{\partial S_c} X_3 Y_{3,\beta} n_\beta d\Gamma \tag{3.45}$$

$$\bar{\mathcal{E}}(\mathbf{X},\mathbf{Y}) = -\int_{S_c} D_t X_k(\mathbf{y}) \int_{S_c} C_{mj}^{tk}(\boldsymbol{\xi}-\mathbf{y}) D_m Y_j(\boldsymbol{\xi}) dS(\boldsymbol{\xi}) dS(\mathbf{y}) + \bar{\mathcal{F}}(\mathbf{X},\mathbf{Y}) \tag{3.46}$$

$$\bar{\mathcal{F}}(\mathbf{X},\mathbf{Y}) = \frac{\tau^s}{2}\int_{S_c} X_{3,\beta} Y_{3,\beta} dS \tag{3.47}$$

It is remarked that the system (3.44) still contains three equations and involves three unknown functions $\{u_i^{\Sigma}, t_i^{\Sigma}, u_i^{\Delta}\}$.

3.5.2 Special case with Only In-plane Surface Elasticity

For the special case when only the in-plane surface elasticity is considered, the fully coupled system of governing equations can readily be obtained by setting the residual surface tension to zero in (3.35) and the final result is given by

$$\begin{aligned} \hat{\mathcal{A}}(\tilde{\mathbf{u}}^{s\Sigma},\mathbf{u}^{\Sigma}) &+ \mathcal{B}(\tilde{\mathbf{u}}^{s\Sigma},\mathbf{t}^{\Sigma}) && = \mathcal{R}_1(\tilde{\mathbf{u}}^{s\Sigma}) \\ \mathcal{B}(\tilde{\mathbf{t}}^{\Sigma},\mathbf{u}^{\Sigma}) &+ \mathcal{C}(\tilde{\mathbf{t}}^{\Sigma},\mathbf{t}^{\Sigma}) + \mathcal{D}(\tilde{\mathbf{t}}^{\Sigma},\mathbf{u}^{\Delta}) && = 0 \\ & \mathcal{D}(\mathbf{t}^{\Sigma},\tilde{\mathbf{u}}^{\Delta}) + \hat{\mathcal{E}}(\tilde{\mathbf{u}}^{\Delta},\mathbf{u}^{\Delta}) && = \mathcal{R}_2(\tilde{\mathbf{u}}^{\Delta}) \end{aligned} \tag{3.48}$$

where the additional bilinear integral operators $\hat{\mathcal{A}}$ and $\hat{\mathcal{E}}$ are defined by

$$\begin{aligned} \hat{\mathcal{A}}(\mathbf{X},\mathbf{Y}) = {} & \frac{\lambda^s}{2}\int_{S_c} X_{\alpha,\alpha}Y_{\gamma,\gamma}\,dS + \frac{\mu^s}{4}\int_{S_c}\left(X_{\alpha,\beta}+X_{\beta,\alpha}\right)\left(Y_{\alpha,\beta}+Y_{\beta,\alpha}\right)dS \\ & -\frac{\lambda^s}{2}\int_{\partial S_c} X_\alpha n_\alpha Y_{\gamma,\gamma}\,d\Gamma - \frac{\mu^s}{4}\int_{\partial S_c}\left(X_\alpha n_\beta + X_\beta n_\alpha\right)\left(Y_{\alpha,\beta}+Y_{\beta,\alpha}\right)d\Gamma \end{aligned} \tag{3.49}$$

$$\hat{\mathcal{E}}(\mathbf{X},\mathbf{Y}) = -\int_{S_c} D_t X_k(\mathbf{y})\int_{S_c} C_{mj}^{tk}(\boldsymbol{\xi}-\mathbf{y})D_m Y_j(\boldsymbol{\xi})\,dS(\boldsymbol{\xi})\,dS(\mathbf{y}) + \hat{\mathcal{F}}(\mathbf{X},\mathbf{Y}) \tag{3.50}$$

$$\hat{\mathcal{F}}(\mathbf{X},\mathbf{Y}) = \frac{\lambda^s}{2}\int_{S_c} X_{\alpha,\alpha}Y_{\beta,\beta}\,dS + \frac{\mu^s}{4}\int_{S_c}\left(X_{\alpha,\beta}+X_{\beta,\alpha}\right)\left(Y_{\alpha,\beta}+Y_{\beta,\alpha}\right)dS \tag{3.51}$$

Again, the system (3.48) still contains three equations and involves the same three unknown functions $\{u_i^{\Sigma}, t_i^{\Sigma}, u_i^{\Delta}\}$.

CHAPTER 4
NUMERICAL IMPLEMENTATION

In this chapter, essential components required in the numerical implementation including the discretization and numerical integration are briefly discussed. In general, standard procedures for the weakly singular SGBEM (e.g., Li and Mear 1998, Li *et al.* 1998, Rungamornrat 2006, Rungamornrat and Mear 2008) and those for the standard finite element method (e.g., Bathe 1990, Hughes 2000, Zienkiewicz and Taylor 2000) are utilized to form the discretized system of linear algebraic equations.

4.1 Discretization

Standard Galerkin approximation is employed in the discretization of the system of governing equations (3.35), (3.44), and (3.48). Since all involved boundary integrals governing the bulk material contain only weakly singular kernels of $\mathcal{O}(1/r)$, continuous (C^0) interpolation functions are utilized everywhere in the approximation of both trial and test functions. In particular, the following approximation for the test functions and the trial functions is introduced:

$$\tilde{u}_i^{s\Sigma} = \sum_{p=1}^{N} \tilde{U}_{3(p-1)+i}^{s\Sigma} \Phi_p \; ; \qquad u_i^{\Sigma} = \sum_{q=1}^{N} U_{3(q-1)+i}^{\Sigma} \Phi_q \tag{4.1}$$

$$\tilde{u}_i^{\Delta} = \sum_{p=1}^{N} \tilde{U}_{3(p-1)+i} \Phi_p \; ; \qquad u_i^{\Delta} = \sum_{q=1}^{N} U_{3(q-1)+i}^{\Delta} \Phi_q \tag{4.2}$$

$$\tilde{t}_i^{\Sigma} = \sum_{p=1}^{N} \tilde{T}_{3(p-1)+i} \Phi_p \; ; \qquad t_i^{\Sigma} = \sum_{q=1}^{N} T_{3(q-1)+i}^{\Sigma} \Phi_q \tag{4.3}$$

where N is the number of nodal points; Φ_p is nodal basis functions at the node p; Φ_q is nodal basis functions at the node q; $U_{3(q-1)+i}^{\Sigma}$, $U_{3(q-1)+i}^{\Delta}$, and $T_{3(q-1)+i}^{\Sigma}$ are nodal degrees of freedom associated with the sum of the displacement, the jump of the displacement and the sum of the traction across the crack surfaces, respectively; and $\tilde{U}_{3(p-1)+i}^{s\Sigma}$, $\tilde{U}_{3(p-1)+i}$, and $\tilde{T}_{3(p-1)+i}$ are arbitrary nodal quantities.

4.1.1 General Case

Substituting (4.1)-(4.3) into (3.35) along with using the arbitrariness of $\tilde{U}^{s\Sigma}_{3(p-1)+i}$, $\tilde{U}_{3(p-1)+i}$, and $\tilde{T}_{3(p-1)+i}$, leads to a system of linear algebraic equations as

$$\begin{bmatrix} \mathbf{A} & \mathbf{B} & \mathbf{0} \\ \mathbf{B}^T & \mathbf{C} & \mathbf{D} \\ \mathbf{0} & \mathbf{D}^T & \mathbf{E} \end{bmatrix} \begin{Bmatrix} \mathbf{U}^{\Sigma} \\ \mathbf{T}^{\Sigma} \\ \mathbf{U}^{\Delta} \end{Bmatrix} = \begin{Bmatrix} \mathbf{R}_1 \\ \mathbf{0} \\ \mathbf{R}_2 \end{Bmatrix} \tag{4.4}$$

where the sub-matrices $\mathbf{A}, \mathbf{B}, \mathbf{C}, \mathbf{D}, \mathbf{E}$ are associated with the bilinear operators $\mathcal{A}, \mathcal{B}, \mathcal{C}, \mathcal{D}, \mathcal{E}$; sub-vectors $\mathbf{R}_1, \mathbf{R}_2$ correspond to the linear operators $\mathcal{R}_1, \mathcal{R}_2$; $\mathbf{U}^{\Sigma}$ is a vector of nodal quantities of the sum of the displacement; $\mathbf{U}^{\Delta}$ is a vector of nodal quantities of the jump of the displacement and $\mathbf{T}^{\Sigma}$ is a vector of nodal quantities of the sum of the traction. The sub-matrices $\mathbf{A}, \mathbf{B}, \mathbf{C}, \mathbf{D}, \mathbf{E}$ and sub-vectors $\mathbf{R}_1, \mathbf{R}_2$ are given explicitly by

$$\begin{aligned} [\mathbf{A}]_{3(p-1)+\alpha,3(q-1)+\beta} &= \frac{\lambda^s}{2}\int_{S_c} \Phi_{p,\alpha}(\underset{\sim}{y})\Phi_{q,\beta}(\underset{\sim}{y})dS(\underset{\sim}{y}) - \frac{\lambda^s}{2}\int_{\partial S_c} \Phi_{p}(\underset{\sim}{y})\Phi_{q,\beta}(\underset{\sim}{y})n_\alpha d\Gamma(\underset{\sim}{y}) \\ &\quad + \frac{\mu^s}{2}\left(\int_{S_c} \Phi_{p,\beta}(\underset{\sim}{y})\Phi_{q,\alpha}(\underset{\sim}{y})dS(\underset{\sim}{y}) + \delta_{\alpha\beta}\int_{S_c} \Phi_{p,\gamma}(\underset{\sim}{y})\Phi_{q,\gamma}(\underset{\sim}{y})dS(\underset{\sim}{y}) \right) \\ &\quad - \frac{\mu^s}{2}\left(\int_{\partial S_c} \Phi_{p}(\underset{\sim}{y})\Phi_{q,\alpha}(\underset{\sim}{y})n_\beta d\Gamma(\underset{\sim}{y}) + \delta_{\alpha\beta}\int_{\partial S_c} \Phi_{p}(\underset{\sim}{y})\Phi_{q,\gamma}(\underset{\sim}{y})n_\gamma d\Gamma(\underset{\sim}{y}) \right) \end{aligned} \tag{4.5}$$

$$[\mathbf{A}]_{3(p-1)+3,3(q-1)+3} = \frac{\tau^s}{2}\int_{S_c} \Phi_{p,\gamma}(\underset{\sim}{y})\Phi_{q,\gamma}(\underset{\sim}{y})dS(\underset{\sim}{y}) - \frac{\tau^s}{2}\int_{\partial S_c} \Phi_{p}(\underset{\sim}{y})\Phi_{q,\gamma}(\underset{\sim}{y})n_\gamma d\Gamma(\underset{\sim}{y}) \tag{4.6}$$

$$[\mathbf{B}]_{3(p-1)+i,3(q-1)+j} = \frac{1}{2}\int_{S_c} \delta_{ij}\Phi_{p}(\underset{\sim}{y})\Phi_{q}(\underset{\sim}{y})dS(\underset{\sim}{y}) \tag{4.7}$$

$$[\mathbf{C}]_{3(p-1)+i,3(q-1)+j} = -\int_{S_c} \Phi_{p}(\underset{\sim}{y})\int_{S_c} U^i_j(\xi-\underset{\sim}{y})\Phi_{q}(\xi)dS(\xi)dS(\underset{\sim}{y}) \tag{4.8}$$

$$\begin{aligned} [\mathbf{D}]_{3(p-1)+i,3(q-1)+j} &= -\int_{S_c} \Phi_{p}(\underset{\sim}{y})\int_{S_c} G^i_{mj}(\boldsymbol{\xi}-\underset{\sim}{y})D_m\Phi_{q}(\boldsymbol{\xi})dS(\boldsymbol{\xi})dS(\underset{\sim}{y}) \\ &\quad + \int_{S_c} \Phi_{p}(\underset{\sim}{y})\int_{S_c} H^i_{mj}(\boldsymbol{\xi}-\underset{\sim}{y})n_m(\boldsymbol{\xi})\Phi_{q}(\boldsymbol{\xi})dS(\boldsymbol{\xi})dS(\underset{\sim}{y}) \end{aligned} \tag{4.9}$$

$$[\mathbf{E}]_{3(p-1)+i,3(q-1)+j} = -\int_{S_c} D_t \Phi_p(\underset{\sim}{y}) \int_{S_c} C_{mj}^{ti}(\xi - \underset{\sim}{y}) D_m \Phi_q(\xi) dS(\xi) dS(\underset{\sim}{y}) + [\mathbf{F}]_{3(p-1)+i,3(q-1)+j} \tag{4.10}$$

$$[\mathbf{F}]_{3(p-1)+\alpha,3(q-1)+\beta} = \frac{\lambda^s}{2} \int_{S_c} \Phi_{p,\alpha}(\underset{\sim}{y}) \Phi_{q,\beta}(\underset{\sim}{y}) dS(\underset{\sim}{y}) + \frac{\mu^s}{2} \left(\int_{S_c} \Phi_{p,\beta}(\underset{\sim}{y}) \Phi_{q,\alpha}(\underset{\sim}{y}) dS(\underset{\sim}{y}) + \delta_{\alpha\beta} \int_{S_c} \Phi_{p,\gamma}(\underset{\sim}{y}) \Phi_{q,\gamma}(\underset{\sim}{y}) dS(\underset{\sim}{y}) \right) \tag{4.11}$$

$$[\mathbf{F}]_{3(p-1)+3,3(q-1)+3} = \frac{\tau^s}{2} \int_{S_c} \Phi_{p,\gamma}(\underset{\sim}{y}) \Phi_{q,\gamma}(\underset{\sim}{y}) dS(\underset{\sim}{y}) \tag{4.12}$$

$$[\mathbf{R}_1]_{3(p-1)+i} = \frac{1}{2} \int_{S_c} \Phi_p(\underset{\sim}{y}) t_i^{0\Sigma}(\underset{\sim}{y}) dS(\underset{\sim}{y}); \quad [\mathbf{R}_2]_{3(p-1)+i} = \frac{1}{2} \int_{S_c} \Phi_p(\underset{\sim}{y}) t_i^{0\Delta}(\underset{\sim}{y}) dS(\underset{\sim}{y}) \tag{4.13}$$

$$[\mathbf{U}^{\Sigma}]_{3(q-1)+i} = U^{\Sigma}_{3(q-1)+i}; \quad [\mathbf{U}^{\Delta}]_{3(q-1)+i} = U^{\Delta}_{3(q-1)+i}; \quad [\mathbf{T}^{\Sigma}]_{3(q-1)+i} = T^{\Sigma}_{3(q-1)+i} \tag{4.14}$$

4.1.2 Special Case with only Residual Surface Tension

By applying the same procedure as that employed in the general case to (3.44), it leads to a system of linear algebraic equations as follows

$$\begin{bmatrix} \bar{\mathbf{A}} & \mathbf{B} & \mathbf{0} \\ \mathbf{B}^T & \mathbf{C} & \mathbf{D} \\ \mathbf{0} & \mathbf{D}^T & \bar{\mathbf{E}} \end{bmatrix} \begin{Bmatrix} \mathbf{U}^{\Sigma} \\ \mathbf{T}^{\Sigma} \\ \mathbf{U}^{\Delta} \end{Bmatrix} = \begin{Bmatrix} \mathbf{R}_1 \\ \mathbf{0} \\ \mathbf{R}_2 \end{Bmatrix} \tag{4.15}$$

where the sub-matrices $\bar{\mathbf{A}}, \mathbf{B}, \mathbf{C}, \mathbf{D}, \bar{\mathbf{E}}$ are associated with the bilinear operators $\bar{\mathcal{A}}, \mathcal{B}, \mathcal{C}, \mathcal{D}, \bar{\mathcal{E}}$; sub-vectors $\mathbf{R}_1, \mathbf{R}_2$ correspond to the linear operators $\mathcal{R}_1, \mathcal{R}_2$; $\mathbf{U}^{\Sigma}$ is a vector of nodal quantities of the sum of the displacement; $\mathbf{U}^{\Delta}$ is a vector of nodal quantities of the jump of the displacement and $\mathbf{T}^{\Sigma}$ is a vector of nodal quantities of the sum of the traction. The additional sub-matrices $\bar{\mathbf{A}}$ and $\bar{\mathbf{E}}$ are given explicitly by

$$[\bar{\mathbf{A}}]_{3(p-1)+\alpha,3(q-1)+\beta} = 0 \tag{4.16}$$

$$[\bar{\mathbf{A}}]_{3(p-1)+3,3(q-1)+3} = \frac{\tau^s}{2} \int_{S_c} \Phi_{p,\gamma}(\underset{\sim}{y}) \Phi_{q,\gamma}(\underset{\sim}{y}) dS(\underset{\sim}{y}) - \frac{\tau^s}{2} \int_{\partial S_c} \Phi_p(\underset{\sim}{y}) \Phi_{q,\gamma}(\underset{\sim}{y}) n_\gamma d\Gamma(\underset{\sim}{y}) \tag{4.17}$$

$$[\bar{\mathbf{E}}]_{3(p-1)+i,3(q-1)+j} = -\int_{S_c} D_t \Phi_p(\underset{\sim}{y}) \int_{S_c} C_{mj}^{ti}(\xi - \underset{\sim}{y}) D_m \Phi_q(\xi) dS(\xi) dS(\underset{\sim}{y}) + [\bar{\mathbf{F}}]_{3(p-1)+i,3(q-1)+j} \tag{4.18}$$

$$[\bar{\mathbf{F}}]_{3(p-1)+\alpha,3(q-1)+\beta}=0 \tag{4.19}$$

$$[\bar{\mathbf{F}}]_{3(p-1)+3,3(q-1)+3}=\frac{\tau^s}{2}\int_{S_c}\Phi_{p,\gamma}(\underset{\sim}{y})\Phi_{q,\gamma}(\underset{\sim}{y})dS(\underset{\sim}{y}) \tag{4.20}$$

4.1.3 Special Case with only In-plane Surface Elasticity

The discretized system of linear algebraic equations of the governing equations (3.48) can also be obtained in the same manner and the final result is given by

$$\begin{bmatrix}\hat{\mathbf{A}} & \mathbf{B} & \mathbf{0}\\ \mathbf{B}^T & \mathbf{C} & \mathbf{D}\\ \mathbf{0} & \mathbf{D}^T & \hat{\mathbf{E}}\end{bmatrix}\begin{Bmatrix}\mathbf{U}^{\Sigma}\\ \mathbf{T}^{\Sigma}\\ \mathbf{U}^{\Delta}\end{Bmatrix}=\begin{Bmatrix}\mathbf{R}_1\\ \mathbf{0}\\ \mathbf{R}_2\end{Bmatrix} \tag{4.21}$$

where the sub-matrices $\hat{\mathbf{A}}, \mathbf{B}, \mathbf{C}, \mathbf{D}, \hat{\mathbf{E}}$ are associated with the bilinear operators $\hat{\mathcal{A}}, \mathcal{B}, \mathcal{C}, \mathcal{D}, \hat{\mathcal{E}}$; sub-vectors $\mathbf{R}_1, \mathbf{R}_2$ correspond to the linear operators $\mathcal{R}_1, \mathcal{R}_2$; $\mathbf{U}^{\Sigma}$ is a vector of nodal quantities of the sum of the displacement; $\mathbf{U}^{\Delta}$ is a vector of nodal quantities of the jump of the displacement and $\mathbf{T}^{\Sigma}$ is a vector of nodal quantities of the sum of the traction. The additional sub-matrices $\hat{\mathbf{A}}$ and $\hat{\mathbf{E}}$ are given explicitly by

$$\begin{aligned}[\hat{\mathbf{A}}]_{3(p-1)+\alpha,3(q-1)+\beta}=&\frac{\lambda^s}{2}\int_{S_c}\Phi_{p,\alpha}(\underset{\sim}{y})\Phi_{q,\beta}(\underset{\sim}{y})dS(\underset{\sim}{y})-\frac{\lambda^s}{2}\int_{\partial S_c}\Phi_{p}(\underset{\sim}{y})\Phi_{q,\beta}(\underset{\sim}{y})n_\alpha d\Gamma(\underset{\sim}{y})\\&+\frac{\mu^s}{2}\left(\int_{S_c}\Phi_{p,\beta}(\underset{\sim}{y})\Phi_{q,\alpha}(\underset{\sim}{y})dS(\underset{\sim}{y})+\delta_{\alpha\beta}\int_{S_c}\Phi_{p,\gamma}(\underset{\sim}{y})\Phi_{q,\gamma}(\underset{\sim}{y})dS(\underset{\sim}{y})\right)\\&-\frac{\mu^s}{2}\left(\int_{\partial S_c}\Phi_{p}(\underset{\sim}{y})\Phi_{q,\alpha}(\underset{\sim}{y})n_\beta d\Gamma(\underset{\sim}{y})+\delta_{\alpha\beta}\int_{\partial S_c}\Phi_{p}(\underset{\sim}{y})\Phi_{q,\gamma}(\underset{\sim}{y})n_\gamma d\Gamma(\underset{\sim}{y})\right)\end{aligned} \tag{4.22}$$

$$[\hat{\mathbf{A}}]_{3(p-1)+3,3(q-1)+3}=0 \tag{4.23}$$

$$[\hat{\mathbf{E}}]_{3(p-1)+i,3(q-1)+j}=-\int_{S_c}D_t\Phi_p(\underset{\sim}{y})\int_{S_c}C^{ti}_{mj}(\underset{\sim}{\xi}-\underset{\sim}{y})D_m\Phi_q(\underset{\sim}{\xi})dS(\underset{\sim}{\xi})dS(\underset{\sim}{y})+[\hat{\mathbf{F}}]_{3(p-1)+i,3(q-1)+j} \tag{4.24}$$

$$\begin{aligned}[\hat{\mathbf{F}}]_{3(p-1)+\alpha,3(q-1)+\beta}=&\frac{\lambda^s}{2}\int_{S_c}\Phi_{p,\alpha}(\underset{\sim}{y})\Phi_{q,\beta}(\underset{\sim}{y})dS(\underset{\sim}{y})\\&+\frac{\mu^s}{2}\left(\int_{S_c}\Phi_{p,\beta}(\underset{\sim}{y})\Phi_{q,\alpha}(\underset{\sim}{y})dS(\underset{\sim}{y})+\delta_{\alpha\beta}\int_{S_c}\Phi_{p,\gamma}(\underset{\sim}{y})\Phi_{q,\gamma}(\underset{\sim}{y})dS(\underset{\sim}{y})\right)\end{aligned} \tag{4.25}$$

$$[\hat{\mathbf{F}}]_{3(p-1)+3,3(q-1)+3}=0 \tag{4.26}$$

4.2. Numerical Integration

To evaluate the sub-matrices $\mathbf{A}$, $\bar{\mathbf{A}}$, $\hat{\mathbf{A}}$, $\mathbf{B}$, $\mathbf{C}$, $\mathbf{D}$, $\mathbf{E}$, $\bar{\mathbf{E}}$, $\hat{\mathbf{E}}$ and sub-vectors $\mathbf{R}_1$, $\mathbf{R}_2$ numerically, the single and double surface integrals must be properly treated. All single surface integrals contain regular integrands and can be efficiently and accurately integrated using standard Gaussian quadrature. Unlike single surface integrals, double surface integrals can be categorized into three types depending on a pair of elements resulting from the discretization of the surface S_c.

The first type is termed a regular double surface integral since its integrand is not singular with only mild variation. This type of integral arises when both elements in a pair are relatively remote in comparison with their characteristic size. Similar to the single surface integral, all regular double surface integrals can be accurately integrated by Gaussian quadrature.

The second type, termed weakly singular double surface integrals, arises when both elements in a pair are identical and, therefore, the integrand is weakly singular due to the involved kernels. Although these integrals exist in an ordinary sense (sense of Riemann), it was pointed out by Xiao (1998) that they cannot be accurately integrated by standard Gaussian quadrature. To circumvent such difficulty, similar techniques based on integrand regularization via a series of transformations proposed by Li *et al.* (1985), Hayami and Brebbia (1988) and Xiao (1998) are employed.

The last type of double surface integrals, which are considered most challenging, is a nearly singular integral. The integrand of these integrals is nearly singular since both elements in a pair are relatively close in comparison with their characteristic size and this renders the kernels appearing in those integrals nearly singular and exhibiting rapid variation. Similar to the weakly singular integrals, Gaussian quadrature cannot be used to integrate nearly singular integrals efficiently. Special techniques proposed by Hayami (1992), Hayami and Matsumoto (1994) and Xiao (1998) are adopted to perform the numerical integration.

4.3 Shape Functions

As clearly discussed in the literature review, the singularity of the stress along the crack front of nano-sized cracks with the presence of surface stresses is still unclear. Some investigators pointed out that the stress along the crack front of nano-sized crack should be finite (e.g., Kim *et al.* 2010, Kim *et al.* 2011, Kim *et al.* 2011, Nan and Wang

2012). Other studies have concluded in the opposite direction that the stress along crack front of nano-sized crack is still singular; however the order of singularity reduces from square-root singularity to logarithmic singularity (e.g., Sendova and Walton 2010, Kim *et al.* 2013). In the current study, it is postulated that the singularity of the stress along the crack front disappears when the surface stresses is taken into account. As a result, standard isoparametric C^0 elements are employed everywhere to approximate all test and trial functions appearing in the governing equations of nano-sized crack problems. However, for some special cases when the influence of the surface stresses is ignored in certain directions, the special crack-tip shape functions proposed by Li *et al.* (1998) to accurately capture the right behavior of the near tip field are still required. The standard isoparametric shape functions can be easily found in Bathe (1990), Hughes (2000) and Zienkiewicz and Taylor (2000). The special crack-tip shape functions can be referred to the work of Li *et al.* (1998). The usage of the shape functions (standard shape functions or special crack-tip shape functions) in the present study can be summarized as follows:

- For the general case, when the full version of Gurtin-Murdoch model is considered, the standard shape functions are used in the approximation of all components of primary unknowns.
- For the special case, when the simplified version of Gurtin-Murdoch model without the surface elastic constants is considered, the special crack-tip shape functions are employed to approximate the in-plane components of $\underset{\sim}{\boldsymbol{u}}^{\Delta}$ and $\underset{\sim}{\tilde{\boldsymbol{u}}}^{\Delta}$ whereas the standard shape functions are utilized to discretize all remaining quantities.
- For the special case, when the simplified version of Gurtin-Murdoch model without the residual surface tension is considered, the special crack-tip shape functions are employed to approximate the out-of-plane components of $\underset{\sim}{\boldsymbol{u}}^{\Delta}$ and $\underset{\sim}{\tilde{\boldsymbol{u}}}^{\Delta}$ whereas the standard shape functions are adopted to discretize all remaining quantities.

CHAPTER 5
NUMERICAL RESULTS

To verify the formulation and numerical implementation of the proposed method for solving nano-sized cracks problems, a penny-shaped crack embedded in an isotropic, linearly elastic, unbounded domain under pure mode-I loading conditions is considered first. Results of the crack opening displacement and the vertical stress in the vicinity of the crack front are compared with existing benchmark solutions (Intarit *et al.* 2012, Intarit 2013). Once the technique is fully tested, the parametric study is performed for this particular problem to elucidate the influence of surface stresses and the size-dependent behaviors of the predicted solutions. Then, the same penny-shaped crack is investigated for mixed-mode loading conditions. To further demonstrate the capability of the current method in solving cracks of arbitrary shapes and multiple cracks, an elliptical crack under mode-I and mixed-mode loading conditions and two coplanar cracks under mode-I loading are considered respectively in the remaining of this chapter.

In the analysis, three different levels of mesh refinement are adopted to examine the convergence of numerical results. Nine-node isoparametric elements are used to discretize the entire crack front, whereas the rest of the crack surface is discretized by eight-node and six-node isoparametric elements. Young's modulus and Poisson's ratio for the bulk material are taken as $E = 107\ GPa$ and $\nu = 0.33$, respectively, and the surface elastic constants and the residual surface tension are chosen identical to those utilized by Intarit *et al.* (2012) and Intarit (2013) (i.e., $\lambda^s = 4.4939\ N/m$, $\mu^s = 2.7779\ N/m$, $\tau^s = 0.6056\ N/m$). These above material properties are used for all following numerical examples in this dissertation. For convenience in the numerical analysis, all quantities involved in the key governing equations are properly normalized. For instance, the unknown sum of the traction and the prescribed traction on the top surface of the two-thickness layers are normalized by the shear modulus μ (i.e., $t_0^{\Sigma} = t^{\Sigma}/\mu$ and $\sigma_{i0} = \sigma_i^0/\mu$); the unknown sum and jump of the displacement across the crack surface are normalized by a special length scale $\Lambda = \kappa^s/\mu = 0.24983\ nm$ (i.e., $u_0^{\Delta} = u^{\Delta}/\Lambda$ and $u_0^{\Sigma} = u^{\Sigma}/\Lambda$) where $\kappa^s = \left|\lambda^s + 2\mu^s\right|$; and all characteristic lengths representing the geometry of the crack such as the crack radius a, the semi-major axis a, and the semi-minor axis b used in following examples are normalized by the length scale Λ (e.g., $a_0 = a/\Lambda$ and $b_0 = b/\Lambda$).

5.1 Penny-Shaped Crack under Pure Mode-I Loading

As a means for verifying the current technique, the problem of a penny-shaped crack of radius *a* embedded in an isotropic, linear elastic infinite medium is considered (Figure 5.1(a)). The crack is subjected to self-equilibrated, uniformly distributed normal traction $t_3^+ = -t_3^- = \sigma_0$. The three meshes of the crack surface used in the numerical study are shown in Figure 5.1(b).

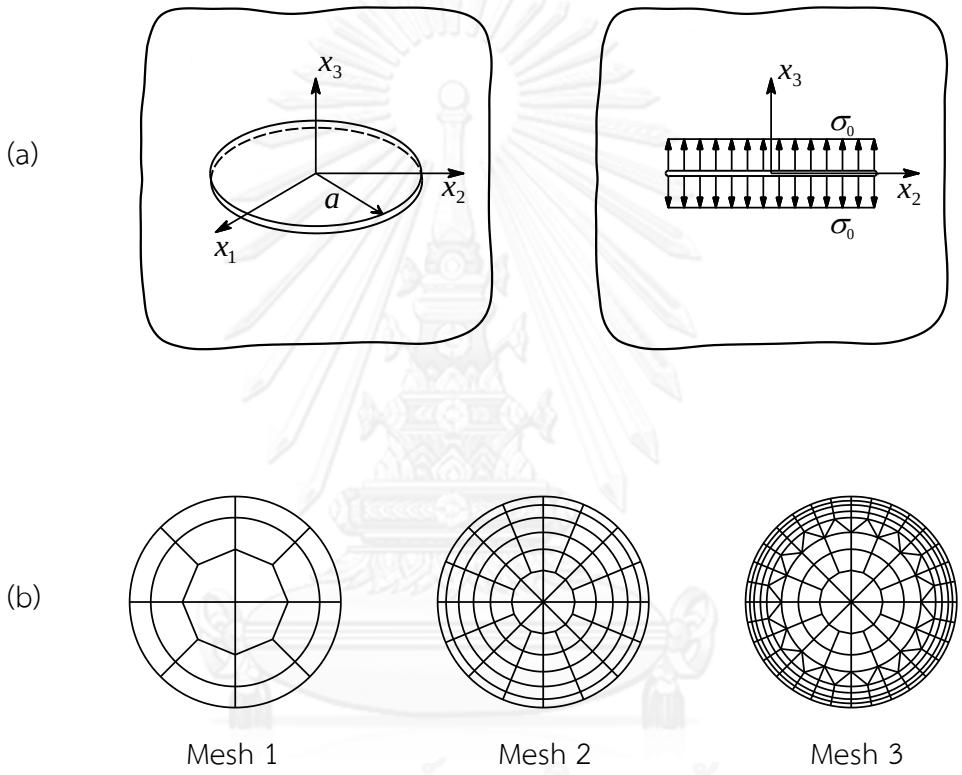

Figure 5.1: (a) Schematic of a penny-shaped crack of radius a embedded in an isotropic, linear elastic infinite medium subjected to uniformly distributed normal traction $t_3^+ = -t_3^- = \sigma_0$; (b) Meshes adopted in the analysis. Mesh 1: 20 elements and 77 nodes. Mesh 2: 88 elements and 297 nodes. Mesh 3: 216 elements and 665 nodes.

5.1.1 Verification

This problem has been previously solved by Intarit *et al.* (2012) and Intarit (2013) using Hankel integral transforms along with a solution technique for dual integral equations and their results are used as the benchmark solution to validate the proposed FEM-SGBEM technique. In this numerical example, results for mode-I loading

conditions are presented for three different models. The model-1 represents the classical case without the surface stress effects. It should be noted that, for this particular case, the classical solution of the crack opening displacement and the stress in the vicinity of crack front can be found in Tada *et al.* (2000) and Kachanov *et al.* (2004), respectively. The model-2 is associated with a simplified version of Gurtin-Murdoch surface elasticity model (the first special case) in which the residual surface tension (τ^s) is only considered. The model-3 corresponds a full version of Gurtin-Murdoch surface elasticity model where both the surface elastic constants (λ^s, μ^s) and the residual surface tension (τ^s) are included.

The normalized crack opening displacement and the normalized vertical stresses near the crack front, when the influence of surface stresses is taken into account, are reported in Figures 5.2-5.3 along with the benchmark solution generated by a technique proposed by Intarit *et al.* (2012) and Intarit (2013). It is seen that the numerical results are slightly mesh dependent and that they are highly accurate and almost indistinguishable from the analytical solution for both the crack opening displacement and near-tip vertical stresses σ_{33} for the model-2 and model-3. It can also be pointed out from the results shown in Figure 5.2 that the two models incorporating the surface stresses with (model-3) and without (model-2) the influence of the in-plane surface elasticity yield results significantly different from those predicted by the classical model (model-1). While both the residual surface tension and the in-plane surface elasticity contribute to such discrepancy, the influence of the residual surface tension seems more significant in the case of mode-I loading conditions. The medium tends to be much stiffer than the classical case, when the full version of the surface stress model is considered in the analysis.

5.1.2 Parametric Study

To further examine the influence of the residual surface tension (τ^s) on the predicted solution of mode-I crack problems, the normalized crack opening displacement and the normalized vertical stress σ_{33} for different values of the residual surface tension τ^s ranging from 0.1 to 1.0 *N/m* (with the surface elastic constants and the bulk material properties remaining fixed) are shown in Figure 5.4. It can be concluded that the residual surface tension exhibits significant role on the crack opening displacement and the vertical stress σ_{33} for mode-I loading conditions. In particular, as τ^s becomes larger, the deviation of results from the classical case

(without the surface stresses) significantly increases and, clearly, it renders the elastic medium much stiffer.

The investigation of the influence of the surface elasticity constants (λ^s, μ^s) on the solution of cracks under mode-I loading conditions is also considered. The normalized crack opening displacement and the normalized vertical stress σ_{33} in the vicinity of the crack front for different values of the surface elasticity constants (λ^s, μ^s) ranging from 0, 0.1, 1 and 10 times of their initial value (with the residual surface tension and the bulk material properties remaining fixed) are reported in Figure 5.5. This numerical study is performed only for the model-3 where the full version of Gurtin-Murdoch surface elasticity is considered. It can be concluded from this set of results that the surface elasticity constants exhibit the slight influence on the crack opening displacement and almost no influence on the vertical stress for mode-I loading conditions. However, as the surface elasticity constants become larger, the deviation of results from those predicted by the model-2 still increases a bit and, clearly, it makes the bulk material a bit stiffer.

To demonstrate the size-dependent behavior of results due to the presence of the surface stresses, the crack opening displacements and the near-tip vertical stresses are illustrated in Figure 5.6 for all three models. It is evident that, by including the surface stress effects in the mathematical model, the predicted solutions apparently exhibit size-dependent behavior. In particular, the normalized crack opening displacements and the normalized vertical stresses in the vicinity of the crack front of the model-2 and model-3 depend significantly on the crack size and this is in contrast with the model-1 where the normalized crack opening displacements and normalized vertical stresses are, upon the proper normalization, independent of the crack radius.

5.2 Penny-Shaped Crack under Mixed Mode Loading

In this section, a penny-shaped crack in an unbounded medium under mixed-mode loading conditions (i.e., mode-II and mode-III loading conditions) is investigated to demonstrate the capability of the proposed FEM-SGBEM coupling in the analysis of nano-sized crack problems. This numerical example should provide the complete information and insight of the influence of the surface stresses on elastic responses and fracture data within the context of three-dimensional problems. In the Gurtin-Murdoch surface elasticity model, the surface elastic constants are related to the in-

plane terms in the governing equations of the surface and should significantly affects the in-plane behavior of cracks under mixed-mode loading conditions. Therefore, similar to the previous problem, three different models are considered in this case. The model-1 is the classical model when the surface stresses are ignored. The classical solution of the crack sliding displacements and stresses in the vicinity of the crack front can be found in Kachanov *et al.* (2004). The model-2 is associated with a simplified version of Gurtin-Murdoch surface elasticity model where the in-plane surface elasticity is only treated. The last model, model-3, again corresponds to the full version of Gurtin-Murdoch model.

Let us consider a penny-shaped crack of radius a embedded in an isotropic, linear elastic infinite medium as indicated in Figure 5.7(a). The crack is subjected to the self-equilibrated, uniformly distributed shear traction $t_1^+ = -t_1^- = \tau_0$. Three meshes, adopted as depicted in Figure 5.7(b), are employed in the analysis.

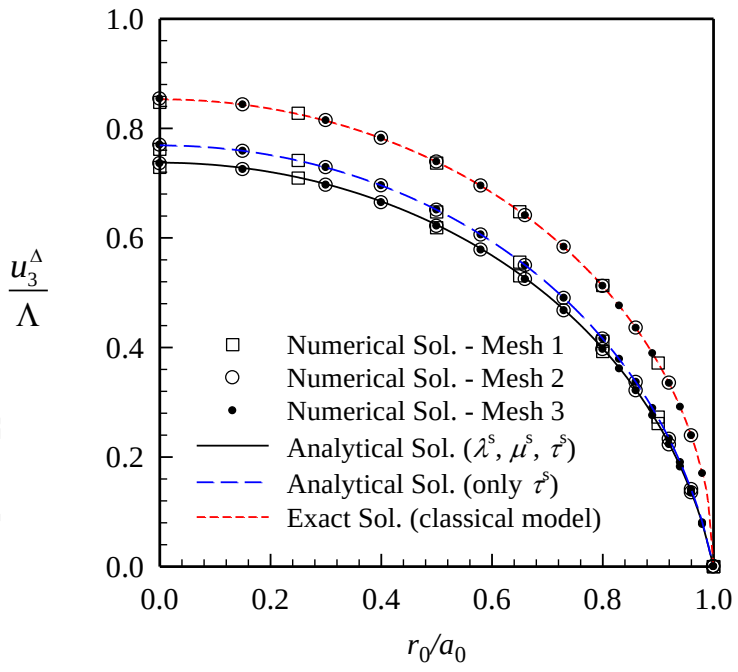

Figure 5.2: Comparison of the normalized crack opening displacements of a penny-shaped crack under uniformly distributed normal traction obtained from three different models for $E = 107\,GPa$, $\nu = 0.33$, $\lambda^s = 4.4939\,N/m$, $\mu^s = 2.7779\,N/m$ and $\tau^s = 0.6056\,N/m$.

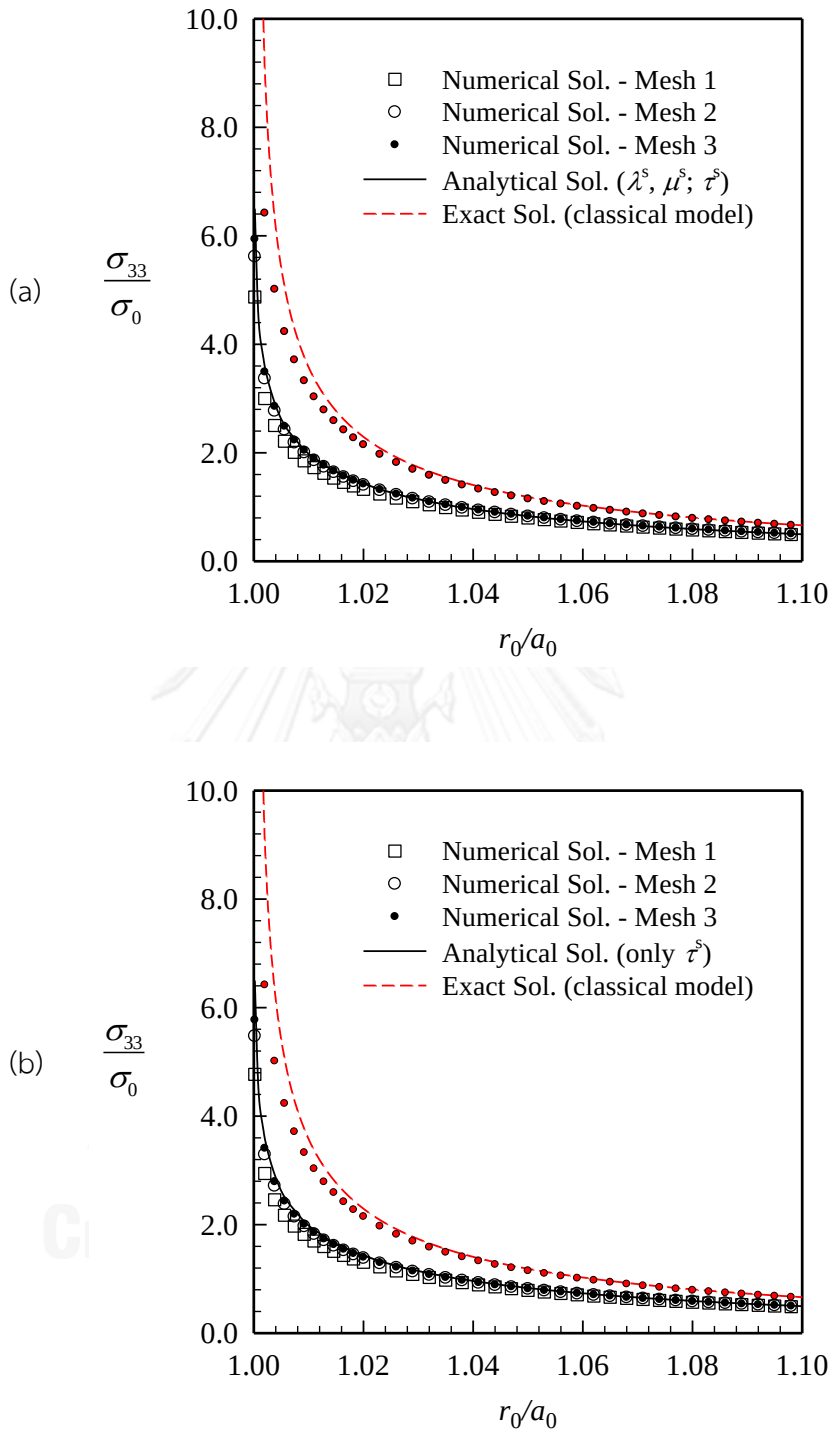

Figure 5.3: Normalized vertical stresses σ_{33}/σ_0 in the vicinity of the crack-front of a penny-shaped crack under uniformly distributed normal traction for $E = 107\,GPa$, $\nu = 0.33$, $\lambda^s = 4.4939\,N/m$, $\mu^s = 2.7779\,N/m$ and $\tau^s = 0.6056\,N/m$: results for (a) model-3 and (b) model-2.

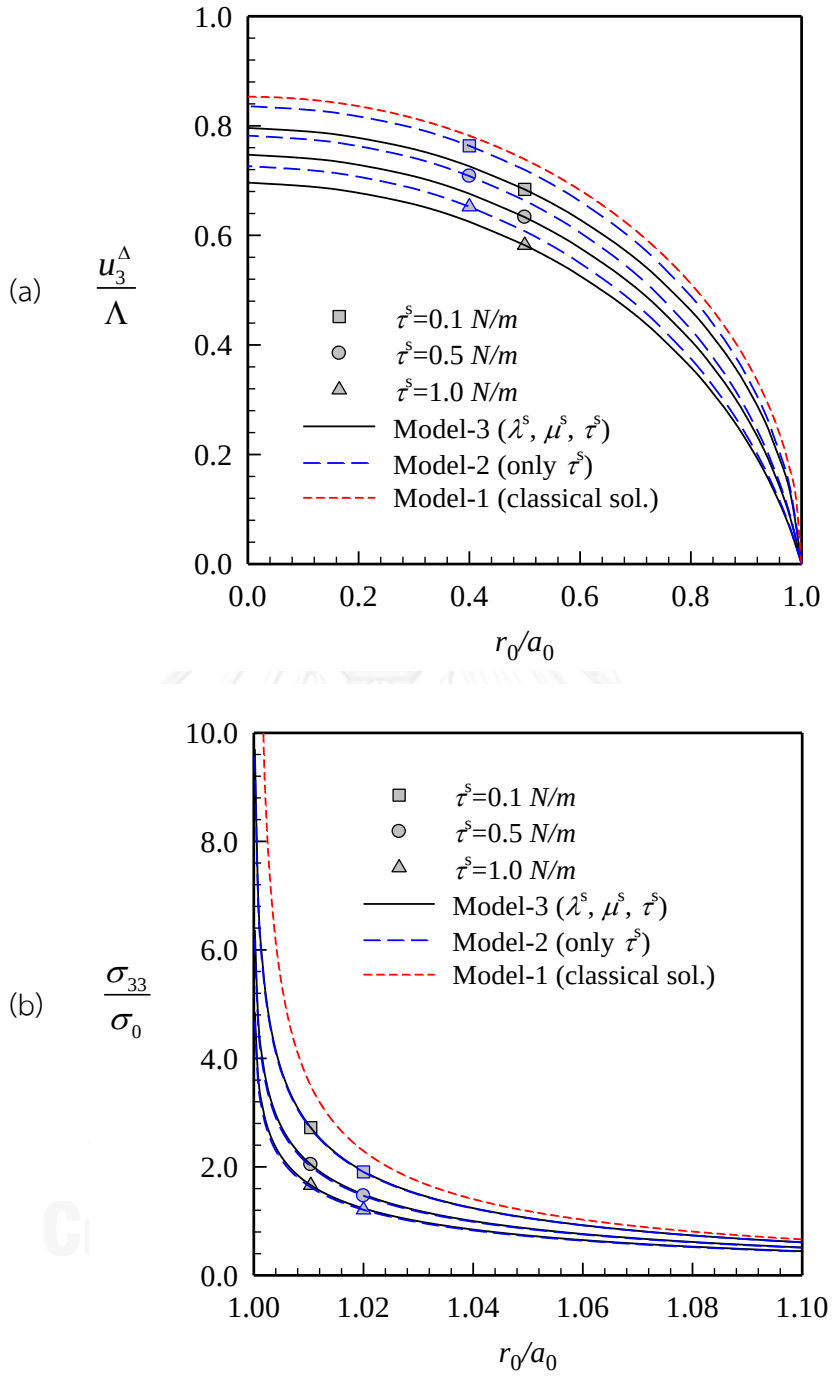

Figure 5.4: Penny-shaped crack under uniformly distributed normal traction for different residual surface tension τ^s ranging from 0.1 to 1 *N/m;* $E = 107\,GPa$, $\nu = 0.33$, $\lambda^s = 4.4939\,N/m$, $\mu^s = 2.7779\,N/m$: (a) normalized crack opening displacements and (b) normalized near-tip vertical stresses σ_{33}/σ_0 obtained by using mesh-3.

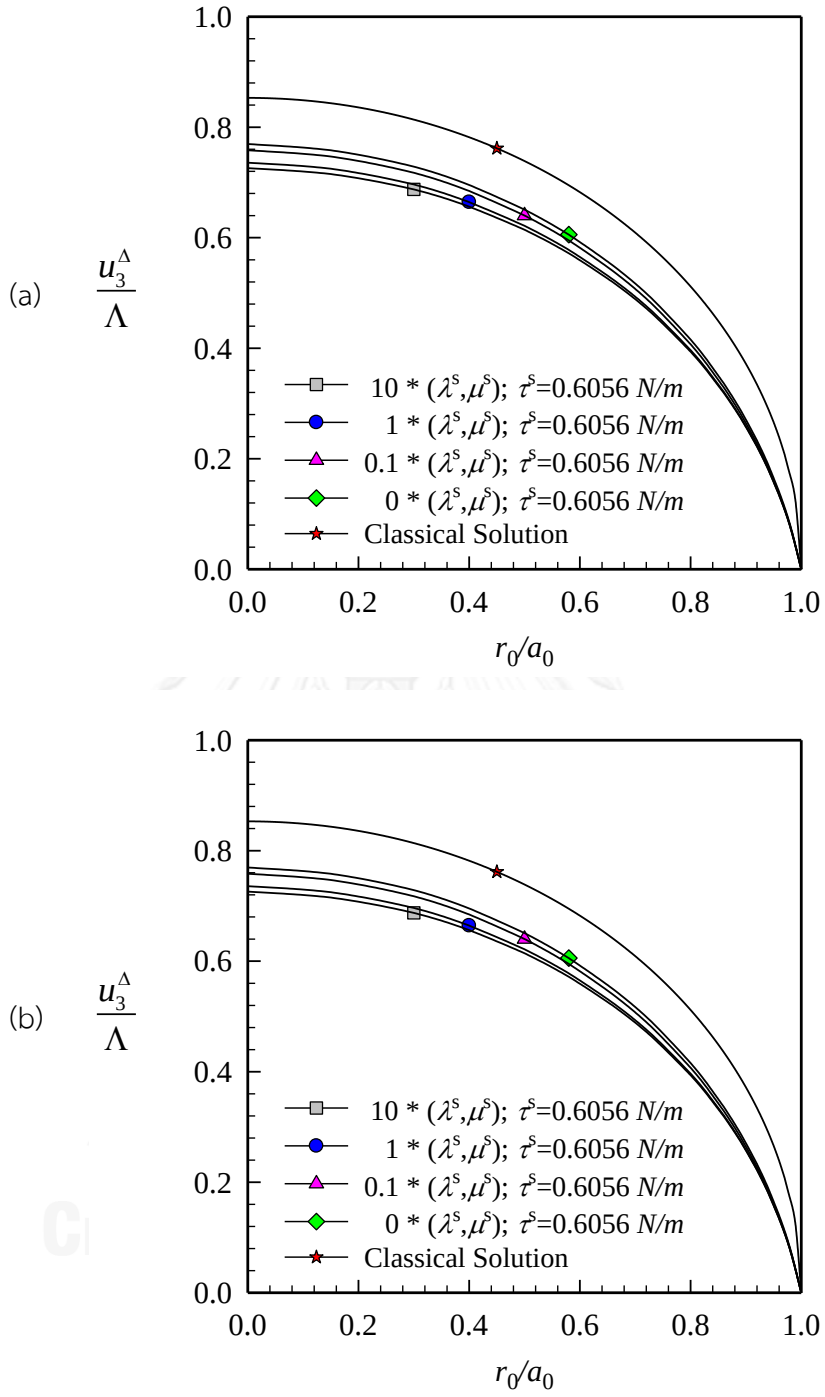

Figure 5.5: Penny-shaped crack under uniformly distributed normal traction, for different surface elasticity constants (λ^s, μ^s) ranging from 0; 0.1; 1 and 10 times of their initial value ($\lambda^s = 4.4939\,N/m$, $\mu^s = 2.7779\,N/m$); $E = 107\,GPa$, $\nu = 0.33$, $\tau^s = 0.6056\,N/m$: (a) normalized crack opening displacements and (b) normalized near-tip vertical stresses obtained by using mesh-3.

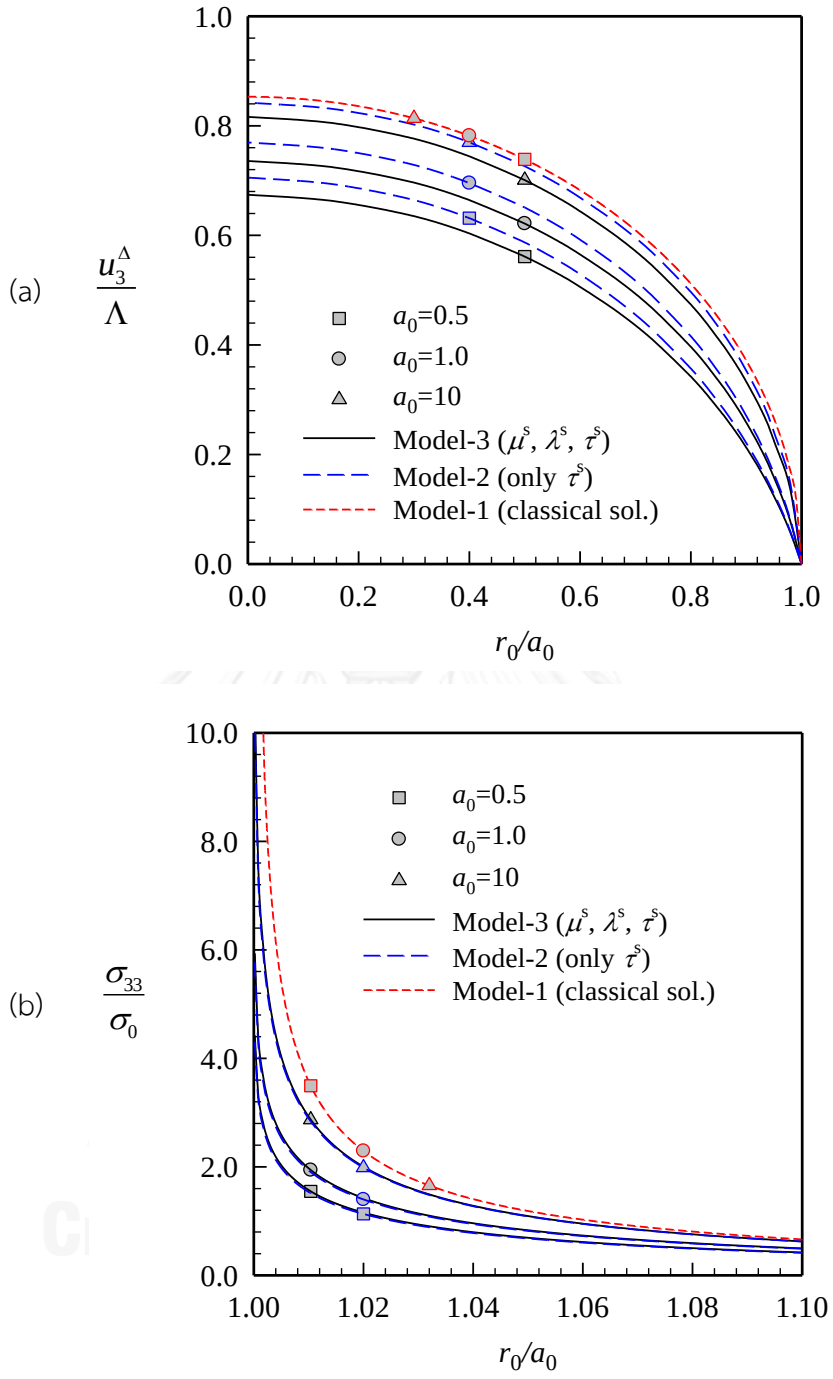

Figure 5.6: Penny-shaped crack under uniformly distributed normal traction, for three different crack radii $a_0 = a/\Lambda = 0.5, 1.0, 10$, and for $E = 107\,GPa$, $\nu = 0.33$, $\lambda^s = 4.4939\,N/m$, $\mu^s = 2.7779\,N/m$, $\tau^s = 0.6056\,N/m$: (a) normalized crack opening displacements and (b) normalized near-tip vertical stresses obtained by using mesh-3.

Results for the crack sliding displacements (CSD) and the stresses in the vicinity of the crack front along the x_1-direction (the direction of the applied shear traction) are reported in Figure 5.8. It is seen that numerical solutions exhibit very good convergence for both the CSD and the near-tip stresses. It can be pointed out from results in Figure 5.8(a) that the surface stresses significantly influence the CSD. Especially, by comparing the CSD predicted by the model-2 and the model-3, the discrepancy between them cannot be well recognized; as a results, it can be concluded that the in-plane elastic constants prominently affect the CSD of cracks under in-plane loading conditions whereas the influence of the residual surface tension on the CSD is insignificant. It also can be argued from Figure 5.8(b) that the shear stress σ_{13} near the crack front is strongly influenced by the surface stresses. The magnitude of the predicted stresses near the crack front reduces considerably from the classical solution when the surface stresses are present. In particular, the in-plane elastic constants affect substantially the in-plane quantities for cracks under in-plane loadings in comparison with the residual surface tension.

To further understand the role of each parameter in the Gurtin-Murdoch model on the predicted solutions of mixed-mode crack problems, following four cases obtained by varying the value of the in-plane elastic constants and the residual surface tension are considered:

- Case 1: Both the in-plane elastic constants (λ^s, μ^s) are varied from 0, 1, 5 and 10 times of their initial value ($\lambda^s = 4.4939\ N/m$, $\mu^s = 2.7779\ N/m$) whereas the residual surface tension remains fixed.
- Case 2: The residual surface tension (τ^s) is ranged from 0, 1, 5 and 10 times of its initial value ($\tau^s = 0.6056\ N/m$) whereas the in-plane elastic constants remain fixed.
- Case 3: Only the parameter λ^s is varied from 0, 1, 5 and 10 times of its initial value ($\lambda^s = 4.4939\ N/m$) whereas all remaining parameters remain fixed.
- Case 4: Only the parameter μ^s is varied from 0, 1, 5 and 10 times of its initial value ($\mu^s = 2.7779\ N/m$) whereas all remaining parameters remain fixed.

The normalized CSD and the normalized shear stresses in the vicinity of the crack front along the x_1-direction are reported in Figures 5.9-5.10 for all four cases. It can be seen that the surface elastic constants (λ^s, μ^s) in the Gurtin-Murdoch model significantly reduce the CSD and the shear stresses near the crack front, whereas the residual surface tension almost have no effect on the predicted solution of mixed-

mode crack problems. It can be also pointed out that the parameter μ^s in the Gurtin-Murdoch model exhibits more prominent effect on the CSD and the near-tip shear stresses in comparison with the parameter λ^s (see Figure 5.9(c)-(d) and Figure 5.10(c)-(d)).

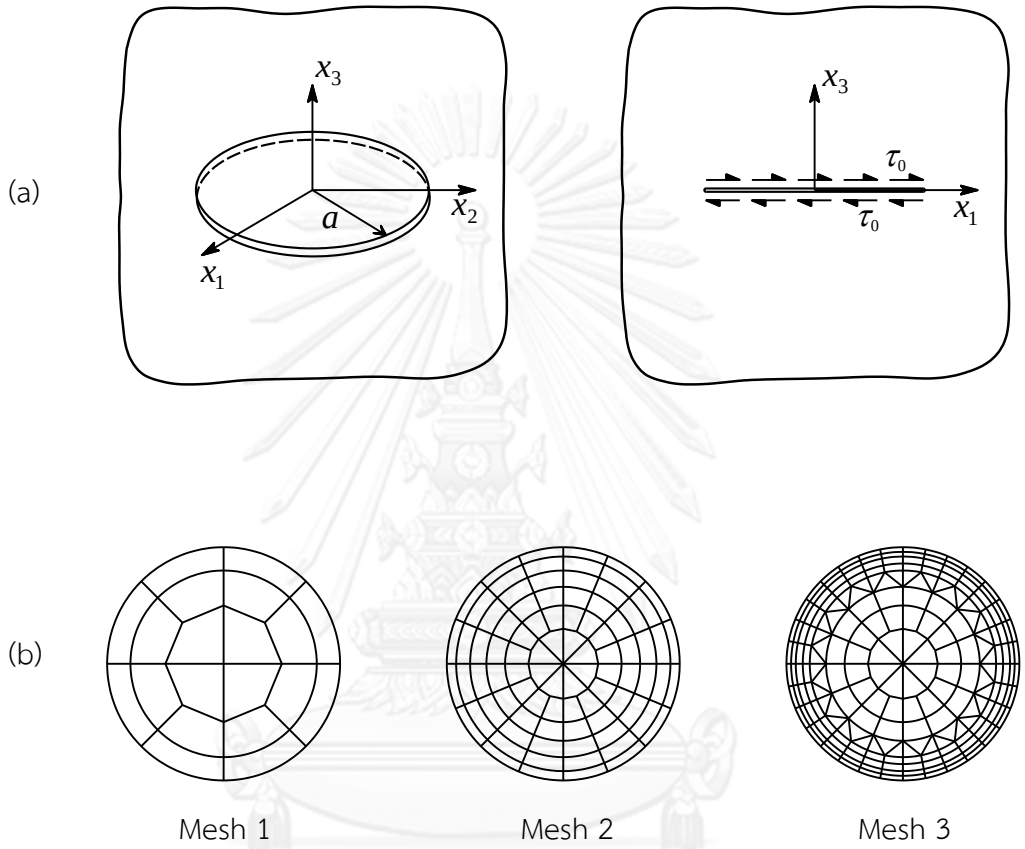

Figure 5.7: (a) Schematic of a penny-shaped crack of radius a embedded in an isotropic, linear elastic infinite medium subjected to uniformly distributed shear traction $t_1^+ = -t_1^- = \tau_0$; (b) meshes adopted in the analysis. Mesh 1: 20 elements and 77 nodes. Mesh 2: 88 elements and 297 nodes. Mesh 3: 216 elements and 665 nodes.

To investigate the size-dependent behavior of the solution of mixed-mode crack problems due to the presence of the surface stresses, the CSD and the shear stresses in the vicinity of the crack-front for different crack radii $a_0 = 0.5, 1.0, 10$ are considered. Results of the crack sliding displacement and the shear stresses along the x_1-direction are shown in Figure 5.11.

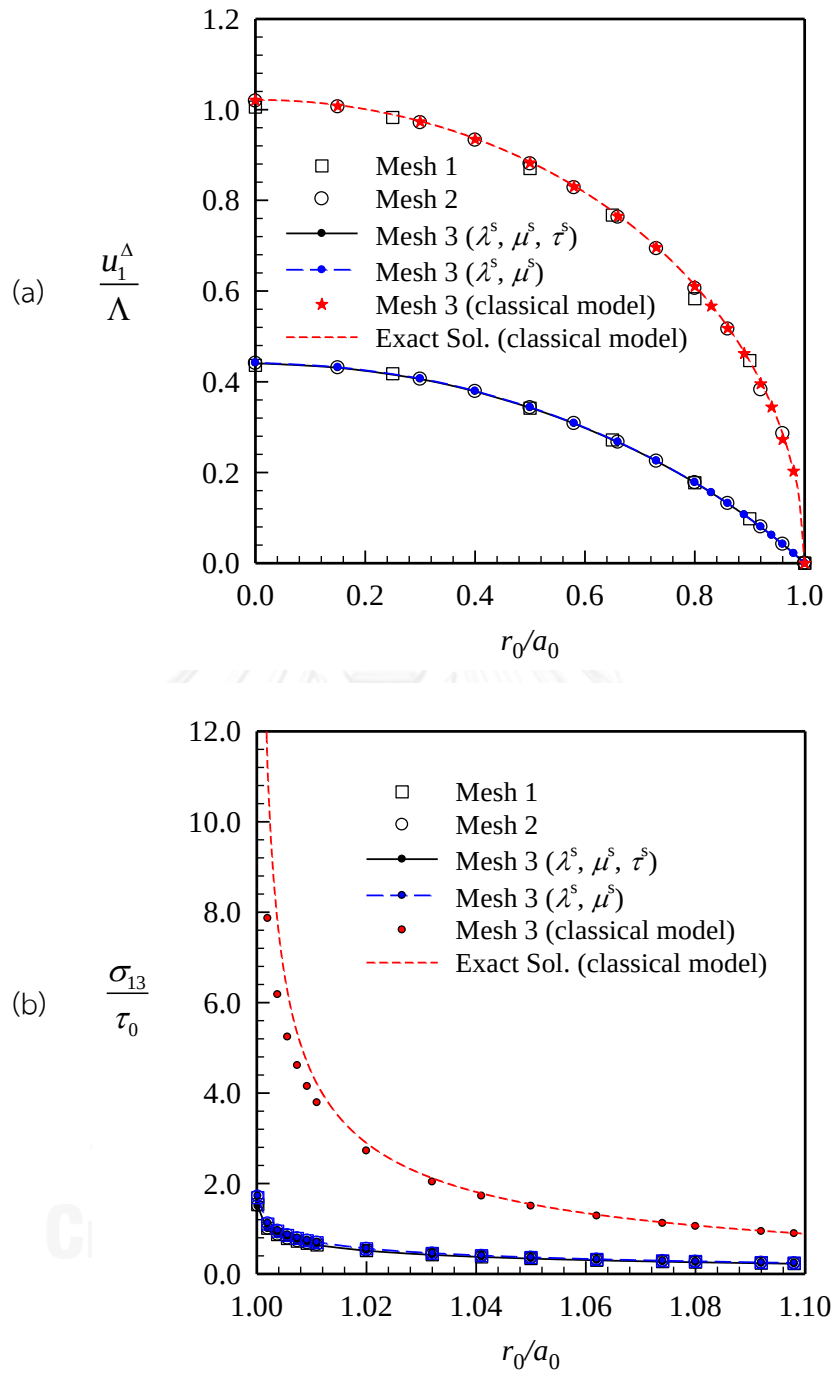

Figure 5.8: A penny-shaped crack under uniformly distributed shear traction, for $E = 107\,GPa$, $\nu = 0.33$, $\lambda^s = 4.4939\ N/m$, $\mu^s = 2.7779\ N/m$, $\tau^s = 0.6056\ N/m$: (a) normalized crack sliding displacements and (b) normalized near-tip shear stress along the x_1-direction.

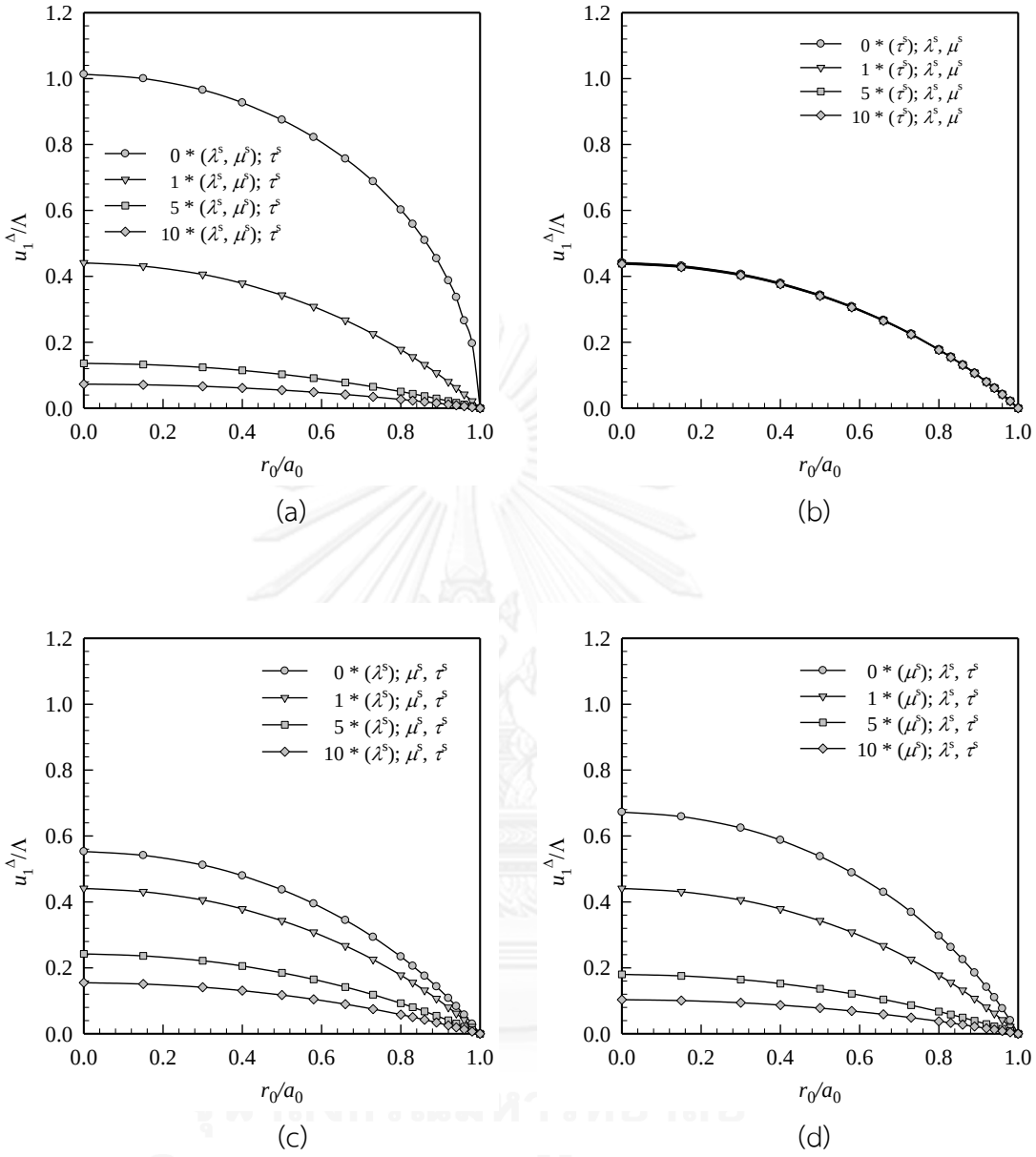

Figure 5.9: Normalized crack sliding displacements of a penny-shaped crack under uniformly distributed shear traction for $E = 107\,GPa$, $\nu = 0.33$ in four cases: (a) different values of (λ^s, μ^s) with $\tau^s = 0.6056\ N/m$; (b) different values of τ^s with $\lambda^s = 4.4939\ N/m$, $\mu^s = 2.7779\ N/m$; (c) different values of λ^s with $\mu^s = 2.7779\ N/m$, $\tau^s = 0.6056\ N/m$ and (d) different values of μ^s with $\lambda^s = 4.4939\ N/m$, $\tau^s = 0.6056\ N/m$ obtained by using mesh-3.

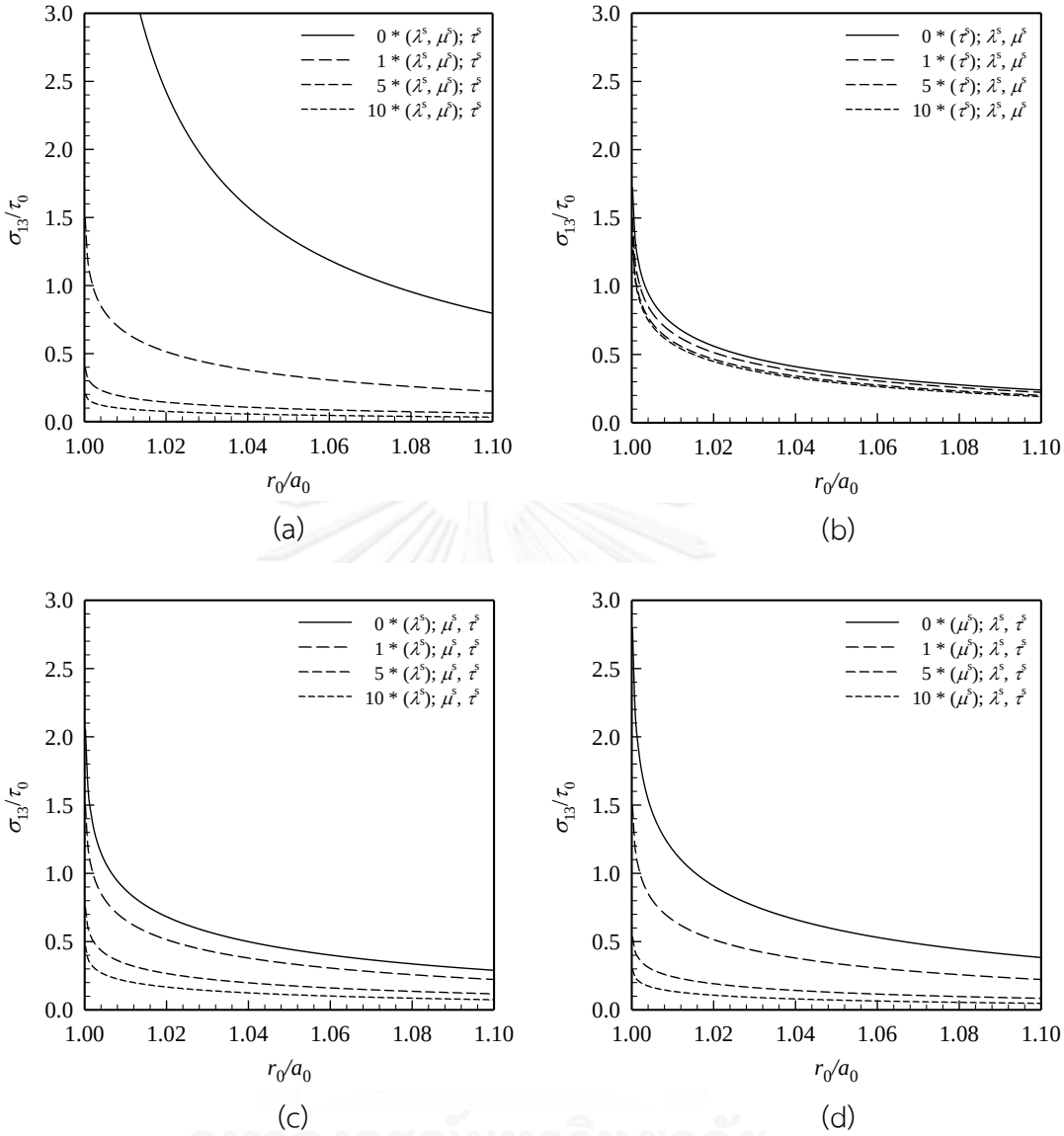

Figure 5.10: Normalized near-tip shear stresses of a penny-shaped crack under uniformly distributed shear traction for $E = 107\,GPa$, $\nu = 0.33$ in four cases: (a) different values of (λ^s, μ^s) ; (b) different values of τ^s; (c) different values of λ^s and (d) different values of μ^s obtained by using mesh-3.

It can be seen in Figure 5.11 that the normalized CSD and the normalized shear stresses in the vicinity of the crack front along the x_1-direction obtained from the model-2 and model-3 are apparently size-dependent. This finding agrees with the case of mode-I loading conditions. When the crack-size decreases, the influence of the surface stresses on elastic responses of cracks subjected to mixed-mode loading conditions becomes more significant in the sense that the medium is stiffer.

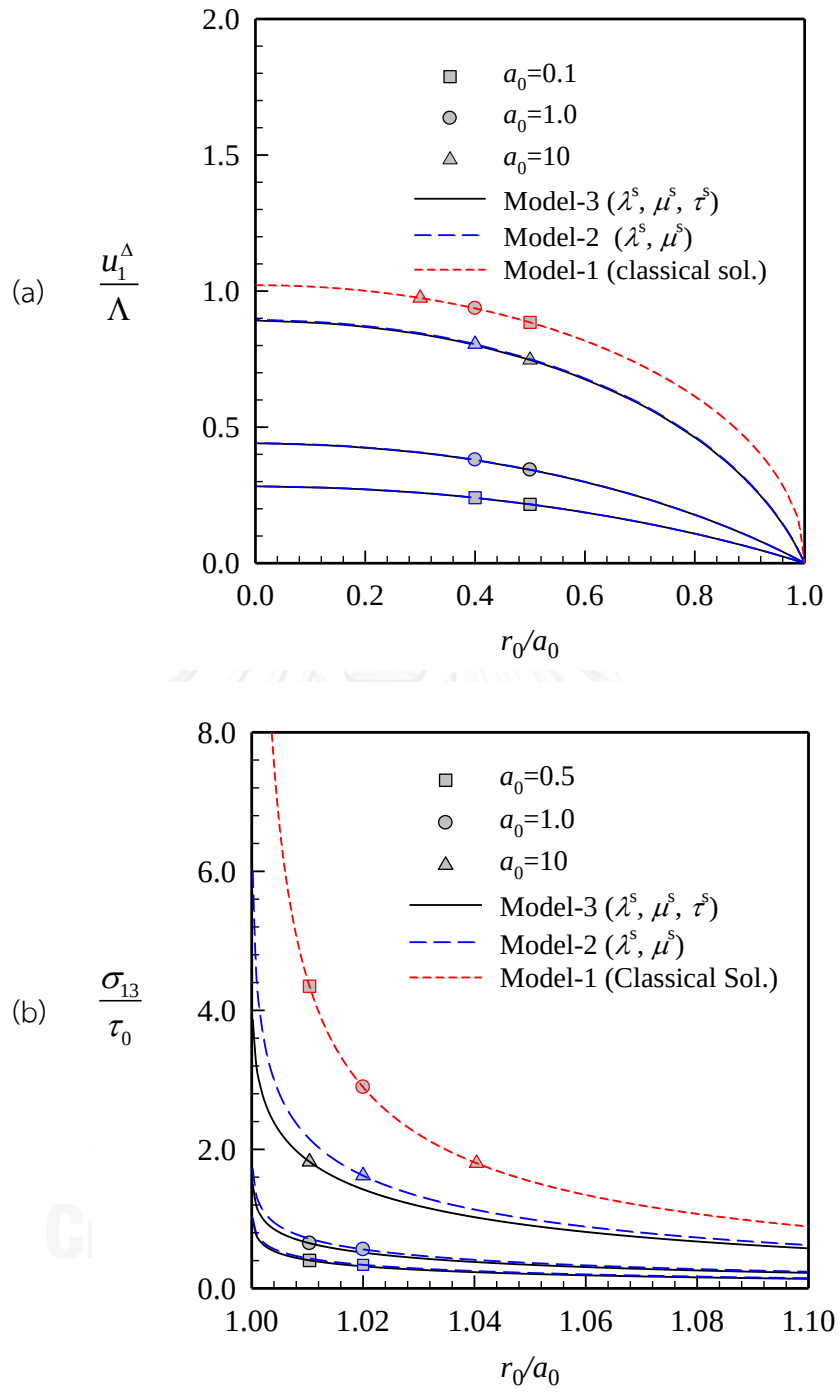

Figure 5.11: A penny-shaped crack under uniformly distributed shear traction, for different crack radii $a_0 = a/\Lambda = 0.5, 1.0, 10$, for $E = 107\,GPa$, $\nu = 0.33$, $\lambda^s = 4.4939\,N/m$, $\mu^s = 2.7779\,N/m$ and $\tau^s = 0.6056\,N/m$: (a) normalized crack sliding displacements and (b) normalized near-tip shear stresses obtained by using mesh-3.

5.3 Elliptical Crack

To demonstrate the capability of the proposed FEM-SGBEM coupling technique for treating crack problems of arbitrary shapes with consideration of the surface stress effects, an elliptical crack embedded in an isotropic, linear elastic infinite domain is considered (see Figure 5.12(a)). The material in which the crack is embedded is Si [100] where properties of the bulk material are $E = 107\,GPa$, $\nu = 0.33$ and the surface elastic constants and the residual surface tension are obtained from Miller and Shenoy (2000). The crack-front is parameterized in terms the angle θ by

$$x_1 = a\cos\theta, \quad x_2 = b\sin\theta, \quad x_3 = 0; \quad \theta \in [0, 2\pi] \tag{5.1}$$

where a and b are the major and minor semi-axes of the crack, respectively. In this numerical example, two loading conditions are investigated. The first case is associated with the crack subjected to the self-equilibrated, uniformly distributed normal traction $t_3^+ = -t_3^- = \sigma_0$ (see Figure 5.12(b)) whereas the other case corresponds to the crack subjected to the self-equilibrated, uniformly distributed shear traction $t_2^+ = -t_2^- = \tau_0$ (see Figure 5.12(c)). Numerical results are presented for three different aspect ratios $a/b = 1, 2, 3$ and three meshes shown in Figure 5.12(d) are adopted to model the elliptical crack (Mesh 1 has 20 elements and 77 nodes; Mesh 2 has 88 elements and 297 nodes and Mesh 3 has 216 elements and 665 nodes).

5.3.1 Normal Traction

For this particular loading condition, results obtained from three different models indicated below are presented and compared:

- Model-1 represents the classical model without the influence of the surface stresses. The classical solution of the crack opening displacements and the vertical stresses in the vicinity of crack front can be found in Zeng-shen (1982) and Kassir and Sih (1975), respectively.
- Model-2 is associated with the simplified version of Gurtin-Murdoch model without the contribution of surface elastic constants.
- Model-3 is the full version of Gurtin-Murdoch model where the surface elastic constants (λ^s, μ^s) and the residual surface tension (τ^s) are included.

The convergence study of the normalized crack opening displacement (COD) and the normalized vertical stress along the minor axis for the aspect ratio $a/b = 2$

using the model-2 and model-3 are reported in Figure 5.13. As can be seen from this Figure, the predicted solutions for COD and the vertical stresses near the crack front show good convergence. The normalized CODs and the normalized vertical stresses σ_{33}/σ_0 along the minor axis of the crack are also presented in Figure 5.14 for the aspect ratios $a/b=1,2,3$ and all three models. As can be observed in Figure 5.14, when the aspect ratio a/b increases, the influence of the surface stresses on the CODs and the near-tip vertical stresses decreases. It can also be remarked that for the mode-I crack problem, the difference between solutions predicted by the full version and simplified version of Gurtin-Murdoch model is insignificant. As a result, the simplified version of Gurtin-Murdoch model can be utilized to investigate the nano-scale influence of mode-I crack problems to simplify the calculation.

In order to investigate the role of the residual surface tension on responses of cracks under the mode-I loading conditions, the normalized CODs and the normalized vertical stresses σ_{33}/σ_0 are computed for different values of the residual surface tension τ^s ranging from 0.1 to 1.0 N/m. Solutions obtained from the model-3 are reported in Figure 5.15 for the aspect ratio $a/b=2$. It can be concluded from this set of results that the influence of the residual surface tension is also significant and the medium becomes much stiffer when τ^s increases.

To examine the size-dependent behavior of predicted results due to the presence of the residual surface tension, the CODs and the near-tip vertical stresses for $b_0=0.5,1.0,10$ and the aspect ratio $a/b=2$ are shown in Figure 5.16. As can be seen in Figure 5.16, the normalized CODs and normalized vertical stresses are clearly size-dependent. This is in contrast with the classical case (i.e., without the surface stress effects) where the solutions are size-independent. In particular, when the crack-size or the aspect ratio decreases, the influence of the surface stresses becomes more significant in the sense that the medium is stiffer.

5.3.2 Shear Traction

Consider, next, an elliptical crack subjected to uniform shear traction τ_0 as shown in Figure 5.12(c). The direction of the applied shear traction is taken in the x_2-direction as shown schematically in Figure 5.12(c). As a consequence of the anti-symmetric nature of the applied load, only mode-II (sliding mode) and mode-III (tearing mode) responses are investigated. Again, following three different models are considered in the numerical study:

- Model-1 is associated with the classical model where the surface stresses are not included. It is remarked that the classical solution of the crack sliding displacement and the shear stresses in the vicinity of the crack front can be found in Kassir and Sih (1975).
- Model-2 corresponds to the simplified version of Gurtin-Murdoch model where only the in-plane elastic constants are considered.
- Model-3 represents the full version of Gurtin-Murdoch model where both the in-plane elastic constants and the residual surface tension are considered.

The numerical results are obtained using the three meshes as indicated in Figure 5.12(d) to confirm the convergence of numerical solutions. The convergence study of the crack sliding displacement (CSD) and the shear stress σ_{23} in the vicinity of the crack front along the minor-axis are reported in Figure 5.17. It can be observed from these results that the proposed technique yields converged solutions for both the CSD and the shear stress.

The Normalized CSDs and the normalized shear stresses σ_{23}/τ_0 near the crack front along the minor-axis are presented in Figure 5.18 for three aspect ratios $a/b = 1,\ 2,\ 3$ and for three models to show the influence of the surface stresses on responses of mixed-mode cracks. Results shown in Figure 5.18(a) indicate that solutions of the CSDs predicted by the model-2 and model-3 are almost identical, whereas solutions of shear stresses σ_{23} for this particular case (see Figure 5.18(b)) are slightly different. Comparing with the classical solution (model-1), it can be easily recognized that the surface stresses (especially the in-plane elasticity constants) significantly reduce the CSDs and the shear stresses in the neighborhood of the crack front. This confirms that presence of the surface stresses renders the medium much stiffer.

To further examine the influence of the in-plane elastic constants (λ^s, μ^s), these parameters are varied from 0, 0.1, 0.5 and 1 times of their initial value ($\lambda^s = 4.4939\ N/m$, $\mu^s = 2.7779\ N/m$) while the residual surface tension remains fixed. The numerical study is conducted only for two aspect ratios $a/b = 2,\ 3$ and the model-3. The normalized CSDs and the shear stresses σ_{23} in the vicinity of the crack front along the minor-axis are reported in Figures 5.19. It can be seen that the surface elastic constants (λ^s, μ^s) in Gurtin-Murdoch surface elasticity theory significantly reduce the CSD and the near-tip shear stresses, whereas the residual surface tension almost have no effect on the solution of mixed-mode crack problems.

To investigate the size-dependent behavior of the solution of mixed-mode crack problems due to the presence of the surface stresses, the elliptical crack of the aspect ratio $a/b = 2$ is examined for different sizes of the minor semi-axis $b_0 = 0.5, 1.0, 10$. Results of the CSDs and the shear stresses in the vicinity of the crack-front along the minor-axis are shown in Figure 5.20. It can be seen that the normalized CSDs and normalized shear stresses along the minor-axis predicted by the model-2 and model-3 are size-dependent. Again, this is in contrast with the classical case (i.e., without the surface stress effects) where the solutions are essentially size-independent upon proper normalization. When the crack-size decreases, the influence of surface stresses on the predicted responses becomes more significant.

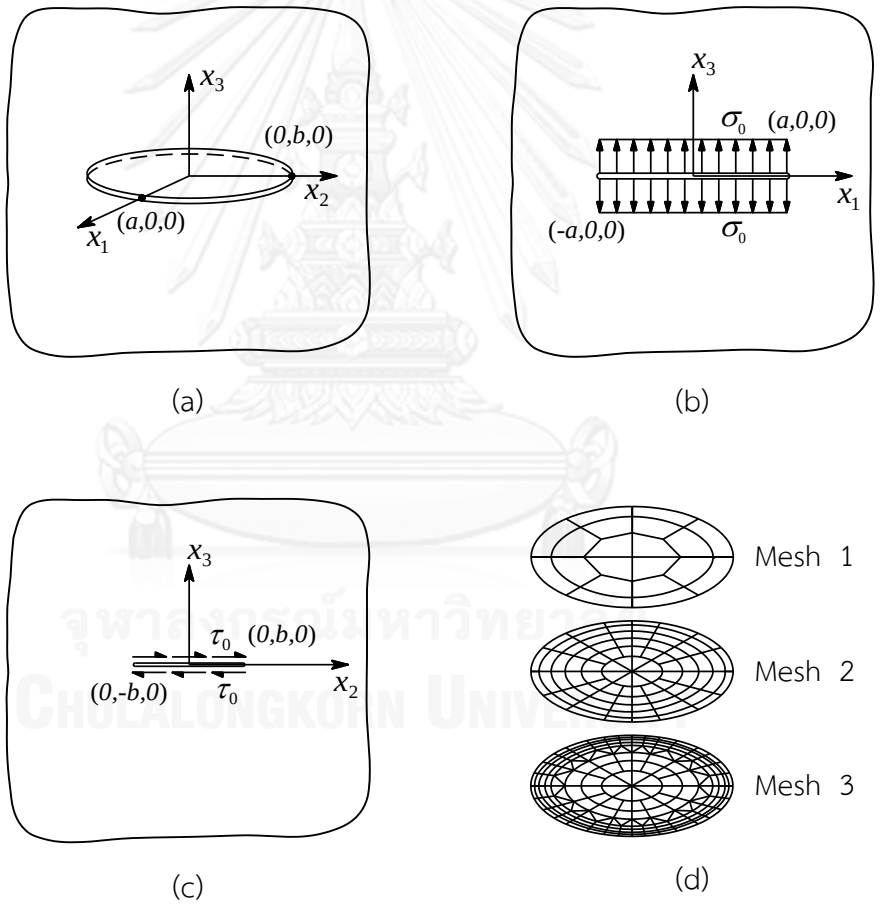

Figure 5.12: (a) Schematic of an elliptical crack embedded in an isotropic, linear elastic infinite medium; (b) both surfaces of the crack subjected to uniformly distributed normal traction $t_3^+ = -t_3^- = \sigma_0$; (c) both surfaces of the crack subjected to uniformly distributed shear traction $t_2^+ = -t_2^- = \tau_0$; (d) meshes used in the analysis.

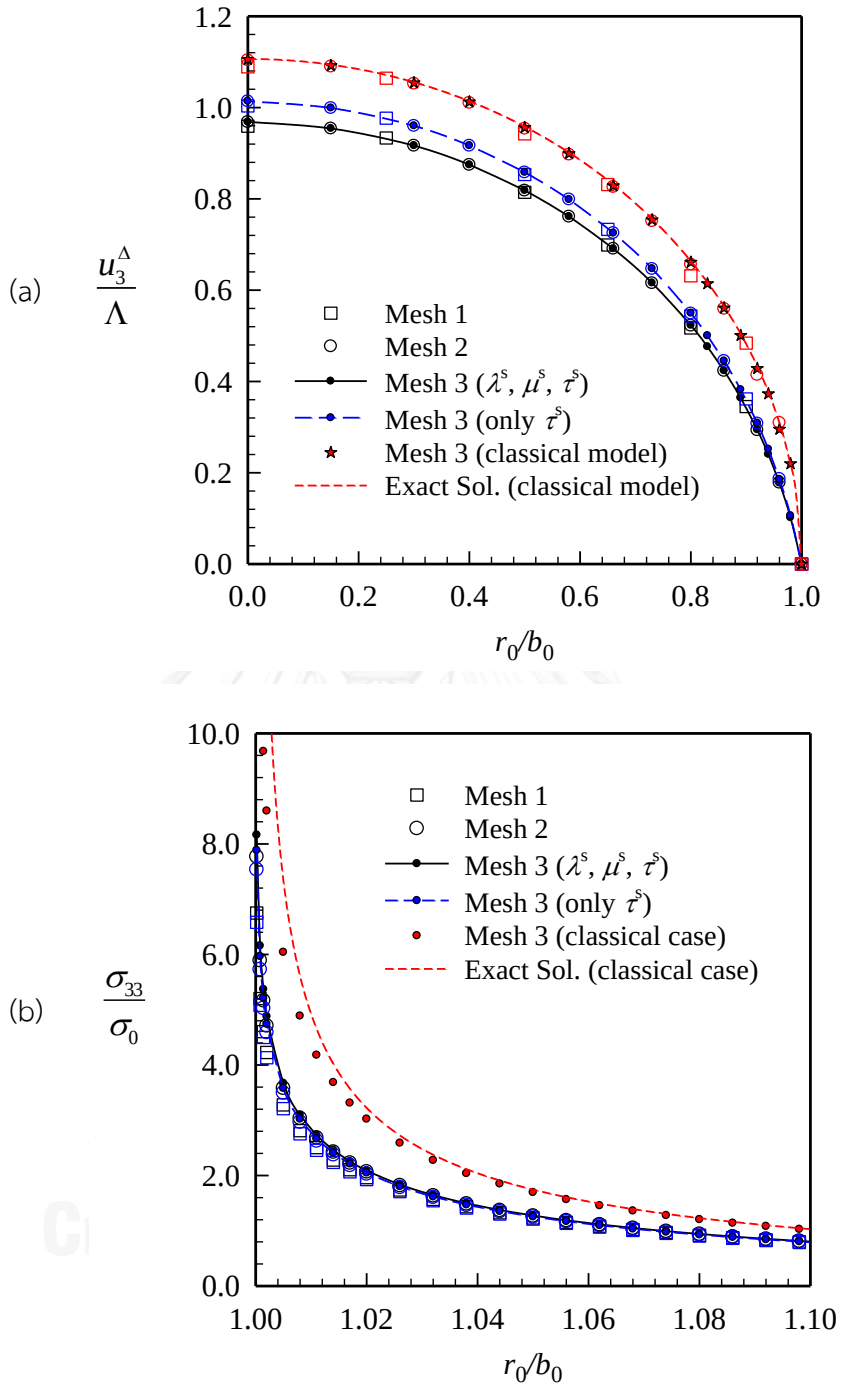

Figure 5.13: Convergence study of an elliptical crack under uniformly distributed normal traction for three different models and the aspect ratio $a/b=2$, for $E=107\,GPa$, $\nu=0.33$, $\lambda^s=4.4939\,N/m$, $\mu^s=2.7779\,N/m$, $\tau^s=0.6056\,N/m$: (a) normalized crack opening displacements along minor-axis and (b) normalized near-tip vertical stresses along the minor-axis.

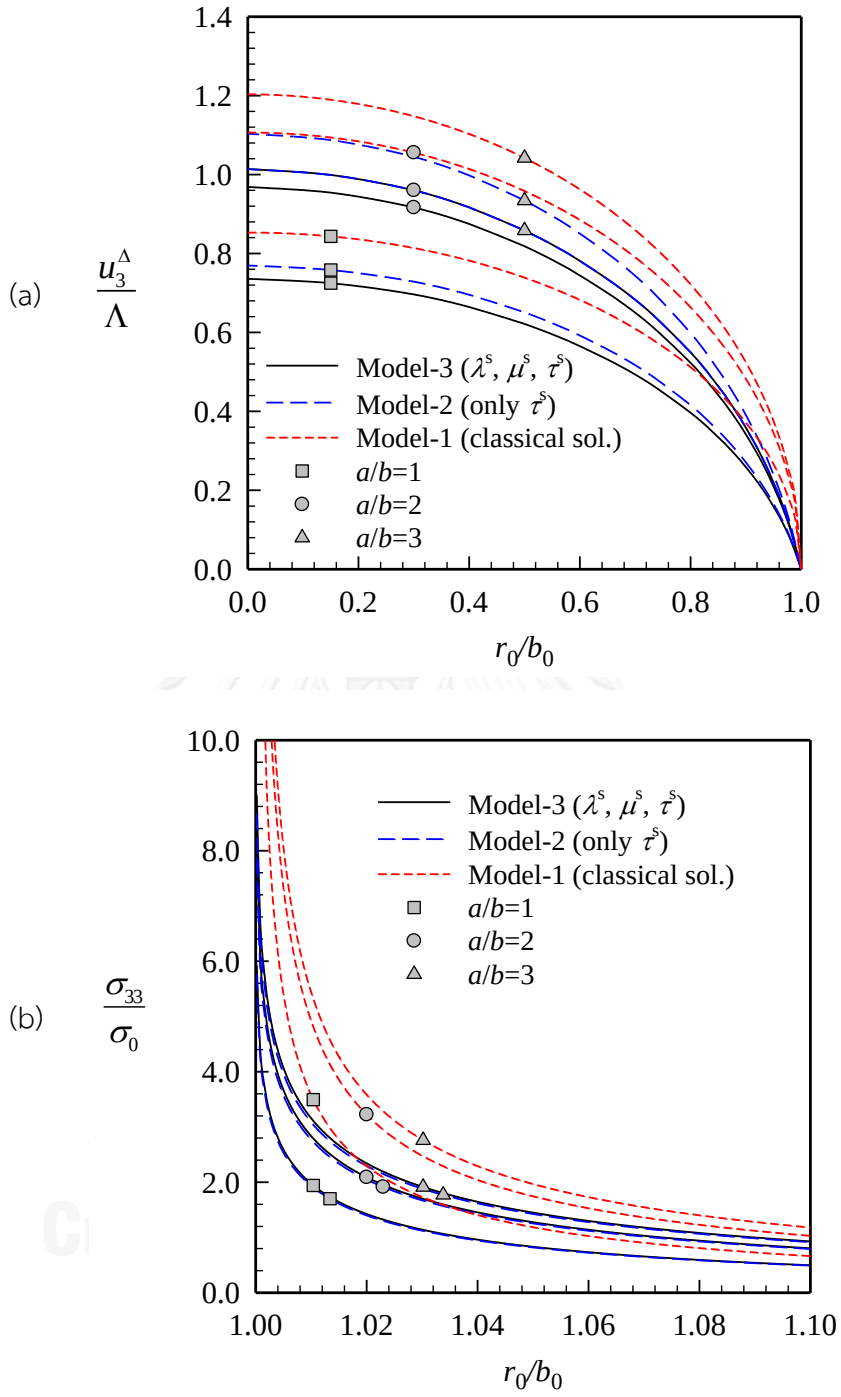

Figure 5.14: Comparison of results of an elliptical crack under uniformly distributed normal traction for three different models and three different aspect ratios $a/b = 1, 2, 3$, for $E = 107\,GPa$, $\nu = 0.33$, $\lambda^s = 4.4939\,N/m$, $\mu^s = 2.7779\,N/m$ and $\tau^s = 0.6056\,N/m$: (a) normalized CODs along minor-axis and (b) normalized near-tip vertical stresses along minor-axis obtained by using mesh-3.

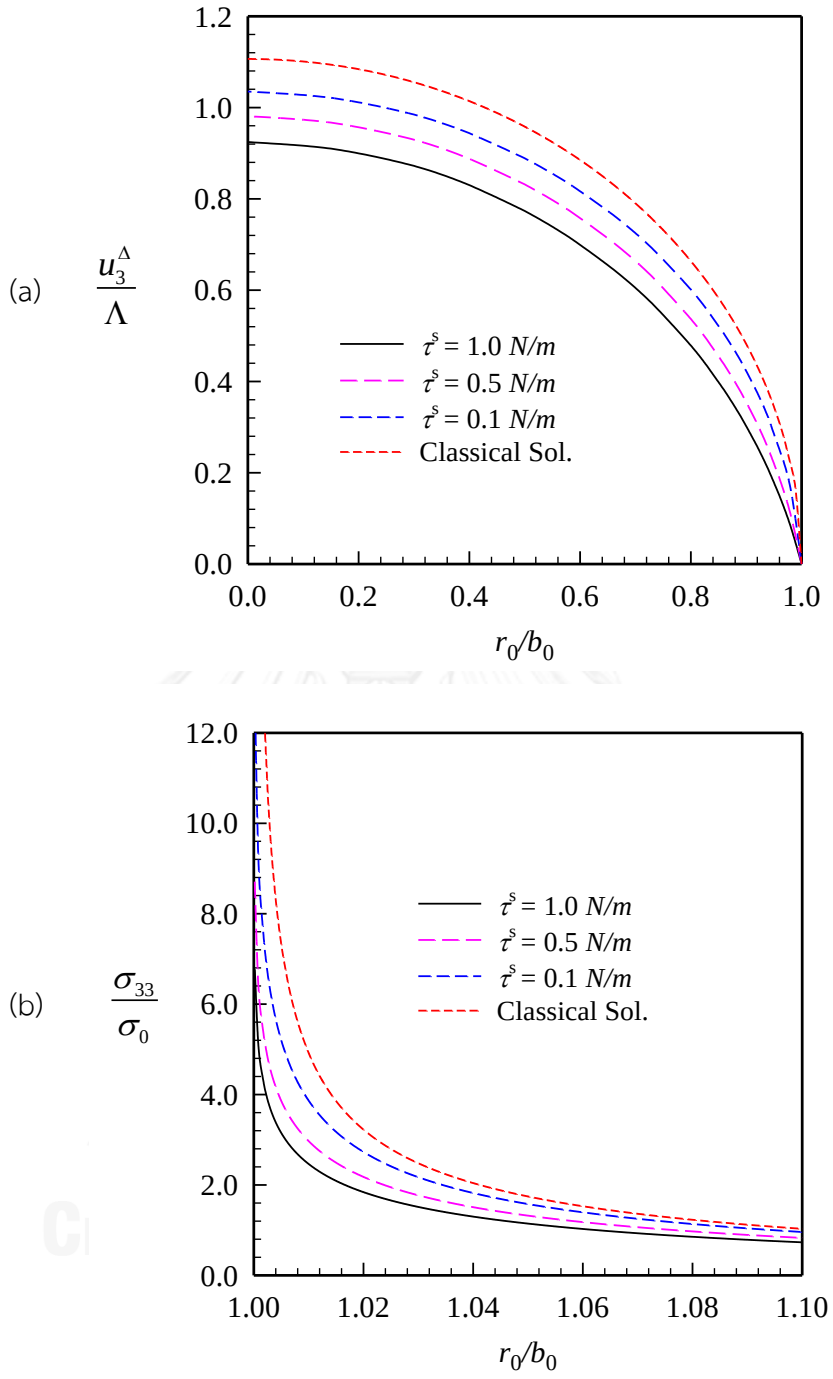

Figure 5.15: Elliptical crack under uniformly distributed normal traction for the model-3 with the aspect ratio $a/b = 2$ and different values of the residual surface tension τ^s, for $E = 107\,GPa$, $\nu = 0.33$, $\lambda^s = 4.4939\,N/m$, $\mu^s = 2.7779\,N/m$: (a) normalized CODs along the minor axis and (b) normalized near-tip vertical stresses along the minor axis obtained by using mesh-3.

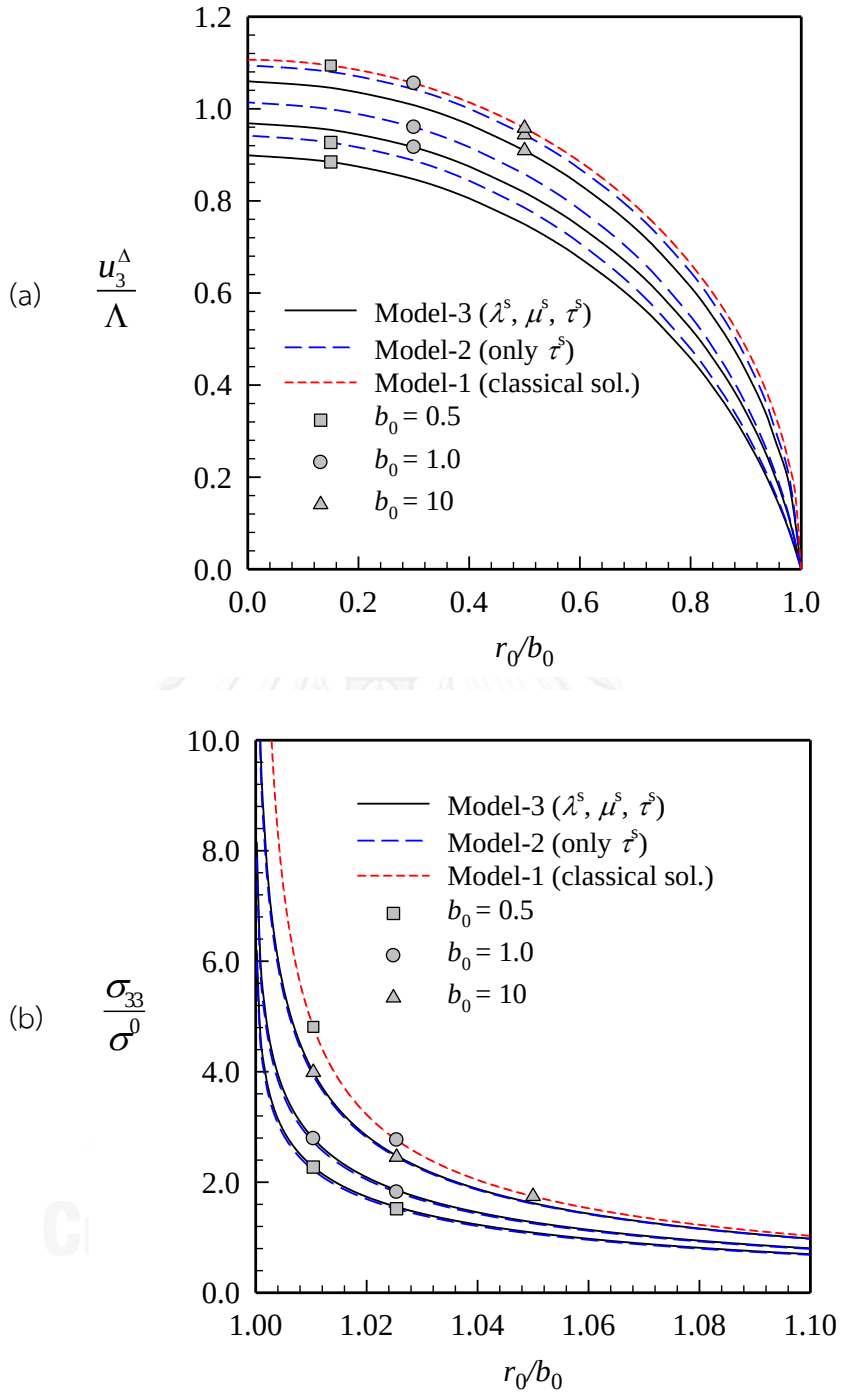

Figure 5.16: Elliptical crack under uniformly distributed normal traction for three different models with different minor semi-axes $b_0 = b/\Lambda = 0.5, 1.0, 10$ and the aspect ratio $a/b = 2$, for $E = 107\,GPa$, $\nu = 0.33$, $\lambda^s = 4.4939\,N/m$, $\mu^s = 2.7779\,N/m$ and $\tau^s = 0.6056\,N/m$: (a) normalized CODs along the minor axis and (b) normalized near-tip vertical stresses along the minor-axis obtained by using mesh-3.

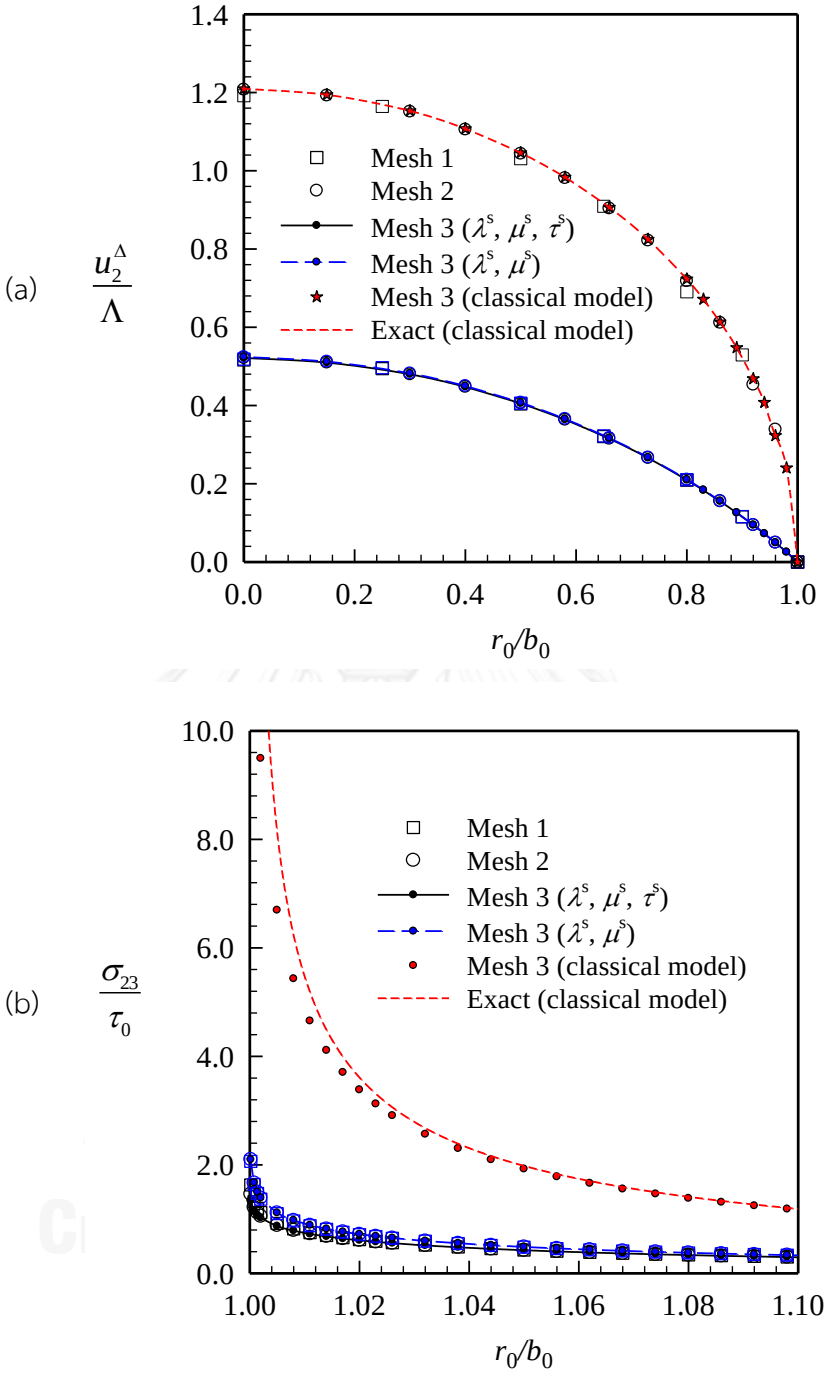

Figure 5.17: Convergence study of an elliptical crack under uniformly distributed shear traction in the x_2-direction with the aspect ratio $a/b = 2$, for $E = 107\,GPa$, $\nu = 0.33$, $\lambda^s = 4.4939\,N/m$, $\mu^s = 2.7779\,N/m$ and $\tau^s = 0.6056\,N/m$, for three different models: (a) normalized CSDs along the minor axis and (b) normalized near-tip shear stresses σ_{23} along the minor-axis.

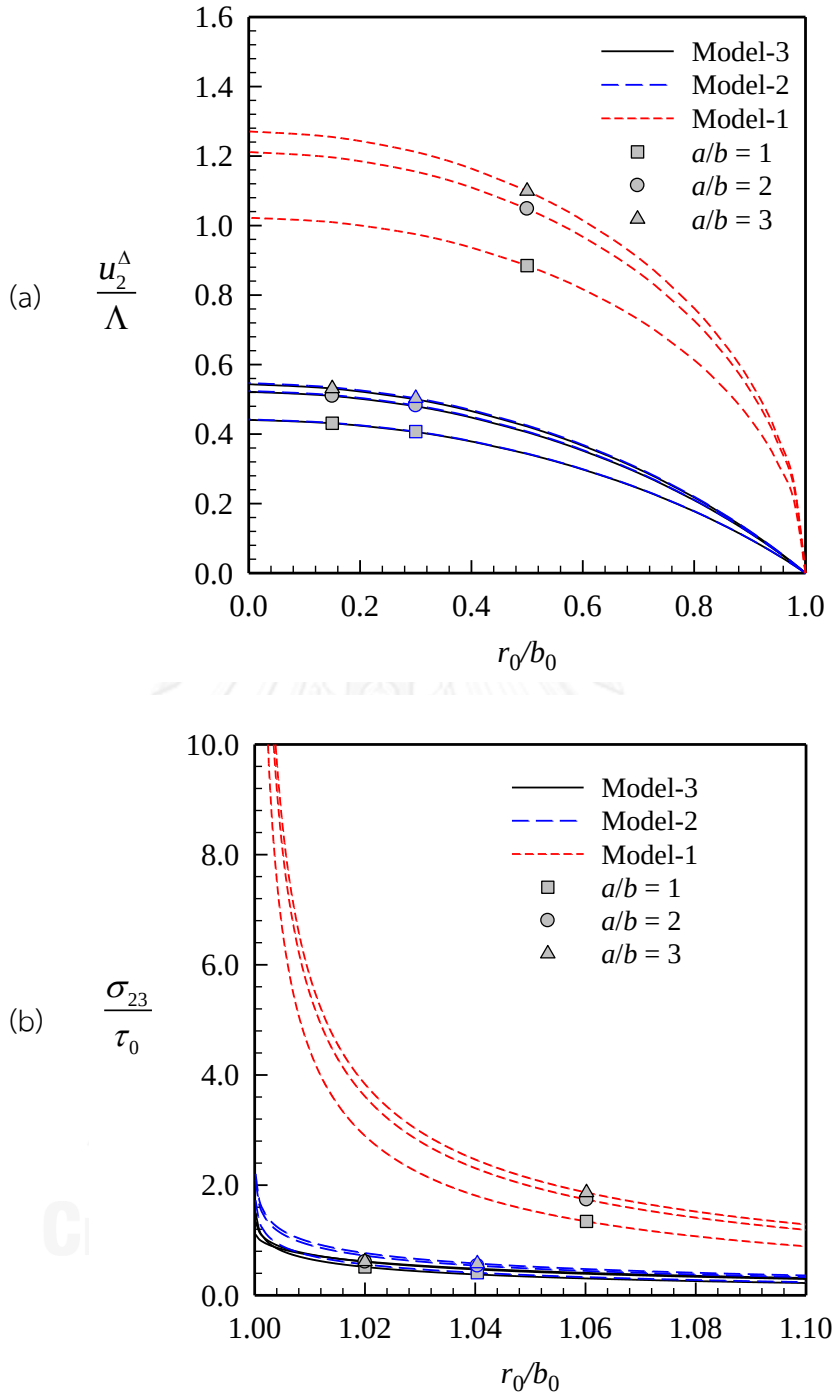

Figure 5.18: Elliptical crack under uniformly distributed shear traction in the x_2-direction with the aspect ratio $a/b = 1, 2, 3$, for $E = 107\,GPa$, $\nu = 0.33$, $\lambda^s = 4.4939\,N/m$, $\mu^s = 2.7779\,N/m$, $\tau^s = 0.6056\,N/m$ and for model-1, model-2, model-3: (a) normalized CSDs along the minor-axis and (b) normalized near-tip shear stresses σ_{23} along the minor-axis obtained by using mesh-3.

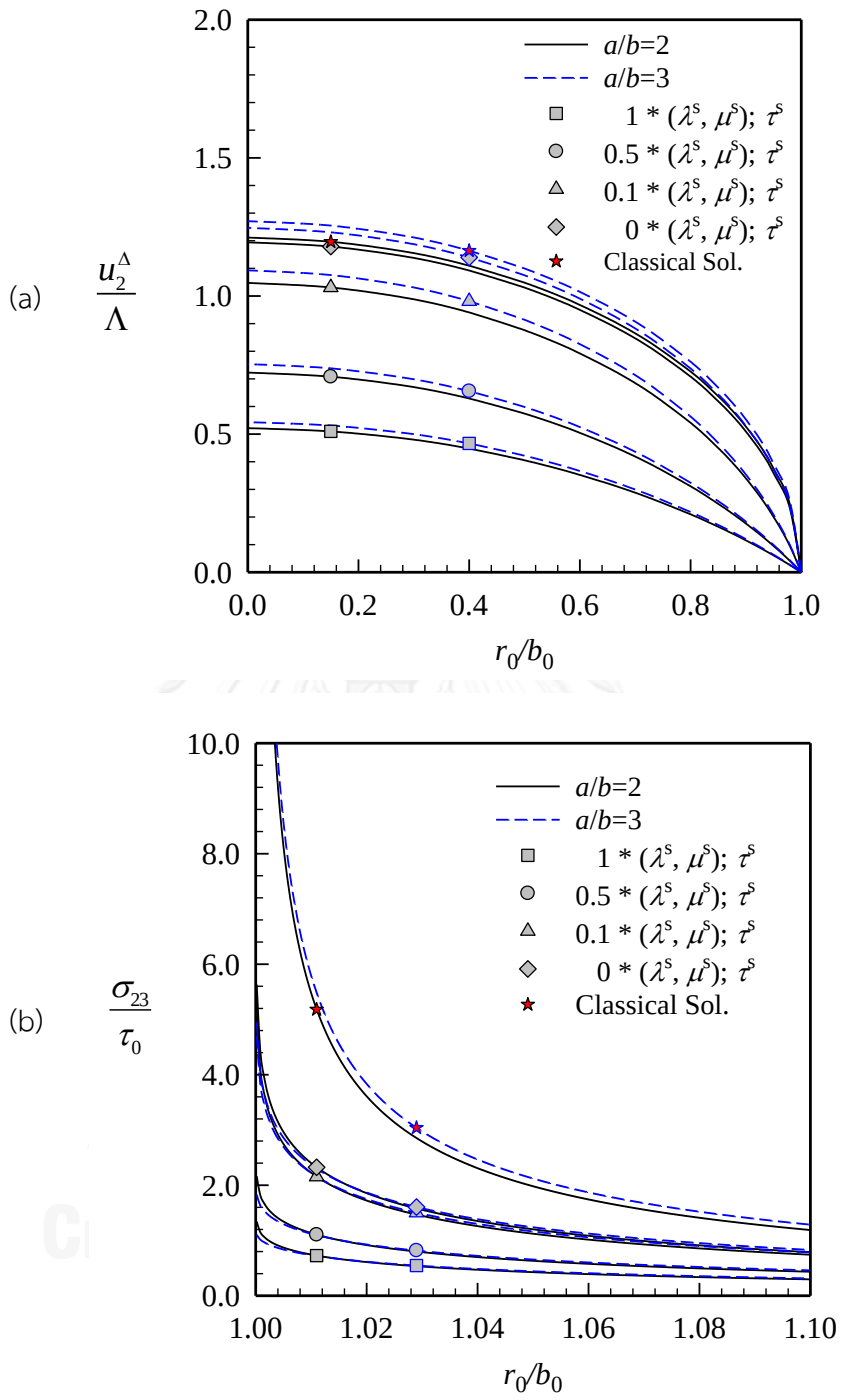

Figure 5.19: Elliptical crack under uniformly distributed shear traction in the x_2-direction for the model-3, the aspect ratios $a/b = 2, 3$ and different values of (λ^s, μ^s) ranging from 0 to 1 time their initial values ($\lambda^s = 4.4939\, N/m$, $\mu^s = 2.7779\, N/m$), $E = 107\, GPa$, $\nu = 0.33$, $\tau^s = 0.6056\, N/m$: (a) normalized CSDs along the minor-axis and (b) normalized near-tip shear stresses σ_{23} along the minor-axis obtained by using mesh-3.

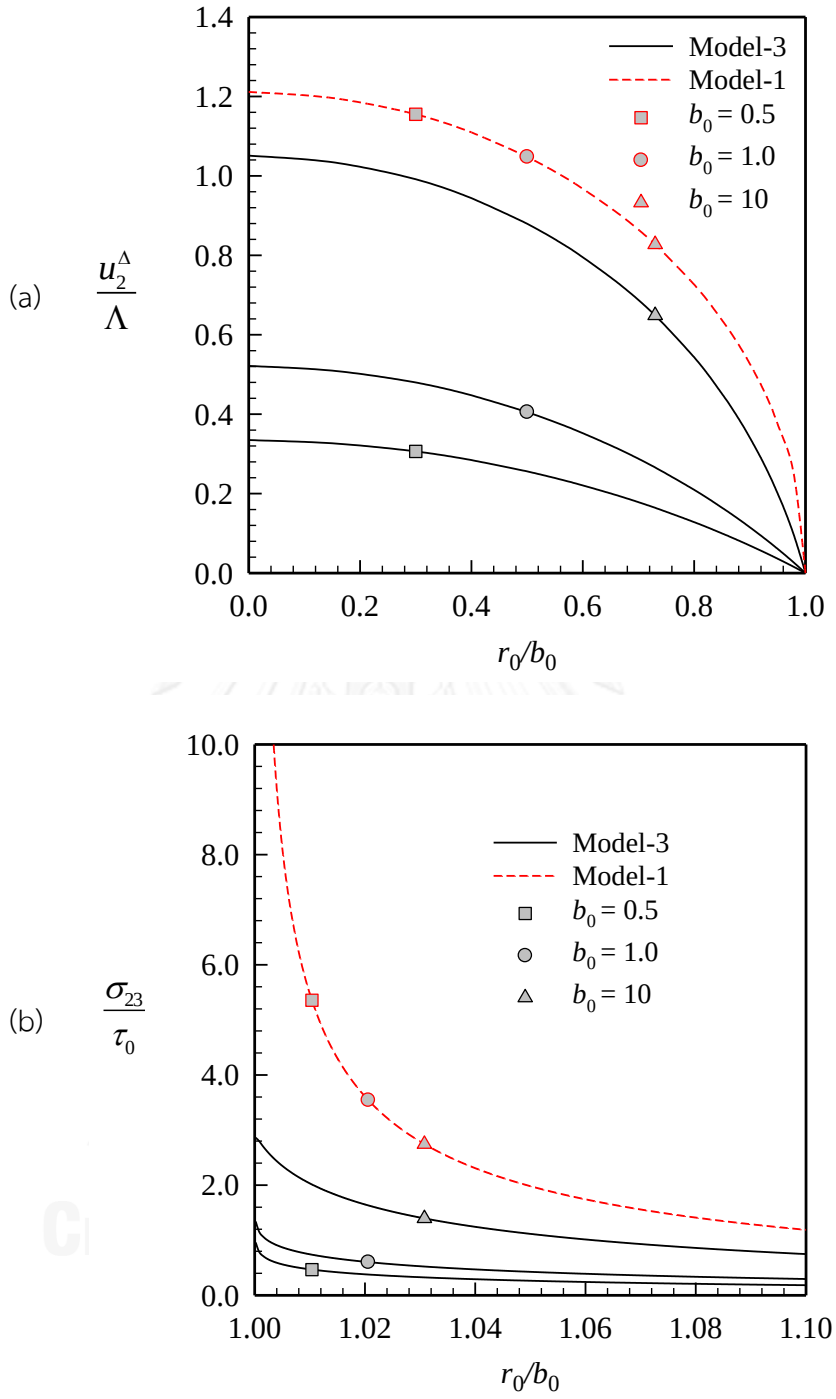

Figure 5.20: Elliptical crack under uniformly distributed shear traction in the x_2-direction for $a/b = 2$, $b_0 = b/\Lambda = 0.5,\ 1.0,\ 10$, for $E = 107\,GPa$, $\nu = 0.33$, $\lambda^s = 4.4939\,N/m$, $\mu^s = 2.7779\,N/m$, $\tau^s = 0.6056\,N/m$ and model-1, model-3: (a) normalized CSDs along the minor-axis and (b) normalized near-tip shear stresses σ_{23} along the minor-axis obtained by using mesh-3.

5.4 Two Coplanar Penny-Shaped Cracks

Finally, to demonstrate another feature of the proposed FEM-SGBEM technique in modeling multiple cracks, in this section, a problem of two interacting penny-shaped cracks embedded in an unbounded domain with consideration of the surface stress effects is investigated.

Consider a pair of co-planar, identical penny-shaped cracks of radius a embedded in an isotropic, linear elastic unbounded domain as shown in Figure 5.21(a). The distance between the centers of the two cracks is denoted by h. Both cracks are subjected to the self-equilibrated, uniformly distributed normal traction $t_3^+ = -t_3^- = \sigma_0$. Young's modulus and Poisson's ratio for the bulk material are taken as $E = 107\ GPa$ and $\nu = 0.33$, respectively. Here, the influence of the interaction between the two cracks on the maximum crack opening displacement (COD) and on the stress in the vicinity of the crack front at a particular point A (see Figure 5.21(a)) is investigated. To investigate the size-dependent behavior, two values of the normalized radius of the crack, $a_0 = a/\Lambda = 1$ and 10 are considered. Three meshes shown in Figure 5.21(b) are used to test the convergence of numerical solutions. For this particular problem the surface stress effects are modeled by the simplified version of Gurtin-Murdoch surface elasticity model with only the residual surface tension ($\tau^s = 0.6056\ N/m$) being treated.

To examine the convergence of the numerical solutions, the normalized CODs and the vertical stresses in the vicinity of the crack front of one of the penny shaped cracks (crack 1) with the normalized radius $a_0 = 1$ are obtained for the three meshes and results are reported in Figure 5.22 for $h/a = 2.2$. The results also are compared with classical solutions which can be found in Fabrikant (1989). It is seen that converged results of the normalized CODs and the near-tip vertical stresses are obtained. The residual surface tension reduced significantly the crack opening displacement and the near-tip vertical stresses.

To study the interaction between the two coplanar cracks, the normalized maximum COD and the normalized vertical stress at the point A are plotted for different values of h/a in Figures 5.23-5.24 for two cases of radius $a_0 = a/\Lambda = 1$ and 10 with three values of the residual surface tension $\tau^s = 0$ (classical solution), $\tau^s = 0.6056\ N/m$, and $\tau^s = 1\ N/m$. It can be seen in Figure 5.23(a) that, in good agreement with all previous examples, the maximum CODs and the vertical stresses in the neighborhood of the crack front decreases when the residual surface tension

increases. The bulk medium becomes much stiffer with the presence of the residual surface tension for cracks under mode-I loading conditions. It can also be seen from Figures 5.23 and 5.24 that the interaction between the two cracks for the classical case is size-independent (i.e., solutions of the two cracks converge asymptotically to that of the single crack in the identical manner). On the contrary, when the residual surface tension is incorporated in the mathematical model, the size-dependent behavior can be clearly observed by comparing results in Figures 5.23(a), (b) and results in Figures 5.24(a), (b), respectively. The decrease in the crack size also lowers the interaction between the two cracks.

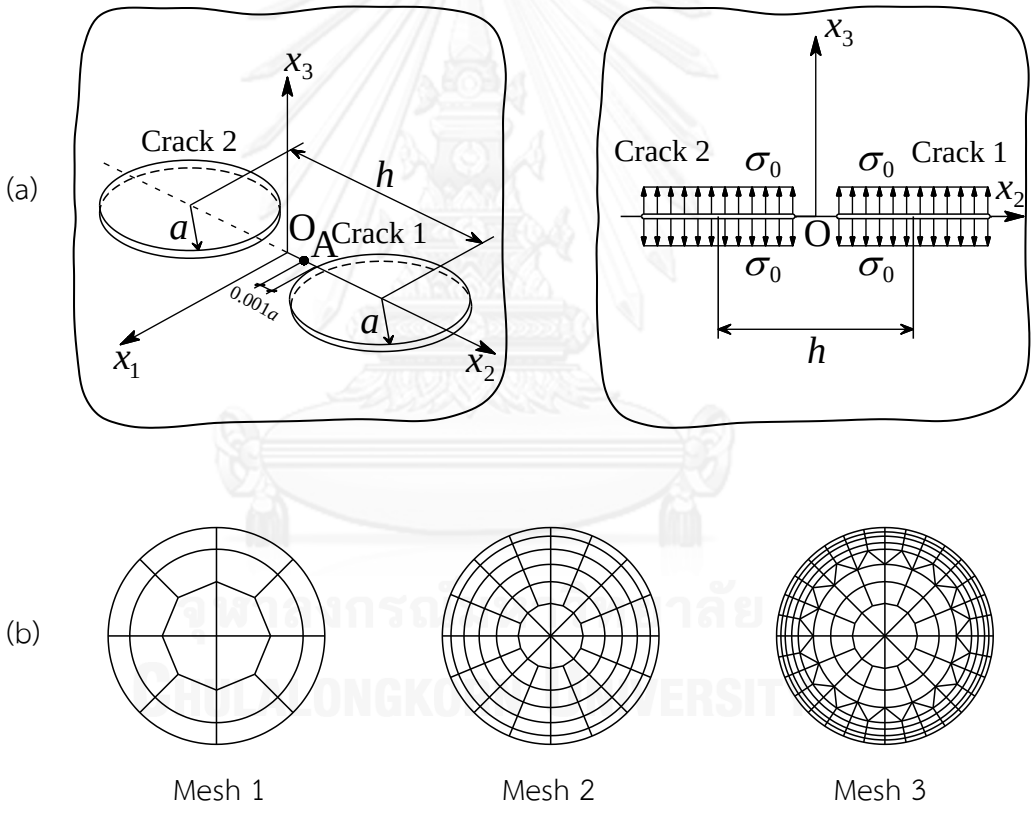

Figure 5.21: (a) Schematic of a pair of penny-shaped cracks of radius a embedded in an isotropic, linear elastic infinite medium subjected to uniformly distributed normal traction $t_3^+ = -t_3^- = \sigma_0$ and (b) meshes adopted for each crack. Mesh-1: 20 elements and 77 nodes. Mesh-2: 88 elements and 297 nodes. Mesh-3: 216 elements and 665 nodes.

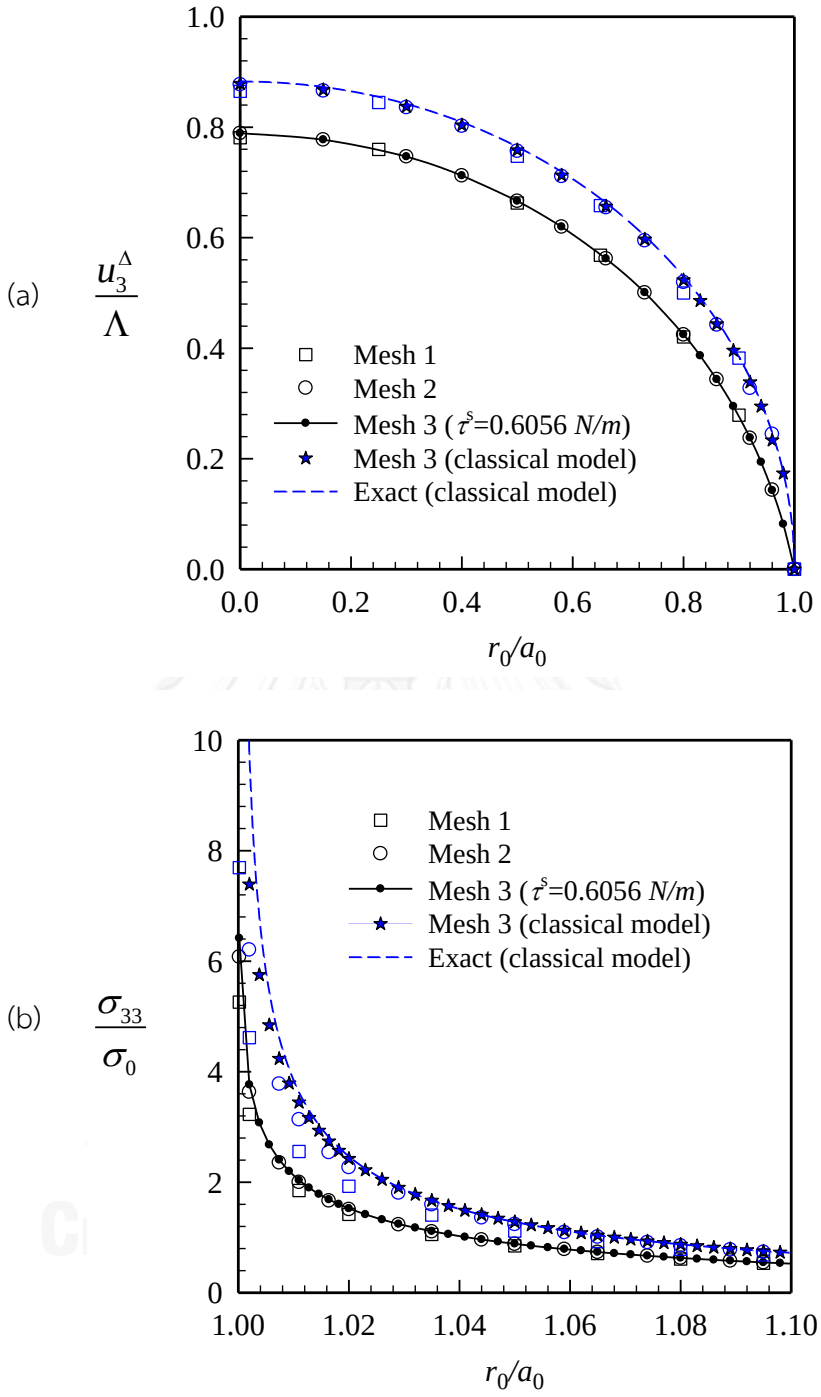

Figure 5.22: A pair of coplanar identical penny-shaped cracks with radius $a_0 = 1$ and $h/a = 2.2$ under uniformly distributed normal traction, for $E = 107\,GPa$, $\nu = 0.33$, and residual surface tension $\tau^s = 0.6056\,N/m$: (a) normalized CODs of crack 1 and (b) normalized near-tip vertical stresses of crack 1.

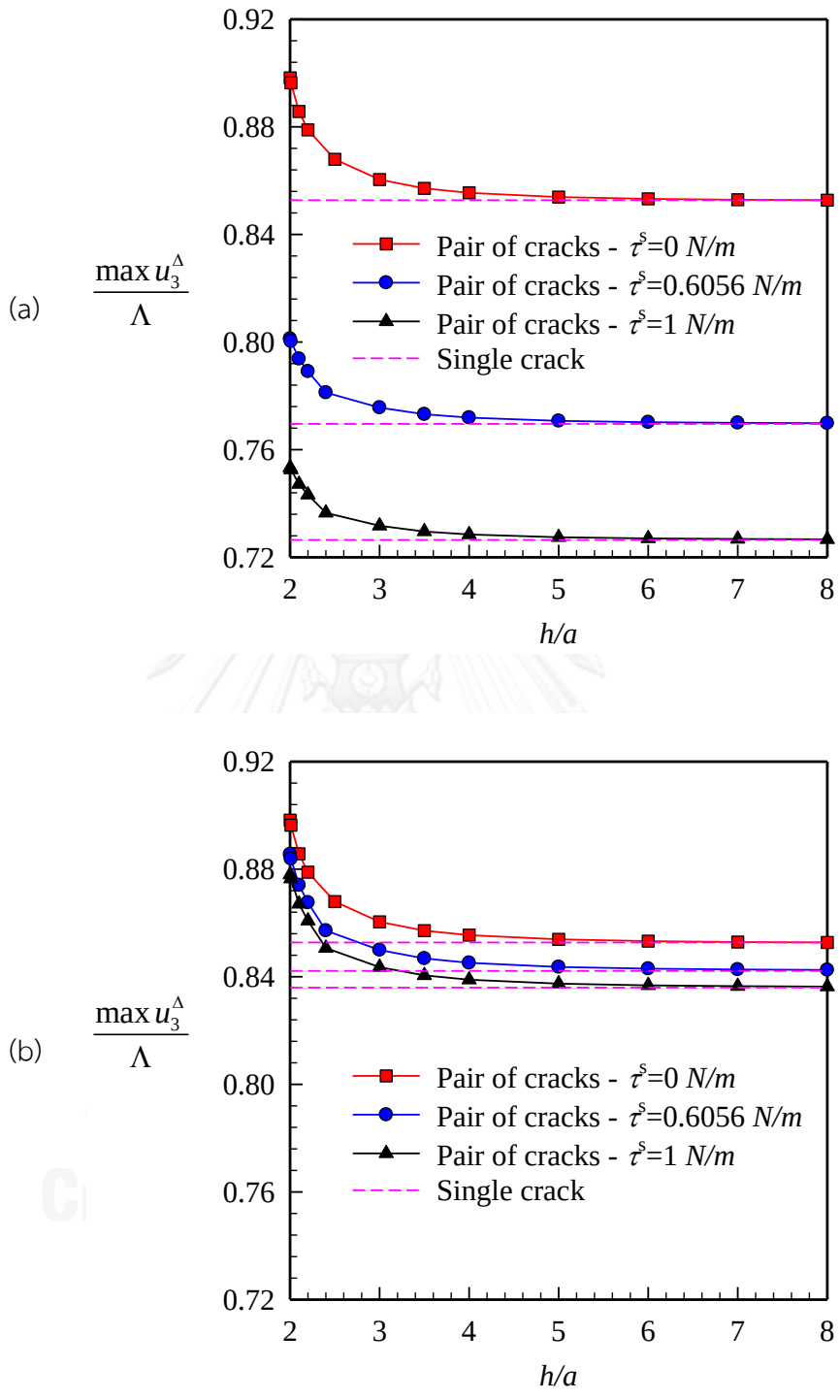

Figure 5.23: Normalized maximum crack opening displacements for a pair of coplanar identical penny-shaped cracks under uniformly distributed normal traction with different values of h/a, for $E=107\,GPa$, $\nu=0.33$, and residual surface tension $\tau^s=0.6056\,N/m$: (a) $a_0=1$ and (b) $a_0=10$ obtained by using mesh-3.

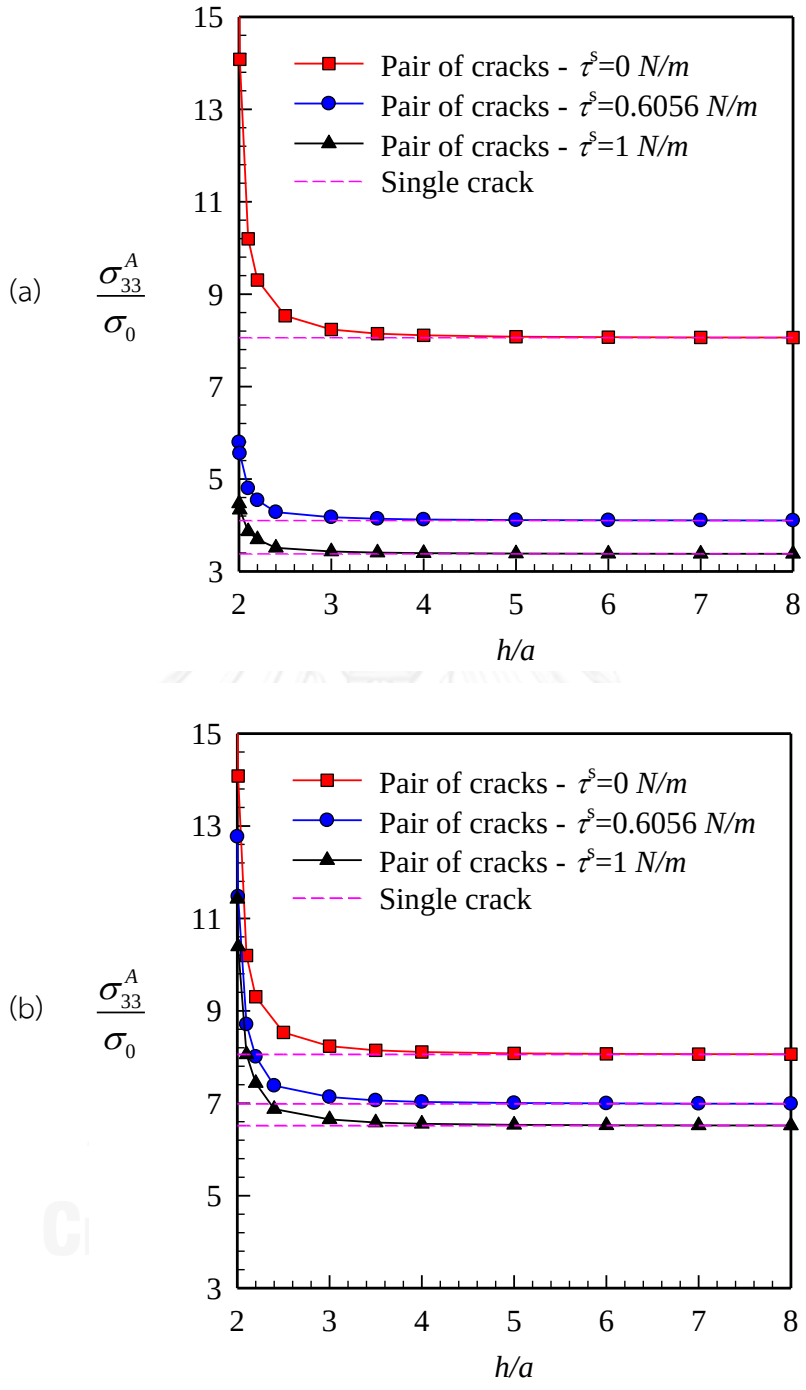

Figure 5.24: Normalized vertical stress at the point A for a pair of coplanar identical penny-shaped cracks under uniformly distributed normal traction with different values of h/a, for $E=107\,GPa$, $\nu=0.33$, and residual surface tension $\tau^s=0.6056\,N/m$: (a) $a_0=1$ and (b) $a_0=10$ obtained by using mesh-3.

CHAPTER 6
CONCLUSIONS

6.1. Summary

A computationally efficient numerical technique capable of modeling planar cracks in three-dimensional, linearly elastic media incorporating the influence of surface stresses has been established. In the formulation of the boundary value problem, the domain decomposition technique has been adopted to separate a cracked body into three parts: (i) an infinitesimally thin layer of materials on the upper crack surface, (ii) an infinitesimally thin layer of materials on the lower crack surface, and (iii) the remaining bulk medium with those two layers being removed. The classical theory of isotropic linear elasticity has been employed to form a system of governing equations of the bulk cracked medium in terms of weakly singular, weak-form boundary integral equations for the sum of the displacement and the jump of the traction across the crack surface of the bulk. Such governing equations possess several desirable features such as the weakly singular nature, simplicity to treat an infinite body and remote loading condition, and applicability to model cracks of arbitrary shapes and under general loading conditions. For both thin layers, they have been modeled as zero-thickness, two-sided surfaces with their behavior being described by Gurtin-Murdoch surface elasticity theory. In the present study, both the full version of Gurtin-Murdoch model including the in-plane surface elasticity and the residual surface tension and its simplified versions without either the in-plane surface elasticity or the residual surface tension are considered. The weight residual technique has been applied to derive the final weak-form statement for the surface part in terms of the same types of primary unknowns as those appearing in the bulk equations. The strong continuity condition of the displacement and traction on the interface of the surface and the bulk medium has been enforced to obtain the fully-coupled system of equations governing the whole medium.

Standard FEM-SGBEM coupling procedure has been implemented to construct numerical solutions of the final coupled system of governing equations. In the discretization, continuous element-based interpolation functions have been employed everywhere in the approximation of trial and test functions. In the present study, it has been postulated, based on the physical evidence and previous investigations, that presence of the surface stresses renders the stress along the crack front of the bulk

medium finite. As the direct consequence, standard C^0-elements have been employed everywhere in the discretization of all primary unknowns on the crack surface when the full version of Gurtin-Murdoch model has been considered. For the special cases, when the simplified version of Gurtin-Murdoch model without either the residual surface tension or the in-plane surface elasticity has been applied, standard C^0-elements have been employed everywhere in the discretization except in a local region along the crack front where either the jump of the out-of-plane displacement or the jump of the in-plane displacement is discretized by special crack-tip elements, respectively, to enhance the capability of the technique to capture the near-tip field. In the construction of a coefficient matrix, standard Gaussian quadrature has been adopted to evaluate all involved regular integrals whereas such quadrature supplemented by a family of suitable transformation has been employed to efficiently compute both weakly singular and nearly singular integrals. The final system of linear algebraic equations has been solved by a selected linear solver.

Extensive numerical experiments have been conducted and obtained results have been compared with available benchmark solutions to validate both the formulation and numerical implementations of the proposed technique. From a convergence study of numerical solutions, it has been found that the FEM-SGBEM coupling technique yields converged solutions with only weak dependence on the mesh refinement. In addition, the capability and the robustness of the proposed method to model relatively complex fracture problems with the treatment of the nano-scale influence have been confirmed via various examples involving mixed-mode loading conditions and interacting cracks.

From an extensive numerical study aiming to examine the influence of the surface stresses present at the crack surface on elastic responses of the bulk cracked medium, it has been found that both the residual surface tension and the in-plane surface elasticity appearing in Gurtin-Murdoch model play a vital role on the responses prediction and can substantially deviate results from the classical solutions. In general, results from the simulations using either the full or simplified version of Gurtin-Murdoch have indicated that the surface stresses tend to increase the local material stiffness in the vicinity of the crack; in particular, the predicted relative crack-face displacements and near-tip stresses are significantly lower than those obtained by the classical model without the contribution of the surface effects. In addition, the size-dependent behavior of the elastic responses predicted by models incorporating either the full or simplified version of Gurtin-Murdoch has been observed. In particular, as the characteristic size of the crack decreases to the intrinsic length scale of materials

(in the range of nano-scale for metals), the influence of both the residual surface tension and the in-plane surface elasticity becomes more prominent.

Results from the investigation of pure mode-I crack problems have indicated that the residual surface tension plays an important role on the reduction of the crack-opening displacement and the vertical stress in the vicinity of the crack front from the classical solution whereas the in-plane surface elasticity exhibits insignificant effect on such quantities. This finding suggests that the simplified version of Gurtin-Murdoch model with only the residual surface tension being treated can be used sufficiently in the modeling of mode-I crack problems to simplify the calculations. On the contrary, for cracks subjected to pure in-plane loading conditions (i.e., mode-II and mode-III loading conditions), the influence of the in-plane surface elasticity on major in-plane quantities such as the crack sliding displacement and the mode-II and mode-III shearing stresses is much more substantial than that of the residual surface tension. As a result, the simplified version of Gurtin-Murdoch model without the residual surface tension yields, in general, similar results to those predicted by a full model incorporating both the residual surface tension and the surface elastic constants. However, for cracks under full mixed-mode loadings, both the residual surface tension and the in-plane surface elasticity can play a crucial role on the predicted responses and the full version of Gurtin-Murdoch model is required.

6.2. Limitations and Directions of Future Research

The present study has provided an alternative computational tool based primarily on an enhanced continuum-based model that can be used to explore the fundamental behavior of nano-scale fractures. Nevertheless, the proposed numerical technique has been developed within the context where the fractures must be modeled as isolated *planar* cracks embedded in a homogeneous, isotropic, linear elastic, infinite bulk medium. To further enhance the modeling capability of the developed technique to treat a wide range of problems and to access more interesting fracture data, following potential extensions are suggested:

(1) the governing equations of the surface part can be extended to treat non-planar cracks;

(2) the formulation can be generalized to treat embedded, near-surface, and surface-breaking cracks in half-space or finite bodies; and

(3) the constitutive model for bulk materials can be extended to treat material anisotropy, non-uniformity, and multi-field material behavior such as piezoelectricity; and

(4) the computation of crucial fracture data such as the T-stress along the crack front can be added.

REFERENCES

Adnan, A. and C. T. Sun (2010). "Evolution of nanoscale defects to planar cracks in a brittle solid." Journal of the Mechanics and Physics of Solids **58**(7): 983-1000.

Bathe, K. J. (1990). Finite Element Procedures, Prentice-Hall, New Jersey.

Blandford, G. E., A. R. Ingraffea and J. A. Liggett (1981). "Two-dimensional stress intensity factor computations using the boundary element method." International Journal for Numerical Methods in Engineering **17**(3): 387-404.

Bonnet, M. (1995). "Regularized direct and indirect symmetric variational BIE formulations for three-dimensional elasticity." Engineering Analysis with Boundary Elements **15**(1): 93-102.

Bonnet, M., G. Maier and C. Polizzotto (1998). "Symmetric Galerkin Boundary Element Methods." Applied Mechanics Reviews **51**(11): 669-704.

Buehler, M. J., F. F. Abraham and H. Gao (2003). "Hyperelasticity governs dynamic fracture at a critical length scale." Nature **426**(6963): 141-146.

Buehler, M. J. and H. Gao (2006). "Dynamical fracture instabilities due to local hyperelasticity at crack tips." Nature **439**(7074): 307-310.

Cammarata, R. C. (1994). "Surface and interface stress effects in thin films." Progress in Surface Science **46**(1): 1-38.

Cammarata, R. C. (1997). "Surface and interface stress effects on interfacial and nanostructured materials." Materials Science and Engineering: A **237**(2): 180-184.

Chen, Q., I. Chasiotis, C. Chen and A. Roy (2008). "Nanoscale and effective mechanical behavior and fracture of silica nanocomposites." Composites Science and Technology **68**(15–16): 3137-3144.

Cruse, T. A. (1988). Boundary element analysis in computational fracture mechanics, Kluwer Academic Publishers, Dordrecht.

Dingreville, R., J. Qu and C. Mohammed (2005). "Surface free energy and its effect on the elastic behavior of nano-sized particles, wires and films." Journal of the Mechanics and Physics of Solids **53**(8): 1827-1854.

Duan, H. L., J. Wang, Z. P. Huang and B. L. Karihaloo (2005). "Eshelby formalism for nano-inhomogeneities." Proceedings of the Royal Society A: Mathematical, Physical and Engineering Science **461**(2062): 3335-3353.

Fabrikant, V. I. (1989). Applications of potential theory in mechanics: a selection of new results, Springer-Verlag New York, LLC.

Fang, Q. H., Y. Liu, Y. W. Liu and B. Y. Huang (2009). "Dislocation emission from an elliptically blunted crack tip with surface effects." Physica B: Condensed Matter **404**(20): 3421-3424.

Fang, Q. H. and Y. W. Liu (2006). "Size-dependent elastic interaction between a screw dislocation and a circular nano-hole with surface stress." physica status solidi (b) **243**(4): R28-R30.

Fang, Q. H., Y. W. Liu, B. Jin and P. H. Wen (2009). "Effect of interface stresses on the image force and stability of an edge dislocation inside a nanoscale cylindrical inclusion." International Journal of Solids and Structures **46**(6): 1413-1422.

Fischer, F. D., T. Waitz, D. Vollath and N. K. Simha (2008). "On the role of surface energy and surface stress in phase-transforming nanoparticles." Progress in Materials Science **53**(3): 481-527.

Frangi, A. and G. Novati (2003). "BEM–FEM coupling for 3D fracture mechanics applications." Computational Mechanics **32**(4-6): 415-422.

Frangi, A., G. Novati, R. Springhetti and M. Rovizzi (2002). "3D fracture analysis by the symmetric Galerkin BEM." Computational Mechanics **28**(3-4): 220-232.

Fu, X. L., G. F. Wang and X. Q. Feng (2008). "Surface effects on the near-tip stress fields of a mode-II crack." International Journal of Fracture **151**(2): 95-106.

Fu, X. L., G. F. Wang and X. Q. Feng (2010). "Surface effects on mode-I crack tip fields: A numerical study." Engineering Fracture Mechanics **77**(7): 1048-1057.

Gao, H. and B. Ji (2003). "Modeling fracture in nanomaterials via a virtual internal bond method." Engineering Fracture Mechanics **70**(14): 1777-1791.

Gibbs, J. W. (1906). The scientific papers of J. Willard Gibbs. Vol. 1, London : Longmans Green.

Gray, L. J., L. F. Martha and A. R. Ingraffea (1990). "Hypersingular integrals in boundary element fracture analysis." International Journal for Numerical Methods in Engineering **29**(6): 1135-1158.

Gu, H. and C. H. Yew (1988). "Finite element solution of a boundary integral equation for mode I embedded three-dimensional fractures." International Journal for Numerical Methods in Engineering **26**(7): 1525-1540.

Gurtin, M. E. and A. I. Murdoch (1975). "A continuum theory of elastic material surfaces." Archive for Rational Mechanics and Analysis **57**(4): 291-323.

Gurtin, M. E. and A. I. Murdoch (1978). "Surface stress in solids." International Journal of Solids and Structures **14**(6): 431-440.

Gurtin, M. E., J. Weissmüller and F. Larché (1998). "A general theory of curved deformable interfaces in solids at equilibrium." Philosophical Magazine A **78**(5): 1093-1109.

Hasheminejad, B. S. M., B. Gheshlaghi, Y. Mirzaei and S. Abbasion (2011). "Free transverse vibrations of cracked nanobeams with surface effects." Thin Solid Films **519**(8): 2477-2482.

Hayami, K. (1992). "A projection transformation method for nearly singular surface boundary element integrals. In: Brebbia, C. A., Orszag, S.A. (eds) Lecture notes in Engineering; 73; 1-2. Springer-Verlag, Berlin."

Hayami, K. and C. A. Brebbia (1988). "Quadrature methods for singular and nearly singular integrals in 3-D boundary element method, Boundary Element X, 237-264, Springer-Verlag, Berlin."

Hayami, K. and H. Matsumoto (1994). "A numerical quadrature for nearly singular boundary element integrals." Engineering Analysis with Boundary Elements **13**(2): 143-154.

He, L. H. and C. W. Lim (2006). "Surface Green function for a soft elastic half-space: Influence of surface stress." International Journal of Solids and Structures **43**(1): 132-143.

He, L. H., C. W. Lim and B. S. Wu (2004). "A continuum model for size-dependent deformation of elastic films of nano-scale thickness." International Journal of Solids and Structures **41**(3–4): 847-857.

Huang, D. W. (2008). "Size-dependent response of ultra-thin films with surface effects." International Journal of Solids and Structures **45**(2): 568-579.

Huang, S., S. Zhang, T. Belytschko, S. S. Terdalkar and T. Zhu (2009). "Mechanics of nanocrack: Fracture, dislocation emission, and amorphization." Journal of the Mechanics and Physics of Solids **57**(5): 840-850.

Hughes, T. J. R. (2000). The finite element method: linear static and dynamic finite element analysis, Dover Publications, New Jersey.

Iijima, S. (1991). "Helical microtubules of graphitic carbon." Nature **354**(6348): 56-58.

Iijima, S. and T. Ichihashi (1993). "Single-shell carbon nanotubes of 1-nm diameter." Nature **363**(6430): 603-605.

Intarit, P. (2013). Solutions of elastic medium with surface stress effects, Chulalongkorn University, Thailand. **Ph.D.**

Intarit, P., T. Senjuntichai, J. Rungamornrat and R. K. N. D. Rajapakse (2012). Stress analysis of penny-shaped crack considering the effects of surface elasticity. Proceedings of 20th

Annual International Conference on Composites or Nano Engineering (ICCE-20), Ramada Beijing North Hotel, Beijing, P.R. China.

Jammes, M., S. G. Mogilevskaya and S. L. Crouch (2009). "Multiple circular nano-inhomogeneities and/or nano-pores in one of two joined isotropic elastic half-planes." Engineering Analysis with Boundary Elements **33**(2): 233-248.

Kachanov, M. L., B. Shafiro and I. Tsukrov (2004). Handbook of Elasticity Solutions, Kluwer Academic Publishers.

Karimi, A., Y. Wang, T. Cselle and M. Morstein (2002). "Fracture mechanisms in nanoscale layered hard thin films." Thin Solid Films **420–421**(0): 275-280.

Kassir, M. K. and G. C. Sih (1975). Three-dimensional Crack Problems: A New Selection of Crack Solutions in Three-dimensional Elasticity, vol. 2, Noordhoff International Publishing, Leyden.

Kim, C., C.-Q. Ru and P. Schiavone (2013). "A clarification of the role of crack-tip conditions in linear elasticity with surface effects." Mathematics and Mechanics of Solids **18**(1): 59-66.

Kim, C. I., P. Schiavone and C. Q. Ru (2010). "Analysis of a mode-III crack in the presence of surface elasticity and a prescribed non-uniform surface traction." Zeitschrift für angewandte Mathematik und Physik **61**(3): 555-564.

Kim, C. I., P. Schiavone and C. Q. Ru (2011). "Analysis of Plane-Strain Crack Problems (Mode-I & Mode-II) in the Presence of Surface Elasticity." Journal of Elasticity **104**(1-2): 397-420.

Kim, C. I., P. Schiavone and C. Q. Ru (2011). "The effect of surface elasticity on a Mode-III interface crack." Archives of Mechanics **63**(3): pp. 267 - 286.

Li, H.-B., G.-M. Han and H. A. Mang (1985). "A new method for evaluating singular integrals in stress analysis of solids by the direct boundary element method." International Journal for Numerical Methods in Engineering **21**(11): 2071-2098.

Li, S. and M. Mear (1998). "Singularity-reduced integral equations for displacement discontinuities in three-dimensional linear elastic media." International Journal of Fracture **93**(1-4): 87-114.

Li, S., M. E. Mear and L. Xiao (1998). "Symmetric weak-form integral equation method for three-dimensional fracture analysis." Computer Methods in Applied Mechanics and Engineering **151**(3–4): 435-459.

Liu, Y. W. and Q. H. Fang (2007). "Analysis of a screw dislocation inside an inhomogeneity with interface stress." Materials Science and Engineering: A **464**(1–2): 117-123.

Masuda-Jindo, K., V. V. Hung and M. Menon (2009). "Fracture and mechanical properties of nanotubes and nanowires." Procedia Engineering **1**(1): 163-166.

Miller, R. E. and V. B. Shenoy (2000). "Size-dependent elastic properties of nanosized structural elements." Nanotechnology **11**(3): 139.

Mogilevskaya, S. G., S. L. Crouch and H. K. Stolarski (2008). "Multiple interacting circular nano-inhomogeneities with surface/interface effects." Journal of the Mechanics and Physics of Solids **56**(6): 2298-2327.

Nan, H. and B. Wang (2012). "Effect of residual surface stress on the fracture of nanoscale materials." Mechanics Research Communications **44**(0): 30-34.

Nan, H. S. and B. L. Wang (2013). "Effect of crack face residual surface stress on nanoscale fracture of piezoelectric materials." Engineering Fracture Mechanics **110**(0): 68-80.

Nix, W. D. and H. Gao (1998). "Indentation size effects in crystalline materials: A law for strain gradient plasticity." Journal of the Mechanics and Physics of Solids **46**(3): 411-425.

Oh, E.-S., J. R. Walton and J. C. Slattery (2005). "A Theory of Fracture Based Upon an Extension of Continuum Mechanics to the Nanoscale." Journal of Applied Mechanics **73**(5): 792-798.

Ou, Z. Y., G. F. Wang and T. J. Wang (2008). "Effect of residual surface tension on the stress concentration around a nanosized spheroidal cavity." International Journal of Engineering Science **46**(5): 475-485.

Pan, E. and F. G. Yuan (2000). "Boundary element analysis of three-dimensional cracks in anisotropic solids." International Journal for Numerical Methods in Engineering **48**(2): 211-237.

Peng, B., M. Locascio, P. Zapol, S. Li, S. L. Mielke, G. C. Schatz and H. D. Espinosa (2008). "Measurements of near-ultimate strength for multiwalled carbon nanotubes and irradiation-induced crosslinking improvements." Nat Nano **3**(10): 626-631.

Phan, A. V. and H. V. Tippur (2009). "Shape-sensitivity-based evaluation of the stress intensity factors at the nanoscale by means of quantized fracture mechanics." Mechanics Research Communications **36**(3): 336-342.

Pinyochotiwong, Y., J. Rungamornrat and T. Senjuntichai (2013). "Rigid frictionless indentation on elastic half space with influence of surface stresses." International Journal of Engineering Science **71**(0): 15-35.

Pugno, N., A. Carpinteri, M. Ippolito, A. Mattoni and L. Colombo (2008). "Atomistic fracture: QFM vs. MD." Engineering Fracture Mechanics **75**(7): 1794-1803.

Qin, E. W., L. Lu, N. R. Tao, J. Tan and K. Lu (2009). "Enhanced fracture toughness and strength in bulk nanocrystalline Cu with nanoscale twin bundles." Acta Materialia **57**(20): 6215-6225.

Rafii-Tabar, H., H. M. Shodja, M. Darabi and A. Dahi (2006). "Molecular dynamics simulation of crack propagation in fcc materials containing clusters of impurities." Mechanics of Materials **38**(3): 243-252.

Ratner, M. A. and D. Ratner (2003). Nanotechnology: A Gentle Introduction to the Next Big Idea, Prentice Hall Professional.

Rungamornrat, J. (2006). "Analysis of 3D cracks in anisotropic multi-material domain with weakly singular SGBEM." Engineering Analysis with Boundary Elements **30**(10): 834-846.

Rungamornrat, J. and M. E. Mear (2008). "A weakly-singular SGBEM for analysis of cracks in 3D anisotropic media." Computer Methods in Applied Mechanics and Engineering **197**(49–50): 4319-4332.

Rungamornrat, J. and M. E. Mear (2008). "Weakly-singular, weak-form integral equations for cracks in three-dimensional anisotropic media." International Journal of Solids and Structures **45**(5): 1283-1301.

Rungamornrat, J. and M. E. Mear (2011). "SGBEM–FEM coupling for analysis of cracks in 3D anisotropic media." International Journal for Numerical Methods in Engineering **86**(2): 224-248.

Rungamornrat, J. and T. Senjuntichai (2009). "Regularized boundary integral representations for dislocations and cracks in smart media." Smart Materials and Structures **18**(7): 074010.

Sáez, A., M. P. Ariza and J. Dominguez (1997). "Three-dimensional fracture analysis in transversely isotropic solids." Engineering Analysis with Boundary Elements **20**(4): 287-298.

Sakib, A. R. N. and A. Adnan (2012). "On the size-dependent critical stress intensity factor of confined brittle nanofilms." Engineering Fracture Mechanics **86**(0): 13-22.

Sander, D. (2003). "Surface stress: implications and measurements." Current Opinion in Solid State and Materials Science **7**(1): 51-57.

Sendova, T. and J. R. Walton (2010). "A New Approach to the Modeling and Analysis of Fracture through Extension of Continuum Mechanics to the Nanoscale." Mathematics and Mechanics of Solids **15**(3): 368-413.

Sharma, P. and S. Ganti (2004). "Size-Dependent Eshelby's Tensor for Embedded Nano-Inclusions Incorporating Surface/Interface Energies." Journal of Applied Mechanics **71**(5): 663-671.

Sharma, P., S. Ganti and N. Bhate (2003). "Effect of surfaces on the size-dependent elastic state of nano-inhomogeneities." Applied Physics Letters **82**(4): 535-537.

Shenoy, V. B. (2002). "Size-dependent rigidities of nanosized torsional elements." International Journal of Solids and Structures **39**(15): 4039-4052.

Shuttleworth, R. (1950). "The Surface Tension of Solids." Proceedings of the Physical Society. Section A **63**(5): 444.

Song, F., G. L. Huang, H. S. Park and X. N. Liu (2011). "A continuum model for the mechanical behavior of nanowires including surface and surface-induced initial stresses." International Journal of Solids and Structures **48**(14–15): 2154-2163.

Sumomogi, T., M. Nakamura, T. Endo, T. Goto and S. Kaji (2002). "Evaluation of surface and subsurface cracks in nanoscale-machined single-crystal silicon by scanning force microscope and scanning laser microscope." Materials Characterization **48**(2–3): 141-145.

Sundararajan, S. and B. Bhushan (2002). "Development of AFM-based techniques to measure mechanical properties of nanoscale structures." Sensors and Actuators A: Physical **101**(3): 338-351.

Sutradhar, A. and G. H. Paulino (2004). "Symmetric Galerkin boundary element computation of T-stress and stress intensity factors for mixed-mode cracks by the interaction integral method." Engineering Analysis with Boundary Elements **28**(11): 1335-1350.

Tada, H., P. C. Paris and G. R. Irwin (2000). The Stress Analysis of Cracks Handbook, American Society of Mechanical Engineers.

Tian, L. and R. K. N. D. Rajapakse (2006). "Analytical Solution for Size-Dependent Elastic Field of a Nanoscale Circular Inhomogeneity." Journal of Applied Mechanics **74**(3): 568-574.

Tian, L. and R. K. N. D. Rajapakse (2007). "Elastic field of an isotropic matrix with a nanoscale elliptical inhomogeneity." International Journal of Solids and Structures **44**(24): 7988-8005.

Wang, G.-F., X.-Q. Feng, T.-J. Wang and W. Gao (2007). "Surface Effects on the Near-Tip Stresses for Mode-I and Mode-III Cracks." Journal of Applied Mechanics **75**(1): 011001-011001.

Wang, G. F. and T. J. Wang (2006). "Deformation around a nanosized elliptical hole with surface effect." Applied Physics Letters **89**(16): -.

Wang, J.-S., X.-Q. Feng, G.-F. Wang and S.-W. Yu (2008). "Twisting of nanowires induced by anisotropic surface stresses." Applied Physics Letters **92**(19): -.

Wu, C. H. (1999). "The effect of surface stress on the configurational equilibrium of voids and cracks." Journal of the Mechanics and Physics of Solids **47**(12): 2469-2492.

Wu, C. H. and M. L. Wang (2000). "The effect of crack-tip point loads on fracture." Journal of the Mechanics and Physics of Solids **48**(11): 2283-2296.

Wu, C. H. and M. L. Wang (2001). "Configurational equilibrium of circular-arc cracks with surface stress." International Journal of Solids and Structures **38**(24–25): 4279-4292.

Xiao, L. (1998). Symmetric weak-form integral equation method for three-dimensional fracture analysis, The University of Texas at Austin, Texas. **Ph.D.**

Xu, G. (1999). "A Variational Boundary Integral Method for the Analysis of Three-Dimensional Cracks of Arbitrary Geometry in Anisotropic Elastic Solids." Journal of Applied Mechanics **67**(2): 403-408.

Xu, G. and M. Ortiz (1993). "A variational boundary integral method for the analysis of 3-D cracks of arbitrary geometry modelled as continuous distributions of dislocation loops." International Journal for Numerical Methods in Engineering **36**(21): 3675-3701.

Yakobson, B. I. (2003). "Nanomechanics. In W. A. Goddard; D. W. Brenner; S. E. Lyshevski; and G. J. Iafrate (eds.). Handbook of nanoscience, engineering, and technology, chapter 17. Florida: CRC Press."

Yan, Y., T. Sumigawa, F. Shang and T. Kitamura (2011). "Cohesive zone criterion for cracking along the Cu/Si interface in nanoscale components." Engineering Fracture Mechanics **78**(17): 2935-2946.

Zeng-shen, C. (1982). "Discussion on the SIF for points on border of elliptical flat crack inside infinite solid under uniform tension." Applied Mathematics and Mechanics **3**(4): 521-526.

Zhang, S., S. L. Mielke, R. Khare, D. Troya, R. S. Ruoff, G. C. Schatz and T. Belytschko (2005). "Mechanics of defects in carbon nanotubes: Atomistic and multiscale simulations." Physical Review B **71**(11): 115403.

Zhao, C. W. and Y. M. Xing (2008). "Nanoscale experimental study of a micro-crack in silicon." Physica B: Condensed Matter **403**(23–24): 4202-4204.

Zhao, C. W. and Y. M. Xing (2010). "Nanoscale deformation analysis of a crack-tip in silicon by geometric phase analysis and numerical moiré method." Optics and Lasers in Engineering **48**(11): 1104-1107.

Zhao, X. J. and R. K. N. D. Rajapakse (2009). "Analytical solutions for a surface-loaded isotropic elastic layer with surface energy effects." International Journal of Engineering Science **47**(11–12): 1433-1444.

Zienkiewicz, O. C. and R. L. Taylor (2000). The finite element method: Solid mechanics, volume 2, Butterworth-Heinemann, Oxford.

APPENDIX

VITA

The author, Binh Thai Nguyen, was born in Hochiminh City, Vietnam, on July 3, 1982. He graduated his Bachelor of Engineering degree in Civil Engineering from Hochiminh City University of Technology in 2005. After graduation, he continued his Master degree in Civil Engineering at Hochiminh City University of technology in the same year and finished his Master of Engineering degree in Civil Engineering major in 2008. In 2010, he achieved the scholarship by ASEAN University Network –Southeast Asia Engineering Education Development Network Project (AUN/SEED-Net) for his doctoral degree in Civil Engineering at Chulalongkorn University under the supervision of Associate Professor Dr. Jaroon Rungamornrat and Professor Dr. Teerapong Senjuntichai. He spent eight months (from October 2012 to May 2013) at Tokyo Institute of Technology, Tokyo, Japan, to conduct a research work with Associate Professor Dr. Anil C. Wijeyewickrema.